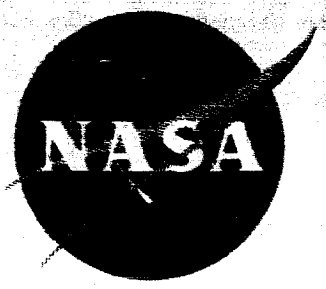

NASA CR-54273

DEVELOPMENT OF IMPROVED SINGLE CRYSTAL GALLIUM PHOSPHIDE SOLAR CELLS

FINAL REPORT

Period June 12, 1963 - August 12, 1964

Prepared for

NATIONAL AERONAUTICS AND SPACE ADMINISTRATION

NASA Contract Number NAS3-2776

MONSANTO RESEARCH CORPORATION

A SUBSIDIARY OF MONSANTO COMPANY

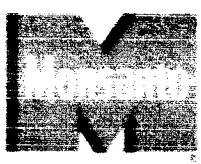

DAYTON LABORATORY

DAYTON, OHIO 45407

NASA CR-54273

DEVELOPMENT OF IMPROVED SINGLE CRYSTAL GALLIUM PHOSPHIDE SOLAR CELLS

Final Report
June 12, 1963 - August 12, 1964

Contract No. NAS3-2776

NATIONAL AERONAUTICS AND SPACE ADMINISTRATION
Technical Management
Space Power Systems Division
NASA - Lewis Research Center
L. R. Scudder

Report Prepared by: W. O. Groves and A. S. Epstein

Edited by: R. A. Ruehrwein

Work Performed by:
Central Research Department
MONSANTO COMPANY
St. Louis, Missouri

TABLE OF CONTENTS

TABLE OF CONTENTS

I. PURPOSE

This is the final report on the 14-month program to develop Single Crystal Gallium Phosphide Solar Cells. The objective of this program was the development of an efficient solar cell operable at temperatures up to 500° C. The approach has been to grow single crystal gallium phosphide by epitaxial deposition from the vapor phase on gallium arsenide substrate followed by removal of the gallium arsenide. Diffused junction cells were then fabricated and the photovoltaic properties of the cells were measured up to high temperatures. The design and performance of the cells were related to the electrical and optical properties of the gallium phosphide.

II. ABSTRACT

Single crystal gallium phosphide has been prepared by synthesis (or transport) and epitaxial deposition on single crystal gallium arsenide using hydrogen chloride in an open tube vapor transport process with gallium and phosphorus (or gallium phosphide) sources. The growth rate and yield of gallium phosphide using this method, and available starting materials, have had limitations imposed by the requirements for obtaining good structure and purity, these ultimately being determined by measurement of solar cell characteristics.

Growth surfaces very nearly free of gross defects, such as bumps and stacking faults, and good epitaxial interfaces can, under favorable conditions, be obtained by pretreating the gallium arsenide substrate wafers with hydrogen and phosphorus vapor at high temperature. A pronounced effect of impurities in the gas stream on the growth habit of bumps has been observed.

The gallium phosphide produced has been highly compensated, electrical properties and analysis indicating impurity levels in the range of 5×10^{18} atoms/cm^3, whereas net carrier levels (n-type) in the low 10^{16} cm^{-3} range are typical for "undoped" <100 > oriented material. Typical mobilities of 100 cm^2/volt cm are measured. The major impurity is silicon, originating in the phosphorus source or from reaction of the gases with silica at high temperature. Rather high concentrations of other metal impurities originate from the same sources as well as in the hydrogen chloride transfer gas - other unidentified contaminants, probably including sulfur, are also present.

Growth direction is found to have a very strong effect on the net carrier concentration of epitaxial gallium phosphide which is not accounted for by analytical data. The order of net carrier density (n-type)

for the different orientations grown under identical conditions is (111)B >(110) >(100) >(111)A.

Doping with tellurium, tin and zinc has been demonstrated.

The open transport and epitaxial deposition of gallium phosphide by water vapor has been investigated briefly, results comparable to those of Frosch[3] being obtained.

The vapor transport and epitaxial deposition of gallium phosphide by water vapor using a close-space technique similar to that of Nicoll[8] has been initiated.

Solar cells have been fabricated from the epitaxially deposited single crystal gallium phosphide using zinc as the diffusant. Two types of cells have been found: (1) those having their major spectral response at about 0.75 μ and referred to as extrinsic and (2) those which have their main response at 0.45 μ and referred to as intrinsic cells.

For the extrinsic cells, at 23° C in sunlight, an open circuit voltage (V_{oc}) of about 0.7 volts with a short circuit current density, J_{sc}, of about 5 ma/cm^2 has been found. Conversion efficiencies between 1.5 and 2% have been noted. Correspondingly, for the 0.45 μ cells a V_{oc} at 23° C of 1.35 volts and a J_{sc} of 1.4 ma/cm^2 have been obtained with a conversion efficiency, measured in sunlight, up to 1%. Cell areas have ranged from 0.2 cm^2 to 0.5 cm^2.

With increasing temperature, the V_{oc} of both types of cells decreases with a temperature coefficient, β, of about 3 mv/deg. The intrinsic cell has a V_{oc} at 350° C of 0.4 volts whereas the extrinsic cell V_{oc} goes to zero at this temperature.

The J_{sc} of the 0.45 μ cell increases with temperature and the temperature variation can be expressed as $J_{sc} \sim e^{-\Delta E/kT}$ with $\Delta E \sim .05$ eV. The extrinsic cell, on the other hand, shows no change in J_{sc} to 200° after which it decreases rapidly. For high temperature operation it is quite

apparent that the intrinsic cell is superior.

The p-n junctions of these cells appear to be graded as evidenced by the capacity-voltage (C-V) relation which suggests a $1/C^3$ variation with voltage. From measurements of the minority carrier diffusion length the minority carrier lifetime in these cells is found to vary between 10^{-10} and 10^{-12} seconds. The I-V characteristics indicate that $n > 2$ in the relationship $I = I_o e^{ev/nkT}$.

Limitation on the solar cell thus far appears to be the series resistance of the junction which should be improved as purer material becomes available.

III. MATERIAL PREPARATION

A. INTRODUCTION

The objective of the work on material preparation has been to prepare high quality single crystal material suitable for critical evaluation of the potential of gallium phosphide in high temperature solar cells. Material objectives for this purpose have been to prepare single crystals up to 10 x 20 x .25 mm in size, free of gross defects such as stacking faults and polycrystalline grain boundaries, and having the following electrical parameters: net carrier level, 10^{16} - 10^{17} cm^{-3} and mobility, 300 cm^2 $volt^{-1}$ sec^{-1} minimum.

Single crystal growth of gallium phosphide by epitaxial deposition from the vapor phase on a suitable substrate is the only currently practicable method for obtaining the uniform large area required. An open tube transport process[1] using a dilute mixture of hydrogen chloride in hydrogen as the carrier gas, with deposition on gallium arsenide substrates, was chosen as the principle preparative method because of the flexibility and convenience; however, other methods, as discussed below, have also been investigated briefly.

Principal efforts have been directed toward increasing growth rates of gallium phosphide to obtain thick self supporting layers, toward improving structure of the deposits, and toward improving the purity. Some early experiments to control net carrier level by doping were discontinued to concentrate on maximizing purity. The latter is considered to be the major factor limiting the open circuit voltage and consequently limiting the high temperature efficiency of solar cells.

B. EXPERIMENTAL

1. Epitaxial Deposition

The open tube transport process used for growth of single crystal

gallium phosphide by vapor phase deposition is a modification of that described previously[1]. The apparatus, shown schematically in Figure 1, consists of a 20 mm I. D. quartz reaction tube containing, respectively, elemental phosphorus, gallium and gallium arsenide substrate in the three separately controlled temperature zones of a three zone furnace, and provision for introducing a dilute mixture of hydrogen chloride in hydrogen. In some experiments gallium phosphide has been used as the source in place of gallium metal.

Source temperatures of 890° to 980° have been used with deposition temperatures of 790° to 870°. A typical temperature profile obtained with one three zone furnace system is shown in Figure 2. Also shown are typical positions of the phosphorus, gallium and gallium arsenide substrate wafers. In a later system the first zone was extended by insertion of a 12" unit to provide a long uniform temperature zone for better control of phosphorus vaporization.

The lines, valves and fittings leading to the quartz transfer tube were of pyrex, teflon or stainless steel to minimize contamination. Prepurified hydrogen (The Matheson Co.) was passed through a Deoxo purifier, then a coil immersed in liquid nitrogen before being metered into the system. In earlier runs, anhydrous hydrogen chloride (Matheson, 99%) was metered directly into the system or passed through a trap containing magnesium perchlorate and mercuric chloride, and cooled in a dry ice slurry, before being metered into the system. In most runs the hydrogen chloride was supplied as a 5% mixture in hydrogen. Alternatively, hydrogen chloride was generated by hydrogen reduction of reagent grade arsenic trichloride (B and A, General Chemical Division, Allied Chemical) in a tube heated to about 800° C. Arsenic trichloride was introduced at a controlled rate by bubbling a portion of the hydrogen stream through a reservoir at 0° C. The elemental arsenic formed in the reduction was condensed before the

gas stream entered the transfer tube.

Red phosphorus from several different sources has been employed. These include "semiconductor" grade from American Agricultural Chemical Co., high purity (99.999% claimed) from L. Light and Co., Ltd., and from Kern Chemical Corp., Monsanto purified phosphorus, and in one run ordinary laboratory grade from Fisher. Some analytical data are included in the discussion section below.

Pure gallium metal (99.9999%) was obtained from Alcoa while polycrystalline gallium phosphide was supplied by Merck.

Gallium arsenide substrate wafers with (100) or (111)B surfaces polished by a standard mechanical-chemical technique were recleaned ultrasonically in concentrated sulfuric acid, rinsed in distilled water, acetone, and absolute ethyl alcohol, then wiped dry with microcloth or lens cleaning tissue just prior to insertion in the reaction tube. Wafers of (111)A and (110) orientation were simply lapped, then given a three minute etch in a polish etch ($HF:HNO_3:H_2O::1:3:4$) before cleaning as above.

The procedure for carrying out an epitaxial deposition was as follows. After loading, the system was flushed with argon or evacuated prior to flushing for at least one hour with hydrogen. The source and deposition zones were then heated to 400° C to prevent condensation while the phosphorus was outgassed for 15 to 20 minutes at a predetermined temperature. The source and substrates were then heated to 1000° C while maintaining the flow of phosphorus. This procedure, which may be considered a further cleaning step, was found necessary to obtain smooth, bump and stacking fault free, (100) growth surfaces. After about one hour (30 minutes at 1000° C) the temperatures of the source and substrate were reduced to the desired transfer and deposition temperatures and the hydrogen chloride flow initiated, all the while maintaining a constant phosphorus zone temperature. For deposition

under low phosphorus pressure this control temperature was lowered after initiating deposition of GaP at the high phosphorus pressure. This procedure was found necessary to avoid decomposition and etching of the GaAs substrates.

At the termination of the run the hydrogen chloride flow was interrupted, then a few minutes allowed for the remaining hydrogen chloride to be swept from the system before, first opening the phosphorus zone to obtain abrupt cooling, then turning off the power to the other zones and allowing them to cool. Thermal stress in some of the thick deposits of gallium phosphide caused breakage of the wafers on cooling. In other experiments this breakage was avoided by a slow cooling (2° per min.) to aid in relieving the thermal strain.

2. Electrical Measurements

Electrical properties, net carrier concentration and Hall mobility, were obtained by standard resistivity and Hall coefficient measurements on monitor Hall bars. The Hall bars, cleaved from polished wafers of high resistivity gallium arsenide, were located adjacent to the wafers during deposition. Contacts to the gallium phosphide surfaces were made by alloying dots of pure indium at 700°-800° C using a strip heater. Consistent results were obtained in all but a few cases. Where determined, net carrier level by voltage-capacitance measurement was in reasonable agreement with the Hall coefficient measurement.

Measurements of some of the thickest deposits were made after removing the gallium arsenide substrate by dissolution in warm concentrated nitric acid.

C. RESULTS AND DISCUSSION

1. Growth Rate

A principle objective of the materials program has been to grow thick self-supporting layers of GaP in order that solar cell

properties might be studied free from possible interfering effects from a GaAs substrate. To achieve this end, either high growth rates or long deposition times must be employed. While the former is to be preferred, structure and purity considerations, as will be discussed later, impose certain limitations on a practicable growth rate.

Run conditions and the resulting growth rates in the open tube HCl transfer system are summarized in Table I. A maximum growth rate of 0.60 μ/min was achieved (Run SC32) and a 200 μ layer grown by increasing the temperature gradient and total flow of HCl and H_2. A maximum thickness of 460 μ was attained by running for 72 hours (Run SC49) at a lower rate.

In the open tube system growth rate is ultimately controlled by the degree of saturation relative to the equilibrium concentration of gallium species in the vapor phase. The GaP-HCl-H_2 system should be analogous to the GaAs-HCl-H_2 system, the thermodynamics of which have been discussed by Ferguson and Gabor.[2] Our system has been operated at high temperatures where the Ga/HCl mole ratios approach unity as may be seen by comparing the HCl flow rates calculated from source loss with the flow meter determinations in column 5 of Table I. The high temperatures have been necessary to obtain good structure but in consequence the yields (and growth rates) are low. At these high temperatures the equilibrium,

$$3\ GaCl(g) + P_2\ (g) \rightleftarrows 2\ GaP(s) + GaCl_3(g) \qquad (1)$$

is shifted strongly to the left and advantage is not taken of the full range of the reaction as the equilibrium shifts to the right on lowering the temperature.

By analogy with the GaAs system[2], increasing phosphorus

pressure should shift the reaction to higher temperature and so favor transport of GaP, increasing growth rates. Such a tendency has been noted (for example, run SC9) but, except at low phosphorus pressures where the rate definitely falls off sharply, other factors mask the effect. In a series of runs (SC36 through SC42) made to determine optimum phosphorus pressures, the growth rate appeared to be independent over a range of P/Ga mole ratios from 0.6 to 3.

The effect of hydrogen on the equilibrium among the gallium chloride species and GaP is complex. The dilution effect shifts the equilibrium (1) to the left, i.e. the reaction is shifted to a lower temperature, but hydrogen reduction of the gallium chlorides lowers the concentration of gallium species at both extremes of the reaction. The behavior of our system suggests that in the range of 900° C. the predominant reaction is

$$GaCl + \frac{1}{2}H_2 + \frac{1}{2}P_2 \rightleftarrows GaP + HCl \qquad (2)$$

Increasing H_2/HCl ratio will shift this reaction to higher temperatures and so favor transport of GaP under our conditions. Increasing the H_2/HCl ratio beyond 150 produced no noticeable effect on growth rates but a decreased growth rate was observed in several runs in which it was reduced. In run SC31 at a H_2 flow of 95 cc/min (vs. normal 150 cc/min) the growth rate of GaP downstream has been sharply reduced although that on the first wafer is normal. In runs SC6 and SC7 doubling the HCl flow rate without correspondingly increasing the H_2 flow actually decreased the overall growth rate. The relative decrease in phosphorus pressure was probably also a factor. The low growth rate in run SC21 might have been contributed to by back diffusion and convection at the very low total flow.

In addition to the thermodynamic limitations, just discussed, on the rate of transfer between a source and sink at two different temperatures, there is the further consideration in our system that deposition is taking place along a temperature gradient. The amount of material available is not controlled by the saturation concentration at the source but by the equilibrium which is established in the deposition zone immediately upstream. Therefore, assuming rapid gas diffusion and attainment of equilibrium, the growth rate along a series of substrates will be proportional to the temperature gradient at a given temperature. This relationship has been roughly confirmed (see SC32 and SC33).

Although the reaction tube wall and support plate provide a large surface for depositions relative to the substrate wafers, nucleation of GaP growth on clean silica surfaces is slow, therefore deposition initially takes place preferentially on the GaAs substrates. As the deposition is prolonged, however, more and more sites are nucleated on the tube wall and support plate, providing competition for growth on the substrates and the growth slows down. This effect may definitely be noted in the data, although masked to a certain extent by the effect of phosphorus pressure. Furthermore, if a temperature differential exists between the substrate and the adjacent wall, the wall will become a preferred site, further reducing growth on the substrate. This has undoubtedly been a factor in this work.

Doping does not appreciably affect growth rate except at very high levels where growth habit of surface bump structure is radically changed (SC16) or the number of bumps is increased to the point that overlapping occurs. A high concentration of overlapping bumps will increase the average layer thickness and hence the apparent growth rate.

2. Effect of Orientation on Growth Rate

The effect of orientation on growth rate is indicated in Table I and given in more detail in Table II. Here the thickness of layers grown on pairs of adjacent Hall bars in the several runs is compared directly. The order of increasing growth rates is seen to be (111)B < (100) <(111)A although there is a wide variation in relative rates from run to run (greater than a factor of two) and between positions in the same run. The variation in relative rates shows a good correlation with position in the furnace, the ratio, < 111 > B/< 100 > increasing on moving downstream; a correlation with P/Ga ratio is doubtful. The series SC50 through SC55 (Table I) indicates that < 110 > growth is slower than < 111 >B, although direct comparison of adjacent Hall bars is not available.

The uniformity of growth across full size wafers appears to be in the reverse order of the growth rate. This is particularly noticeable for the < 111 > A wafers. In a typical case (Figure 11) inside a thick smooth outer rim, a region containing a high concentration of regular faceted holes is followed by a series of irregular steps as the thickness decreases toward the center. This non-uniform growth on the <111 > A surface may be related to rapid attainment of equilibrium with the gas stream causing depletion of that portion of the gas reaching the center of the wafer. If so, higher flow rates or a different flow pattern might improve the growth uniformity.

Thickness uniformity on the slowly grown thick (100) layers is also very poor. These generally have a very thick leading edge and thin sides. The latter is undoubtedly due to the unfavorable temperature profile across the tube as discussed above.

3. Structure

The structural features of concern in this study have been interface irregularity and surface defects. The surface defects include stacking faults and other structural defects associated with bumps on the surface of the epitaxially grown wafers.

An extreme case of interface irregularity including the presence of large voids is illustrated in Figure 3. In this particular case the substrate was heated to 800° C before introducing phosphorus vapor, from a rather impure source, into the gas stream passing over the wafers. It has been found that interface irregularity invariably is associated with conditions under which the GaAs substrate is attached prior to or during initial deposition. This may be by thermal decomposition, etching by oxide impurities, or by hydrogen chloride in the gas stream. Irregular interfaces have also been observed when the growth rates were low, as in runs SC12 and SC21 (Table I). It is interesting to note that even extremely ragged interfaces, such as that illustrated, do not affect surface smoothness of the grown layer.

Stacking faults and other structural defects associated with bumps, in extreme cases, as shown in Figure 4, lead to non-planar junction on diffusion. While the incidence and severity of these defects is greatly reduced by the high temperature phosphorus treatment described in the experimental section above (compare Figure 5 with Figures 6 and 7, for example), they are not completely eliminated.

Three interdependent factors appear to be involved in the formation of bumps: surface preparation; surface orientation; and growth conditions. Surface preparation is critical. The origin of most bumps can be traced to the epitaxial-substrate interface where they have been nucleated by dirt or damage on the surface.

Some attempts have been made to improve upon the standard cleaning technique described in the experimental section but without notable success. For one run, SC24, one of the wafers was simply lapped, etched in polish etch, rinsed in deionized distilled water and dried in a nitrogen jet. The resulting surface was streaked with haze but the bump structure did not correlate with this haze and was equivalent to that of the standard wafer. Another run, SC47, included polished wafers deliberately oxidized by heating in air to determine if this treatment followed by the high temperature treatment in phosphorus could serve as a cleaning procedure. The layer grown on the initially oxidized (100) surface was equivalent to that normally obtained. The layer grown on the (111)B surface which was oxidized to a greater extent contained a very high concentration of stacking faults. The phosphide-arsenide interfaces were very slightly ragged compared with the smooth interfaces of the normally cleaned substrates.

Surface orientation has been recognized as a major factor in the formation of bumps and is the primary, if not the only, cause of the differences observed for different substrates in the same run. The more closely the surface approaches exact < 100 > orientation the more critical do the surface preparation and run conditions become. If the surface is slightly off orientation the growth mechanism apparently permits potential or actual bump sites to be overridden and buried. Perfectly oriented surfaces become covered with incipient bumps, many of which develop into full blown bumps which may then engulf less active neighbors. A systematic study of the effect has not yet been made. Neither has an attempt yet been made to obtain wafers deliberately cut and polished off orientation. On the other hand, the availability of a set of nearly perfectly oriented wafers has increased the sensitivity of the growth experiments to the other factors causing bumps.

A deposit nearly free of bumps is shown in Figure 6. The orientation effect here is evident. A high concentration of bumps appears near the lower edge where the surface was "on orientation" due to slight curvature introduced by polishing. The few isolated bumps (of the "square pyramidal" type) appear to be tipped over with one edge partially buried in the surface. The line at the lower edge was caused by the support holding the wafer in a vertical position.

The growth conditions affecting bump formation include flow rates of H_2, HCl and phosphorus, temperature and temperature gradient at the substrate positions, or, in short, all the conditions discussed above in connection with growth rate. The effect of temperature on the perfection of crystal growth is dramatically illustrated in Figure 7. This wafer, SC32-3, was located in a steep temperature gradient at about 870°. The growth upstream at higher temperatures is smooth, that at lower temperatures downstream covered with bumps. The line of demarcation between the two regions is sharp and at right angles to the gradient.

Even though proper surface orientation, surface preparation and run conditions have been established to produce bump free surfaces, a disturbance in the gas flow such as a sudden pressure drop may initiate bump formation. This is believed to be the cause for the bumps on SC30-3 (Figure 8). The bumps on this 95 μ layer are about one half the size expected for the thickness of the layer and were probably all nucleated at a point midway in the run when a pressure buildup due to plugging of the exit tube was relieved. Similar disturbances may account for bump formation which invariably has been encountered on the thick layers made in very long runs. In these runs it was necessary to periodically melt down a deposit of gallium trichloride forming in the reaction tube outside the furnace. This may have introduced an undesirable pressure fluctuation and upset the normal growth.

A most striking effect is that of impurity dopants on the growth habits of the bumps. This is illustrated in Figures 9 (a), (b), (c) and (d) and 10 (a), (b), (c) and (d). In earlier "undoped" runs using the first HCl source (Figure 9(a) and Figure 5), the bumps tended toward a rounded rectangular base shape with the long axes in the <011 > direction (surface being (100)) frequently with a flattened top. Moderate doping with tellurium produces bumps of the same shape, but very heavy doping with tellurium draws the bumps out into long parallel ridges (Figure 9(c)). Later "undoped" runs using the second HCl source, have produced bumps having the "square pyramidal" configuration illustrated in Figure 9(b). Doping with Zn elongates the bumps in the $<0\bar{1}1>$ direction (Figure 9(d)).

Details at the peaks of some typical bumps are shown in Figure 10 (a), (b), (c) and (d). One feature all have in common is the lack of symmetry expected for a <100 > oriented structure. If we label the slopes of the bumps, A and B, (as for the sides of a pyramid formed by (111) faces on a (100) base) the Te doped bumps are elongated in the B direction <011 > the zinc doped bumps in the A direction $<0\bar{1}1>$. The peak of the bump in each case is symmetrical with the B slopes but displaced in one or the other of the A directions. Displacement in the B direction has never been observed.

The square arrays in Figures 10 (a) and (c) are believed to be stacking faults in the { 111 } planes intersecting the surface. The size of the square corresponds with the base of a pyramid formed by { 111 } planes with its apex at the GaP-GaAs interface. An example of a very high concentration of these "stacking faults" in a cleaved section is shown in Figure 4.

The other short "hash marks" on the B slopes of the bumps in Figures 10 (a), (b), (c) and (d) are small growth steps. These steps also appear in smooth bump free areas of the wafers, but are strong only

if the surface is tipped in the B direction with respect to the (100) plane. The steps probably correspond to the similar feature on epitaxial GaP grown by wet hydrogen vapor transport[3] and identified by Gershenzon and Mikulyak[4] as a growth step terminated by a pair of screw dislocations lying in a (111) plane intersecting the surface.

Although not investigated in such detail similar considerations probably apply to growth in other directions. Typical growth on (111)A, (111)B and (110) surfaces are shown in Figures 11 through 17. Figures 15, 16 and 17 demonstrate the perfection attainable for runs of relatively short duration, the (100) wafer being included for comparison.

The (111)B surfaces usually contain broader lower triangular pyramids and scattered polycrystalline nodules. The latter lead to poor p-n junction characteristics and may be a major factor in causing poor solar cell performance. The (110) surfaces have contained sharp triangular pyramids containing material in an apparent twinned orientation.

4. Purity

The purity of the material, because of its effect on lifetime, is probably the most critical factor affecting the properties of a gallium phosphide solar cell. A study, which will be described later, of open circuit voltage versus impurity level indicates that to attain the theoretical open circuit voltage the total ionized impurity concentration must be reduced to about 10^{17} cm^{-3}, about an order of magnitude lower than presently produced.

Possible sources of contamination of the gallium phosphide grown in this open tube process are: (1) the transfer gas, hydrogen chloride and hydrogen, (2) the source materials, GaP or gallium, and phosphorus, and (3) the materials of construction of the apparatus. To

the extent that these sources have been investigated they will be discussed below.

Electrical data for the "undoped" epitaxial material are listed in Table III, together with identification of the source material and notes on conditions affecting purity. Other deposition conditions may be found in Table I.

The relatively high net carrier levels generally obtained for undoped runs through SC24 may probably be attributed to contamination by the HCl source used. Different phosphorus sources had no effect as may be seen by comparing the data for runs SC5, SC11 and SC17, made under otherwise similar conditions. This HCl source also invariably produced on the source a yellow, fluffy deposit not seen after changing over to the new HCl supply system.

Introduction of a U-tube trap containing $HgCl_2$ and $Mg(ClO_4)_2$ into the HCl line to remove H_2S and water had no effect on the product purity based on the evidence of run SC17. Immersion of the trap in a dry ice slurry may, however, have effected some degree of purification in SC24. In this run the bump habit changed from "rounded rectangular" (Figure 11 (a)) to "square pyramidal" (Figure 11 (b)), characteristic of the later "undoped" material. Furthermore, the open circuit voltage of the corresponding solar cells was higher than obtained from any previous material.

The change over to the new HCl supply system effected a definite improvement in purity, on which only marginal improvement has been made, although as shown below further significant progress can be expected with higher purity HCl sources. With the growth of thicker layers, net carrier levels in the low 10^{16} cm^{-3} range with mobilities of about 100 $cm^2 volt^{-1} sec^{-1}$ have been obtained consistently for the < 100 > orientation.

Hydrogen chloride generated by hydrogen reduction of reagent grade $AsCl_3$ produced results (SC50) no better than the earliest runs. Passing the gases through a dry-ice cooled trap containing $HgCl_2$ and $Mg(ClO_4)_2$, however, reduced the net carrier levels of both <100> and <111>B orientation as compared with the previous run and resulted in the best <111> B material made in this work (possibly excepting SC55-7) in terms of structure (Figure 17), mobility and net carrier level. Also, the high temperature open circuit voltages of cells from all three wafers were the best, for the corresponding orientations, obtained to date.

Any contamination contributed directly by gallium, available commercially in purity of 99.9999% , should be negligible. Boat grown GaP, however, does contain impurities which can be expected to be transferred from the source and reincorporated in the epitaxial deposit. Evaluation of the GaP source used in runs SC12 through SC15 is not available but it would appear to have contained a p-type dopant which compensated the n-type impurities normally present. Thus two of the runs could not be evaluated while a third had a very low net carrier concentration. In SC12, the relatively high net carrier level might be attributed to the effect of the high deposition temperature on the segregation of impurities as will be discussed below.

Analytical data on several phosphorus samples, gallium phosphide and gallium recovered from the source, and epitaxially grown GaP are presented in Table IV. Comparison of the analysis of phosphorus sample AA-222 with those of the GaP products shows phosphorus to be a major source of contamination, however, the impurity levels in the GaP product are generally even higher than those of the phosphorus. Furthermore, since some purification of the phosphorus takes place on sublimation as evidenced by the concentration of impurities in the phosphorus

residue, it seems probable that the greatest source of impurity lies elsewhere. Except for a higher silicon content in the sample of Monsanto phosphorus (M-105), the different phosphorus sources analyzed are equivalent.

To take advantage of the upgrading of the phosphorus source, as has been reported previously[5], attempts were made in runs SC54 and SC55 to minimize the phosphorus evaporation temperature. By using a more readily vaporizable sample of phosphorus (K996), and lowering the pretreatment temperature to 950°, the maximum phosphorus temperature was kept to 400° C and during deposition reduced to 363°C (SC54) and 374° (SC55). The electrical properties of the SC55 samples(Table III) do indicate some modest improvement though solar cell evaluation and analytical data are not yet available. Growth in run SC54 was apparently initiated successfully, but throughout most of the long run the very low phosphorus pressure (caused apparently by a shift in the measuring thermocouples) prevented further growth and caused extensive etching of the substrate. Electrical evaluations are therefore not reliable.

A likely source of contamination by silicon (and by other impurities in the quartz) is through reaction of the gallium chloride with the hot quartz tube. Significant contamination of $GaCl_3$ by silicon, for instance, has been demonstrated on simply passing the vapor through a quartz tube heated to only moderately high temperature.[26] Therefore some other reactor material is highly desirable.

Although neither reduction in silicon contamination nor increase in aluminum contamination (Table IV) was effected by the use of an alumina liner (SC48, SC49), there may be some significance in the lower impurity levels (except copper) of SC49-2, 4. As noted later, the corresponding wafer produced a solar cell having the highest short circuit current

density observed in this work. The apparent improvement in overall impurity as indicated by the increase in mobility of the < 100 > wafers (Table III) in runs SC48 and SC49 may have been due to an effect of the great thickness since it was not obtained in SC52. An increase in some type of impurity is indicated by the increase in net carrier levels, by the dark metallic color of polycrystalline growth (probably due to precipitation in grain boundaries, since single crystal regions were clear) and by the failure of the < 111 > wafers to produce single crystal overgrowths in SC48 and SC49. Among other possible impurities, sulfur would not have been detected by the emission analysis.

Contamination of the gallium source by reaction with the boat material, either SiO_2 or Al_2O_3 at these low temperatures is insignificant. It is interesting to note that all of the source contamination comes from the vapor and virtually all remains in the GaP crust forming over the surface. The latter result is opposed to the conclusions derived from tellurium doping experiments described later.

5. The Effect of Substrate Position on Electrical Properties

A strong impurity segregation accompanying GaP deposition is evident from the trend in carrier level derived for successive Hall bars in the same run. The data for individual <100 > Hall bars, including those intentionally doped, are tabulated in Table V. With few exceptions the net carrier level decreases with position downstream for both doped and "undoped" deposits. The persistent recurrence of an accompanying drop in mobility in the "undoped" runs indicates that the trend is real and due to an increase in a compensating p-type impurity. This is in agreement with an observed darkening of the deposit on the tube wall downstream which indicates an increasing impurity level.

The decreasing carrier level for the runs heavily doped with tellurium, accompanied by a small, but again persistent, increase in mobility shows that the trend here is due to a decrease in the concentration of the n-type dopant, tellurium.

The data for runs SC48 and SC49, in which thick layers were grown using alumina tube liners, show an increasing net carrier level with decreasing mobility, therefore the predominant dopant causing the effect must be n-type. Except in the case of the heavily doped tellurium samples, the identities of the impurities involved are open to speculation. The semiquantitative emission analyses (Table IV) indicate total active impurity levels of $\sim 5 \times 10^{18}$ cm^{-3} whereas the net carrier levels are two orders of magnitude lower.

Similar effects are noted for the <111 >B oriented layers (Table VI) although, as discussed more fully in the next section, the net carrier levels here are much higher. Here, also the predominating trend is toward higher mobilities with decreasing net carrier levels.

6. Effect of Orientation on Electrical Properties

A surprisingly pronounced difference in the electrical properties of GaP grown simultaneously on different orientations is shown by the data of Table III. The order of the segregation is the same as that which has been reported for GaAs[6], but the effect is an order of magnitude or more greater. The data are given in more detail in Table VII where electrical properties of pairs of adjacent Hall bars are compared directly. The analytical data given in Table IV, while showing some trend toward higher impurity levels in <111 > B grown material relative to < 100 >, do not seem to account for the very large differences in net carrier level usually obtained.

7. Doping

Since the net carrier level of "undoped", <100 > oriented, epitaxial GaP is in the 10^{16} cm^{-3} range or lower (Table III), to control the net carrier level in the range up to 10^{19} cm^{-3} n-type, or to produce p-type material, impurity dopants must be added deliberately. Ultimately such control will be required to optimize device characteristics, although the main object of the present work was to obtain maximum purity.

Doping with tellurium and zinc has been accomplished by vaporizing the elements into the H_2-HCl stream from a boat in the first furnace, Sn has been added directly to the gallium source. In the case of tellurium, as will be shown later, almost all of the dopant dissolved in a liquid gallium source. This doped source also was subsequently used to produce heavily n-type epitaxial layers. In the case of zinc, not enough dopant remained in the source to form p-type deposits on reuse, but the zinc did apparently influence the growth habit of the bumps (Figure 10(d)).

Data on electrical properties of these doped samples are summarized in Table VIII. The conditions under which they were made may be found in Table I. For runs SC16, SC18 and SC29 under source, the rate of evaporation of dopant in atoms/unit time based on total weight loss is expressed relative to the rate of consumption of source in cc of solid GaP equivalent per unit time. Thus the expressed doping rate is equivalent to that from a GaP source doped to the same level. In run SC16, using a GaP source, the carrier level of the epitaxial layer is of the same order of magnitude as that of the "source". The results from SC18 are ambiguous because the epitaxial carrier level is only slightly higher than the normal undoped level, but in SC19 the epitaxial carrier level is a factor of twenty less than the "source" level. This is a good indication that the gallium source has dissolved most of the tellurium passing over it. Solution of all of the tellurium would have

produced a concentration equivalent to 2.3×10^{18} cm^{-3} in the original source. Subsequent use of this source did, indeed, produce increasingly doped epitaxial layers as shown by the series SC20 through SC23, and confirms the high solubility of tellurium in gallium. This tendency of the dopant to concentrate in the source will add an additional complication to accurate control of doping.

Comparable results are indicated by two zinc doping runs in one of which zinc was vaporized separately. The zinc weight loss was not obtained, but the approximate temperature is indicated. The results suggest that only a fraction of the zinc in the vapor phase is incorporated in the epitaxial deposit. Thus, in SC30 the doping was insufficient for conversion to p-type although, as noted above, the bump habit was affected.

For SC33 and SC46, the concentration of Sn initially added to the gallium source is again expressed as atoms per cm^3 of GaP equivalent. In both cases the fraction incorporated in the epitaxial deposit(<100 > orientation) was less than 5×10^{-3}.

8. H_2O Transport of GaP

Using the technique described by Frosch[3], GaP has been transported in wet hydrogen and deposited epitaxially on GaAs substrates. The source, GaP from Merck, was maintained at about 1085° C, <111 > B and < 100 > oriented substrate wafers with adjacent Hall bars at 1066° and 1051° respectively, the temperature gradients being 5.5 and 6.2 °C/cm. With a total hydrogen flow rate of 380 cc/min and an initial water vapor pressure of 1.9×10^{-3} atm., the rate of source consumption, 2.8 mg/min., is in excellent agreement with the theoretical transport rate calculated from the equilibrium constant for the reaction given by Thurmond and Frosch.[7]

The weight gain of the < 111 > B substrates is equivalent to a growth rate of 2.04×10^{-7} gm of GaP per cc of carrier gas and so of the same order as the rates reported by Frosch.[3] Heavy deposition

on the cool wall depleted the gas stream sufficiently to cause extensive etching of the edges of the <100 > wafer (Figure 19). The appearance of the < 111 > B deposits (Figure 18) with prominent development of <110 > facets and large area of flat growth is equivalent to that reported by Frosch. The appearance of the <100 > surfaces (Figure 19), however, is much superior, being free of the faceted pits.

Rather than inserting the wafers into the hot furnace according to the procedure of Frosch, the source and substrate were brought to temperature in a stream of hydrogen (380 cc/min) with phosphorus (2. 3 cc P_4/min) to prevent decomposition, the phosphorus flow being continued for 20 minutes after introducti on of the water vapor. In this way a very smooth interface was formed (Figure 20).

The electrical properties of this material have not been obtained by the usual technique; the Hall bars, in the process of heat treatment for alloying In dots,being converted to high resistivity. Simply probing the surfaces with an ohm meter revealed considerable inhomogeneity, the <111 > B surface being conducting, the < 110 > facets nonconducting, while the <100 > surface was conducting at the center, decreasing gradually to zero at the etched sides. These may, however, have been surface effects; capacitance voltage measurement on the < 111 > B deposit indicated a net carrier level of the order of 10^{17} atoms/cm^{-3}. Solar cell characteristics (SC44 Table XII) were equivalent to those of some of the better HCl transported < 100 > material.

9. Close-Space Water Transport of GaP

Using a close-space technique similar to that described by Nicoll[8] GaP has been transported in wet hydrogen and deposited in single crystal < 100 > oriented form on <100 > oriented GaAs substrates.

Both GaP powder and polycrystalline ingot were used as a source. Current efforts, lately begun, are aimed at optimizing conditions. The source powder or ingot was obtained by solution growth from excess Alcoa 99.9999% gallium and American Agricultural Chemical Co. Semiconductor Grade phosphorus. This was held in quartz discs, in a sandwich which included a quartz ring spacer between the surface of the source and the substrate face. Holes in the sides of the quartz discs permitted insertion of thermocouples for measuring temperatures directly adjacent to source and substrate. This assembly was heated in a quartz envelope in a split tube furnace, with separately controllable upper and lower coils, in an atmosphere of wet H_2 saturated with H_2O at 0° C., the H_2 flowing at 1-4 cc/min. A vertical temperature gradient of 20-25° C., between source and substrate was maintained, with the source at 900-950° C. Three-hour runs at source temperature above 900° C. resulted in GaP single crystal deposits, on <100 > oriented GaAs substrate, of 3-7.3 mils thickness, as determined by cleaving, etching in HNO_3, microscopic examination, and X-Ray diffraction. The latter in some cases was able to discern some ternary alloy formation at the interface. The powder sources yielded matte finish deposits. The polycrystalline ingot source slices, evidently because of differences in reactivity with orientation, gave "photographic" images of the source crystal planes on the deposit, with 10 mil spacing. This tendency was substantially diminished with a 20 mil spacing, as the transported species had a better chance to diffuse sideways before depositing. Techniques for smooth deposits will be sought; however, with sufficient deposit built up, mechanical or chemical polishing may be a suitable alternate.

Data are summarized in Table IX.

10. Other Processes

Some thick GaP wafers grown by another epitaxial technique (on a separate company-funded program) have also been made available for this program. The structure of these wafers, grown in the < 111 > A direction, is rather poor and the solar cell characteristics (Samples 521044-1 and 521038 in Table XXX) have also been poor. No particular advantage, at present can be seen in this particular process, but as other processes are developed the material therefrom will continue to be tested.

IV. SOLAR CELL FABRICATION

The fabrication of the epitaxially deposited GaP into solar cells served two mutually beneficial purposes: (1) development of a GaP solar cell and (2) check on the material made.

A. Diffusion

Since the epitaxial deposits were n-type, p-type dopants have been utilized as diffusants to provide the p-n junction for the solar cells. Two diffusants have been utilized namely, zinc and cadmium. Since zinc is known to have a relatively shallow acceptor level[9] and a suitable solubility and diffusion constant in GaP[10] which permits shallow penetration at low temperatures ($\sim$800° C) for short times whereas cadmium diffuses much slower and higher temperatures or considerably longer times are required to achieve the same diffusion depth, most of our investigations have been carried out using zinc as the diffusant. The work with cadmium will be reported in the Appendix (Appendix A).

Our desire to work at relatively low diffusion temperatures (< 900° C) was occasioned by several factors (1) a desire to minimize any heat treatment effects which might occur above 900° C. especially since epitaxial GaP was prepared at $\sim$ 900° C (2) thin epitaxial layers (average of 40 μ), (3) possible effect of the GaAs-GaP interface, (4) poor structure of the epitaxial GaP.

Since little is known about the properties of GaP, efforts were directed toward gaining more information on the general problems connected with p-n junction fabrication including surface concentration, diffusion time, junction depth, junction front and junction delineation techniques, both from the point of making solar cells and evaluating the material produced.

The diffusions were carried out in closed tubes approximately 20 ml in volume using various zinc sources including pure zinc (99.999%), zinc with added phosphorus and zinc-gallium. The samples which consist of epitaxially deposited single crystals of GaP on GaAs substrates rest in the closed tube on a quartz shelf. The zinc source is placed in a graphite boat which is placed under the quartz shelf. Necessary preliminary steps to minimize the contamination from the graphite boat were taken. This includes cleaning the boat in boiling HNO_3 followed by a rinse and then baking in vacuum (10^{-4} mm) for 30 minutes at 900° C to 1100° C. The quartz capsule and plate are boiled in HNO_3 for one hour and rinsed in deionized H_2O and dried with dry nitrogen. The epitaxial samples are cleaned in an ultrasonic bath for 5 minutes in absolute alcohol and 5 minutes in undiluted reagent grade H_2SO_4. This is followed by five thirty-second rinses in distilled water. The water is poured off and replaced by alcohol. The sample is removed from the alcohol bath, just prior to placing it in the diffusion capsule and wiped dry with lens tissue. It is then placed on the silica plate in the diffusion tube, the diffusant source placed in the graphite boat, and the entire apparatus evacuated to 5×10^{-7} mm Hg and sealed off. The diffusion tube is placed in a preheated furnace for a desired time, then removed to the edge of the furnace and allowed to cool to room temperature, whereupon the samples are removed and tested.

Because of the generally poor structure of the epitaxial GaP, diffusion with pure zinc[10] led to generally ragged junctions as noted in Figure 4. Figure 4 shows a cleaved section of one of the epitaxial samples after zinc diffusion that has been etched to delineate the p-n junction. The junction is very ragged with diffusion spikes at an angle which suggests they are parallel to stacking faults. Better junctions were achieved using zinc

with added phosphorus as noted in Figure 21. The effect of the addition of phosphorus on the diffusion of zinc into GaP while not understood may be similar to that noted by Rupprecht and LeMay[11] for zinc diffusion into GaAs under the influence of arsenic vapor with the additional effect of compensation resulting from the diffusion of an electrically active impurity into a region containing deep centers of the opposite type[1]. Best results have been obtained thus far with a Zn/P ratio of 5.8/1.8 with diffusions carried out at 800° C for about 3 minutes. With low lifetimes as noted in Section VF and poor GaP structure, shallow junction depths have generally been utilized.

In Table X are listed the data obtained on GaP samples which have had p-n junctions fabricated into them. The data tabulated is that for zinc diffusions only and includes the run number, slice number, p-type source material and amount used, the diffusion temperature and time, the average surface concentration after diffusion (p-type) and the resultant carrier mobility. These latter were determined from Hall effect and electrical resistivity measurements at room temperature. The last column lists the junction depth determined by junction delineation techniques to be discussed below. In a few cases we used bulk polycrystalline GaP instead of single crystal epitaxial GaP.

The diffusion temperature generally used were between 800 and 850° C although a few samples have been diffused at higher temperature. The 800 to 850° range was found to give better control for shallow junctions and to reduce the occurrence of zinc alloying.

The surface concentrations as deduced from room temperature Hall effect measurements and known junction depths are found to vary from about 10^{18} to $10^{19}/cm^3$ with most of the samples having hole concentrations of $5 \times 10^{18}/cm^3$ or less. The corresponding hole mobility is about 30 cm^2/volt sec.

A diffusion coefficient for zinc as deduced from these experiments ($\sim 10^{-10}$ cm^2/sec at 800° C) is in reasonable agreement with that predicted from Pearson's analysis[10] and by the work of Allison.[12]

That the diffusions do not give the desired degree of control can be deduced from the attempts made to vary the surface concentration by varying the amount of zinc placed in the diffusion tube. The p-surface concentration and mobility as well as the junction depth for two samples with the diffusion temperature and time maintained constant are shown in Table XI. It is noted that reducing the amount of zinc does not necessarily imply a consistent reduction in the surface concentration or a consistency in the observed junction depth.

As further support to the statement of a lack of control on diffusion it is also observed that for certain samples (see NA23 SC19-3, NA23 SC13-6, Table XI for example) having higher initial carrier concentrations, junction depths are deeper than for those of lower initial carrier concentrations - the amount of zinc kept the same as is the temperature and time.

It has also been observed that starting material which was initially p-type gives rise to a p-n junction when zinc is diffused (shallow) into it. This was particularly true of samples SC13-4 and SC21-3 (see Table X).

It is believed that all of these examples cited may be related to the fact that most of the starting materials are compensated.

B. Junction Delineation

The following procedure has been used for delineating the p-n junction formed by zinc diffusion:

The single crystal epitaxial layers which are generally grown in the <100> or <111> orientation are cleaved and delineated by etching in conc. (48%) HF for about 3 minutes at room temperature under the

influence of light (an American Optical microscope lamp can be used). Following the etching action the samples are rinsed in H_2O and alcohol and then mounted on an object slide with plasticine and leveled to bring the cleavage plane exactly at right angles to the optical axis of the microscope. The junction depth is measured directly with an optical microscope equipped with incident lighting, a stable mechanical stage and a calibrated eyepiece scale. Measurements are usually made at magnifications of 500 diameters.

Another etch that may be used is the copper stain etch consisting of 10 gms $CuSO_4$ and 0.3 ml HF in 100 ml H_2O. The etching is also carried out in the presence of light. Figures 4 and 21 are examples of the delineation technique.

C. Contacts to p and n Faces

Following the diffusion cycle, the back side of the wafer is lapped back to remove the diffused zinc. Since n-type GaAs substrates have been used as supports for the epitaxial layer, a 50%-50% AuSn alloy is evaporated onto this substrate followed by evaporated nickel. The sample is then placed in a tube in a furnace where it is evacuated and then flushed with argon. The alloying is carried out at $\sim$ 550° C in an argon atmosphere.

The contact to the diffused p-type face is made by evaporating silver through a mask onto the specimen heated to $\sim$ 200° C.

Similar procedures have been used on bulk GaP.

D. Etching

The cells have generally been etched with aqua regia with the contacts masked. The etch has generally improved the short circuit current density (at room temperature) and has been found to be controllable.

V. EVALUATION

A. Solar Cell Characteristics

Both the open circuit voltage (V_{oc}) and the short circuit current densities (J_{sc}) of the fabricated cells were routinely measured using both a tungsten source calibrated with a silicon solar cell for a 100 mw/cm^2 output and sunlight. The tungsten source temperature was 2800° K.; the emitted light however has a peak intensity (through water) at a wavelength of about 0.8 μ which is far removed from the peak response of GaP cells - 0.45 μ. Therefore, the values obtained from tungsten were expected to routinely give lower values of J_{sc} and this was the case. Measurements made in sunlight which has a peak intensity at a wavelength of about 0.45 microns were made by placing the sample outside a window directly in the sun's rays. Total intensity of the sunlight was measured with a standard silicon solar cell and generally was between 80 and 100 mw/cm^2.

For some of the better cells, V-I power curves were taken in sunlight and conversion efficiencies deduced using the sunlight input intensity as measured with a standard silicon solar cell.

The cells were generally made in shapes which were either rectangular or closely approached a rectangle. Areas used in the measurements were taken to include the entire cell with top contacts. A traveling microscope was used to determine the length and width of the cells from which the area could be deduced.

Measurements of open circuit voltage and short circuit currents were made with an Applied Physics electrometer and a Hewlett Packard Microvolt ammeter, Model No. 425A respectively.

The solar cell, for temperature measurement of the open

circuit voltage and short circuit current was mounted in a cell holder of lavite (Figure 22) with provisions for a Chromel-Alumel thermocouple under the solar cell. The cell holder was inserted into a Hoskins muffle furnace, type FD 104. The top of the cell holder has an opening so that a source suitably mounted and focused at the top of the furnace can provide the desired intensity through a glass filter to the cell. For the source a G. E. Projector Spotlight, 150 PAR/SP, has been used. The variation of intensity can be accomodated by adjusting the separation between the source and sample. An experiment was carried out at two temperatures (23° C and 225° C) to check the relationship and determine where the V_{oc} of the cell saturates with distance, L. Figure 23 is a plot of these measurements. A check was also made at the higher temperature (225° C) in order to determine whether with the expected shift of the peak response to longer wavelength at higher temperature the source setting at 23° C would still be valid at higher temperatures. Experiment showed that it was. In fact, as expected, saturation of V_{oc} with distance occurred at a greater distance (lower intensity). It will be noted that even with the largest separation (L = 20") (lowest intensity utilized) there is less than a 10% variation in V_{oc}. The setting normally used was L = 10" or within the saturation region. To avoid any undue heating the light was turned on only to take a reading and then for only a short time (a few seconds).

In order to further check ourselves, open circuit voltage measurements with temperature were made using the sun as a source. The measurements were taken starting at 12:30 p. m. with the sample directly illuminated by the sun. The sun was south to southwest and the day was bright and clear. From monitoring with a standard silicon solar cell, the intensity was found to be 90 mw/cm^2. The

results of the measurements and the comparison with the tungsten source illumination with the source-sample separation set at L = 10" and L = 20" are shown in Figure 24 for sample NA33 SC37-3. Good agreement was found between sunlight measurements and the L = 10" measurements. It was also noted that there is at most only a few percent difference in V_{oc} between the L = 10", sunlight measurement and the L = 20" measurements.

At lower temperature (< 150° C) some differences were noted in the measurements between sunlight and the L = 10" case. This may be due to surface or junction effects. Such large differences have not always been observed although some bending is generally noted around room temperature.

In Table XII are shown the V_{oc}, J_{sc} of the solar cells* evaluated at room temperature in tungsten and in sunlight together with the areas, the spectral response peaks and the conversion efficiency measured in sunlight using a standard silicon solar cell to measure the sun's intensity. From the data one notes that for the main spectral response peak at 0.45 μ, the highest open circuit voltage obtained is 1.35 volts and the highest short circuit current density in sunlight is 2.0 ma/cm^2. The highest conversion efficiency obtained at this wavelength was 1.1% for an area of about 0.5 cm^2. For samples having their main response at 0.7 μ which is at a wavelength longer than the band gap and is assumed due to extrinsic effects one notes a short circuit current density

* These cells have been fabricated using zinc as the diffusant. For cells fabricated using cadmium to make the p-n junction, the reader is referred to Appendix A and Table XVIII and for evaluation to Table XXIX. For cells evaluated from epitaxial GaP prepared by other techniques but using zinc diffusion, reference should be made to Appendix B and Table XXX.

of 5 ma/cm^2, an open circuit voltage of 0.7 volts and an indicated conversion efficiency of 1.6 to 2.5%. We will discuss some of these results further in the discussion section.

Table XIII is a tabulation of the temperature coefficient of open circuit voltage vs. temperature for typical solar cells having the 0.45 μ spectral response and the 0.7 μ response. Also found are the slopes of the short circuit current density - temperature curves for the above solar cells. Curves of V_{oc}, J_{sc} with temperature for GaP solar cells with 0.45 μ and 0.7 μ response are found in Figure 25 and 26. More curves on V_{oc}-temp. will be found in Figure 37.

From our data we note that the 0.45 μ cell has a temperature coefficient of open circuit voltage of about 3 mv/deg, the voltage decreasing with increasing temperature. This coefficient, β, as will be noted later is in good agreement with classical theory. The short circuit current density of the GaP solar cell having a 0.45 μ response increases with increasing temperature following a relationship which can be expressed as

$$J_{sc} \sim e^{\Delta E/kT}$$

Where Δ E the activation energy is of the order of 0.05 eV.

In the case of the extrinsic cell (0.7 μ) the short circuit current density is independent of temperature to 200° C, decreasing after that; the temperature coefficient of the open circuit voltage for these extrinsic cells is 3 mv/deg.

B. Optical Measurements

The spectral response measurements on the GaP solar cells were made on a Bausch and Lomb Monochromator Cat. No. 33-86-40

with a plane circular grating blazed for 0.5 μ.

The experimental procedure followed was a standard method. The source used was a tungsten lamp. The solar cell was mounted so that it was in the exit beam of the Monochromator. A constant slit of 2 mm was held during the entire scan for the solar cell and a Reeder thermocouple in the wavelength interval 0.35 to 0.9 μ. The scan was made first with the solar cell and then with the thermocouple as a detector with all other conditions held constant. A ratio was then taken between the response of the solar cell and the thermocouple and plotted as relative response. In Figure 27 are given typical relative spectral response curves having peaks at 0.45 μ and 0.7 μ. Table XIV lists for typical samples the spectral response peaks normalized relative to the thermocouple. (The magnitude of the peaks are given in terms of μa/μv where the μv represents the voltage output of the thermocouple which can be related to a thermocouple energy using the standard - .46 μw/μv). The short circuit currents are measured with a Hewlett Packard DC Microvolt ammeter, Model 425A. Two main spectral response regions are noted, namely, one around 0.45 μ and another broad region at 0.7μ. The peaks at ~ 0.53 μ and ~ 0.6 μ can be controlled and/or removed by controlling the growth conditions as noted in Section VII.

C. Sheet Resistance and Surface Concentration

While serious consideration of the p-layer sheet resistance is premature, estimates of this parameter for some of the epitaxial samples shown in Table X has been found to vary from about 10 ohms (NA11, AP88-2) to about 100 ohms (NA1, AP62-2). In general, this term has not been optimized. As expected a variation with surface concentration does change the sheet resistance but the dependence is not always in as direct a manner as expected.

That the sheet resistance is not of primary importance at this time can perhaps be most easily seen from Figure 28 where an improvement of only about 15% is seen in the efficiency for sample NA31 SC34-3 which is increased with grid structure from 0.94% to 1.13%, only a minor improvement at present. The gridded solar cell, sample NA31 SC34-3, is shown in Figure 29. Grid spacings are .4 cm, thickness of grid stripe is .016 mm. Total area of the cell is 0.57 cm^2.

D. I-V Characteristics of Solar Cells

The forward I-V characteristics of these cells have been determined from D.C. measurements and from 60 cycle I-V traces. For all solar cells having the response peak at 0.45 μ the value of n in the current-voltage relationship

$$I = I_o \exp\left(\frac{eV}{nkT} - 1\right) \qquad (3)$$

is found to be considerably greater than 2, with evidence from capacity-voltage data discussed in a subsequent paragraph, that wide space charge layers exist in many of the cells. These are believed to be similar to the characteristics reported by Gershenzon and Mikulyak[9] for their diffused junctions in gallium phosphide. These authors suggest that the characteristics result from a nearly compensated layer right at the junction.

In the case of the extrinsic cells characterized by a peak response at 0.7 μ, the value of n in Eq. (3) is found to be about 2 which suggests from the work of Sah, Noyce and Shockley[16] that recombination center mechanisms may predominate in these cells.

The saturation current density, $J_o = I_o/A$, for both types of cells are found to be around 10^{-8} amperes/cm^2 at 300° K which is orders of magnitude higher than one would predict for an ideal GaP

p-n junction. It should be noted that the junction areas range from about 0.1 to 0.5 cm^2.

In Table XV are listed values of n for some of the solar cells measured and the saturation current density. In two cases we have attempted to deduce information about the nature of the recombination centers from the forward I-V temperature characteristics assuming the forward currents to be dominated by recombination currents of the type discussed by Sah, Noyce and Shockley.[16] It was assumed that if the recombination currents result from a single level near the center of the forbidden band gap then one might expect to find from a plot of $I_o T^{-5/2}$ vs. $1/T$ that the slope of the curve would represent the activation energy of the center if it were the dominant level. Hence a slope of about 1.15 eV was looked for. It was noted that the slopes for the two cases, NA25 SC25-3 and NA21 SC21-3 were considerably less than this (0.46, 0.18 eV) indicating very likely either that the assumption of a single dominant trapping level is not sufficient description of the space charge region or it is not located near the center of the band. It is possible that multi trapping levels exist and hence make the model invalid for our case.

In the last column of Table XV is given the forward series resistance of the junction at 5 ma for some of our samples. These values are considerably larger than the bulk resistance measured and suggest that the low conversion efficiencies and poor solar characteristics can be accounted for by the poor junction characteristics.

In Figure 30 we have shown the best I-V oscilloscope traces obtained for our intrinsic 0.45 μ response cells and the extrinsic 0.7 μ response cells. Figure 31 is a typical I-V trace for the 0.45 μ response cell and Figure 32 is a trace obtained on sample NA24 SC13-6

showing a negative resistance in the forward direction.

E. Series Junction Resistance

As already noted above, at low forward currents at room temperature, the I-V characteristics follow an I-V characteristic with $n > 2$ which suggests dominance by recombination currents in the space charge region. With increasing forward current, the current appears generally to "saturate" with the inference of a high series junction resistance predominating as noted in the last column of Table XV. The resistance quoted was obtained after subtraction of the bulk and lead resistances. There is little likelihood that the level of operation of the solar cell is high enough such that operation in the "injection" region of the forward I-V characteristic is usually reached, thus in general accounting for the poor solar cell characteristics.

Figure 33 gives D. C. forward I-V characteristics at room temperature of some sample cells. The so-called "saturation" can be seen on most of the curves.

F. Diffusion Length Measurements

Using the method of Logan and Chynoweth[13], room temperature measurements of diffusion length have been made on mesas of some of the solar cells. From a plot of $1/C/A$ (capacity/area)$^{-1}$ vs. Jp (photo current density of the cell with reverse bias) the minority carrier diffusion length can be determined. Such a plot is shown in Figure 34 for sample NA16 SC13-6 (from the plot, $L_D = 150$ Å). Some values obtained by this method are shown in Table XVI. Diffusion lengths have ranged from about 150 Å to about 5000 Å. Using a carrier diffusion constant of 2.5 cm^2/sec the values of the diffusion length correspond to values of minority carrier lifetime

varying from 10^{-12} to 10^{-10} sec. The generally short lifetimes are in accord with those reported in GaP by Gershenzon and Mikulyak[9] (about 10^{-10} sec. for injected carriers at low bias and the workers at the Westinghouse Research Laboratories[14] (about 10^{-12} sec).

Calculation of the diffusion length from spectral response data using the relation of Lamond and Dale[15]

$$\frac{I_{p_1}}{I_{p_2}} = \frac{1 + \frac{1}{\alpha_2 L_p}}{1 + \alpha_1 L_p} \exp\left[-X_j (\alpha_1 - \alpha_2) \right] \qquad (4)$$

where I_{p_1} is the current at the peak response wavelength, I_{p_2} is the current for wavelength of half peak response, α_1 , α_2 are the absorption coefficients at these points, X_j is the junction depth, L_p is the diffusion length, gives for solar cell sample NA1, AP62-2 a diffusion length of about 0.8×10^{-4} cm which is in fair agreement with the above results. Assuming a carrier diffusion coefficient of 2 cm^2/volt sec, one calculates a lifetime of 3×10^{-9} sec which is somewhat higher than noted above but probably less accurate considering the approximate nature of the values substituted into Eq. (4).

G. Capacity-Voltage Measurements

Capacity-voltage measurements taken on mesas of the fabricated solar cells generally support the idea that the p-n junctions are graded and appear to follow a $1/C^3$ law as seen in Table XVI. Figure 35 shows a plot of the capacity vs. voltage for sample NA21 SC19-5. It appears to follow the $1/C^3$ law. It has been

possible to fit, generally, the capacity-voltage data to the following types of equations:

$$V_a + V_i = - \frac{qa}{12\epsilon} \left(\frac{\epsilon}{C/A} \right)^3 \tag{5}$$

$$V_a + V_i = - \frac{qa}{12\epsilon} \left(\frac{\epsilon}{C/A} - W_I \right)^3 \tag{5a}$$

$$V_a + V_i = - \frac{qa}{12\epsilon} \left(\frac{\epsilon}{C/A} - W_I \right)^2 \left(\frac{\epsilon}{C/A} + \frac{W_I}{2} \right. \tag{5b}$$

where V_a is the applied reverse voltage, V_i is the built in voltage of GaP, a constant and characteristic of the material. For n-type GaP we have taken $V_i = 2$ volts in order to fit the data.[+] (This agrees with the results of White and Logan[17] and Logan and Chynoweth).[13] In the equations q is the electronic charge, ϵ the dielectric constant, C the capacity of the junction, A the cross sectional area of the junction and a is a concentration gradient in the graded junction. W_I is introduced into the equations to fit our experimental results. It signifies that the space charge layer of the junction is extremely wide and infers that the space charge layer is intrinsic so that we may in these samples talk about a p-I-n cell. In Table VII reference is made to calculations from the data using eqs. (5-5b). One notes that some of the samples with higher short circuit current densities have smaller "I" layers and also the diffusion length is greater than the "I" layer. This is especially true for mesa sample NA16 SC13-6.

[+] Fixing the parameter V_i necessitates introduction of another term, since plots of $1/C^3$ vs. V give rise to impossibly large values of built in voltage in some cases as high as 10 volts.

The "I" layer or W_I as calculated for the samples in Table XVI is seen to vary from 150 Å to about 10 μ. The gradient, a, is observed to generally decrease with increasing width of I layer.

The mesas which have been used in these measurements generally have areas in the range of 10^{-3} cm^2.

VI. EFFECT OF VARIOUS PHYSICAL STRUCTURES ON THE GA P SOLAR CELL CHARACTERISTICS

With relatively poor structure of the GaP and use of GaAs substrates, the effect of some of these parameters on solar cell characteristics have been examined.

A. Effect of GaAs Substrate

With the thin (40 micron) epitaxial layers* and the relatively large areas desired, the GaAs substrate has been retained as a support. The possible effect of the GaP-GaAs interface on the GaP solar cell has been examined. The photovoltaic effect of this heterojunction due to absorption of light transmitted by the GaP layer would be to oppose the photovoltaic effect of the GaP p-n junction. Two experiments have been conducted to check this effect.

(1). An experiment was conducted with an epitaxial specimen consisting of n GaP (35 μ) on n+ GaAs. An In-Sn-gold Kovar disc was alloyed into the n+ GaAs substrate and a gold dot (.025 cm dia.) was evaporated on the GaP. The open circuit voltage was observed under a tungsten source to be 0.9 volts with the polarity opposite to that

* In order to further verify that most of the solar energy greater than 2.2 eV is absorbed in a layer of 40 μ, approximate calculations have been carried out and shown in Appendix C which indicate that for a GaP thickness of 15 microns about 80% of the energy > 2.2 eV is absorbed.

expected for the heterojunction (that is, the gold dot was positive and the Kovar disc negative). This potential was therefore primarily that of the photo response of the GaP-Au barrier. A portion of the surface of the GaP including the gold dot was covered with black wax and the sample remeasured. The open circuit voltage was reduced but the polarity remained the same. With black wax completely covering the surface and sides, the open circuit voltage was reduced to about 60 millivolts and the polarity was unchanged.

This experiment indicated that the effect of the GaP-GaAs interface in this sample on the solar characteristics is small.

(2) A second experiment involved making a window directly to the GaP and testing more directly the effect on the solar characteristics with and without the GaP-GaAs.

The procedure involved was to etch out a portion of the GaAs from zinc diffused GaP cells to provide a window directly to the back of the GaP n layer. The GaAs was masked with black wax except for the portion to be etched away. The etch used was $1HF:3HNO_3:2H_2O$. This etch attacks GaP only negligibly.

A sketch of the sample with contacts is shown in Figure 36. Contact 2 is the original back contact of Au-Sn-Ni, contact 3 to the GaP, is made in the same manner. Contact 3 is, as can be seen, smaller than the "window". The top contact 1 employs evaporated silver.

If a photovoltage is developed at the GaP-GaAs interface, open circuit voltages and short circuit currents measured between contacts 1 and 2, which include this interface, should differ from those measured between contacts 1 and 3, which do not. No differences have been noted on making the measurements under a variety of conditions including normal solar cell testing conditions both with our standard test apparatus and in sunlight and with a microscope light using both front and back illumination. These

results seemed to indicate that with our method for making material in the GaP-GaAs interface does not play a significant role in determining the characteristics of the GaP solar cell.

As further comment it is only necessary to compare the V_{oc} of self supporting samples such as NA39 SC47-3 with that obtained for samples which have the GaAs substrate such as NA31 SC34-3 for example to further verify the negligible effect of the interface with our material preparative method:

Sample	V_{oc} Volts (in Sunlight)	Thickness of GaP, μ	Comments
NA31 SC34-3	1.35	35	GaAs substrate
NA39 SC47-3	1.10	125	Self supporting

B. Effect of Top Metal-GaP Contact on Solar Cell

The possible effect of the photo voltage generated by the top metal (silver)-GaP contact on the open circuit voltage of the GaP solar cell was investigated. Successive masking of the contact and the surface of the solar cell with black wax has led to no change in open circuit voltage within the error of the experiment as can be seen from Table XVII. It has been concluded that the effect of the metal contact to the GaP does not effect the open circuit voltage obtained.

C. Effect of Junction Depth on Solar Cell Characteristics

In Table XVIII is given the results of an investigation on the effect of deeper junctions on the solar cell characteristics. Diffusions with samples SC13-6 to SC21-3 were carried out with both shallow ($\sim 0.5\ \mu$) and deeper penetrations (3-5 μ). The results show agreement with what one expects from general solar cell theory.

The open circuit voltage is independent of the junction depth while the short circuit current density decreases using the deeper junction. The results of this investigation would support the use of a shallow junction as opposed to a deep junction.

D. Bump Density

Since the GaP surface is quite irregular, containing large numbers of imperfections of the type shown in Figure 9b, hereafter identified as bumps, an attempt has been made to correlate these bumps with some electric characteristics such as the open circuit voltage. Since all material presently made has these imperfections on the surface, a count has been taken of them using a microscope and recorded in terms of the number of bumps per cell area. Table XIX is a tabulation of the bump density for some of the fabricated cells together with the open circuit voltage and the short circuit current density as measured with a tungsten source. No obvious correlation exists between the bump density and the open circuit voltages. This finding is not at variance with the observations of Gershenzon and Mikulyak[4] that structural defects in GaP need not perturb the electrical properties.

E. Effect of Crystal Orientation on Open Circuit Voltage

The possible effect of crystal orientation on the open circuit voltage of the GaP solar cells was investigated. As noted from Table XX no significant difference was noted which can specifically be related to the orientation.

VII. OPTIMIZATION OF GA P GROWTH CONDITIONS WITH SOLAR CELL SPECTRAL RESPONSE AND ELECTRICAL CHARACTERISTICS

Using the sun as a source and with a series of Schott color filter glasses to delineate the wavelength response of the GaP solar cells, it was found that, with the exception of a few solar cells having their main response at 0.7 μ, most of the cells contribute mainly to the short circuit current from response to wavelengths less than 0.5 μ. This is what one expects from theory. However, of additional interest is the observation that the response peaks of 0.53 μ, 0.58 μ and 0.7 μ (broad), in these cases account for less than 5% of the current and in some cases less than 1%. However, while they may not contribute in these cases to the current directly they can in a detrimental way influence (reduce) the current and/or voltage.

Since these response peaks have in some cases been influenced by altering the zinc concentration it is felt that the spectral response peaks of 0.55 μ, 0.58 μ and 0.7 μ (broad) found in the solar cells are likely associated with impurities or imperfections in the lattice. For ideal solar cell action the response only to the main band edge is desired and hence the removal of the response in the longer wavelength region by varying the crystal growing conditions and also their specific influence on the solar cell are the subject of this section.

The effect of some of the growth conditions used in making epitaxial GaP (i.e., the gallium and phosphorus source temperature and the hydrogen flow rate) on the solar cell spectral response (peaks) and the short circuit current density (J_{sc}) are shown in Table XXI. For these series of experiments the regular diffusion cycle and our standard fabrication technique have been used in making the solar cells**

** See Section IV, this report, on solar cell fabrication.

One notes from Table XXI that for our particular growing technique a (Ga) source temperature of about 900° as compared with the higher source temperature of 935° or 975° appears to give the best combination of major response peak (0.45μ) and highest short circuit current in sunlight. A hydrogen flow rate between 95 cc/min and 500 cc/min appears, on the basis of Table XII, to provide the most desirable solar cell properties. It is beneficial to see whether one cannot narrow, the optimum hydrogen flow rate by considering additional electrical parameters such as the effect of J_{sc} with temperature and the solar cell conversion efficiency* (in sunlight) at room temperature. In Table XXII are listed those samples grown at a (Ga) source temperature of approximately 890° and having only the characteristic 0.45 μ peak response. The above electrical properties are compared for the various hydrogen flow rates from 95 cc/min to 500 cc/min. Since ideally we would expect the short circuit current to change only little with temperature in the range to 300° C, our criterion should be based on looking for samples with small slopes of J_{sc} vs. 1/T. In Table XXII we have indicated the slopes from the J_{sc} vs. 1/T curve assuming that $J_{sc} \alpha e^{-\Delta E/kT}$. It will be seen that the samples having short circuit currents greater than 0.5 ma/cm^2 also exhibit the shallowest slopes and only a single slope ($\sim$ 0.05 eV), whereas those generally with short circuit current densities less than 0.5 ma/cm^2 have either two slopes or a higher slope of .08 eV. It is noted that the samples with the highest or the multiple slopes have been grown with the highest hydrogen flow rate (500 cc/min). There is one exception and that is sample NA30 SC31-3

* Measurement made from open window between 11:00 a.m. and 3:00 p.m. with sample pointed toward sun. A 10% standard silicon solar cell was also measured at the same time to determine the solar intensity - if the incident intensity was lower than 80 mw/cm^2 measurements were not taken.

which in spite of the apparent higher J_{sc} has exhibited no simple dependence of J_{sc} with temperature. The curve was found to be irregular, staying constant then rising, then remaining constant. A check of the conversion efficiency showed in spite of the high J_{sc} and V_{oc} (see following discussion and Table XXIV) a value of only 0.45% which is about half of that expected. The sample unexpectedly revealed an apparent high internal series resistance of unknown origin. Since another sample grown under similar conditions gave poor results it appears that the flow rate of hydrogen of 95 cc/min is not a reliable rate to use. From the data summarized in Table XXII, material grown with hydrogen flow rates between 150 cc/min and about 300 cc/min seem to give the highest values of efficiency. For our work a hydrogen flow rate of about 300 cc/min has been adopted as standard.

Another growth variable that was considered is the phosphorus flow rate (or the P/Ga mole ratio). Data have been obtained to optimize this variable with the other growth conditions kept constant - that is, the Ga source temperature has been maintained at about 900° C., hydrogen flow rate at 300 cc/min and HCl flow rate fixed at about 2 cc/min. A < 100 > crystal orientation is being used. The results are shown in Table XXIII with V_{oc}, J_{sc} and spectral response compared. It can be seen that with a phosphorus flow rate broadly between 0.3 and 0.6 cc/min (or expressed as a P/Ga mole ratio between 0.6 and 1.4) the best electrical properties and spectral response are obtained.

Thus far the effect of the longer wavelength spectral response (0.53, 0.58, 0.7) on the magnitude of the short circuit current has not been tacitly brought out, nor has it actually been determined explicitly how the presence of these responses are detrimental to

solar cell performance. From Table XXI it would appear that in certain cases even with the presence of these responses, short circuit current densities of 0.5 to 1 ma/cm^2 are observed in the sun. On the other hand we note that in some of the cases there appears to be a connection between the presence of response peaks at 0.53 μ, 0.58 μ and 0.7 μ and the low magnitude of the current obtained. These are associated generally with the samples which either have anomalously high mobilities, are initially p-type or have very high resistivity epitaxial layers.

To more clearly show the possible effect of these extraneous responses on the GaP solar cell we consider the relationship of the measured open circuit voltage and the value of the voltage at the knee (V_{knee}) of the forward I-V trace of these samples, i.e., where there is a change in slope and the current increases more rapidly than the voltage. All of our data was taken with a Tektronix Scope Model No. 536 with the current scale at 0.2 ma/cm and the voltage at 0.5 volts/cm. It is known that this value should closely approximate the built in voltage of about 1.5 v for GaP for an ideal case. Further, the open circuit voltage measured in sunlight should be in reasonable agreement with V_{knee} if the internal cell resistance is low.

In Table XXIV are listed the parameters V_{knee}, spectral response peaks, V_{oc} (sunlight) and J_{sc}(sunlight) for some of the above samples. Several effects are noted: (1) in those samples where only the major spectral response is found one observes good correlation between V_{oc} and V_{knee}. (2) The presence of the extraneous peaks appears to be associated with disagreement between V_{knee} and V_{oc}. This may suggest that if we associate these response peaks with impurities, it is possible the location of these impurities (i.e., whether in the p, space charge or n region) and its position with respect to the

Fermi level in these regions may determine its role. It is also possible that photoconducting effects in addition to a photovoltaic effect may occur. (3) In general the presence of these response peaks appears to lower the open circuit voltage below that observed when only the 0.45 response is present. It therefore appears that the open circuit voltage should be a sensitive indicator of sample purity and that these extraneous responses are generally undesirable.

VIII. DISCUSSION

Two main types of GaP solar cells have resulted from this work: (1) An extrinsic cell having its main spectral response at room temperature in a broad band roughly centered at about 0.75 microns, (2) an intrinsic cell having its principal response at about 0.45 microns.

The differences between the cells have been noted in V A, it being readily apparent that the high temperature characteristics of the intrinsic cell are superior and since a primary objective of the development is the feasibility of GaP solar cells for high temperatures our present attention will be focused on the intrinsic cell. Thus far, at room temperature for the intrinsic cell the highest short circuit current density obtained in sunlight, as noted in Section VA has been 2 ma/cm^2, the highest open circuit voltage has been 1.35 volts. Cell areas have ranged from 0.1 to 0.5 cm^2. The temperature coefficient of the open circuit voltage, β, was found to be about 3 mv/deg.

Ideally for GaP, from the maximum rate of carriers generated by solar radiation at the absorption edge of GaP (9.6×10^{16}/cm^2/sec) and with 100% collection efficiency a short circuit current density of 15 ma/cm^2 might be expected. From the relationship of Moss[18]

$$\frac{J_{sc}}{e\Phi} = \frac{kL\,[\,\alpha + kL - (1+\alpha)\exp(t/L - kt)\,]}{(k^2L^2-1)(\cosh t/L + \alpha \sinh t/L)} = Q \text{ (collection efficiency} \quad (6)$$

where J_{sc} is the short circuit current density, e is the electron charge, Φ is the number of photons generated per sec per cm^2, k is the absorption coefficient, L is the carrier diffusion length (hole and electron diffusion lengths are assumed equal), t is the thickness of the p-layer, and α is a surface recombination factor, one can, by assuming appropriate values for kt, kL ($k + < kL$, $kL \sim 1$) and neglecting surface recombination ($\alpha = 0$), estimate a collection efficiency at room temperature of 50%. The short circuit current density is then 7 ma/cm^2.

The calculated values for J_{sc} of about 7 ma/cm^2 is about 3 to 4 times larger than the present observed values. Grimmeiss and coworkers[23] have reported in GaP short circuit currents of up to 5 ma/cm^2 and an open circuit voltage of up to 1.2 volts in small area ($\sim 10^{-3}$ cm^2) GaP photovoltaic cells.

The difference between our observed value of 2 ma/cm^2 and that calculated from theory could be accounted for in terms of short diffusion length or that the material is not as yet under control. The presence of junctions which appear to have wide layers in them arising from the effects of compensation or near compensation when zinc (or another suitable diffusant) is diffused into the n carrier material appears to be good evidence of the material problem and the lack of control in fabricating junctions. This is not to say that junctions with wide I layers are necessarily detrimental to obtaining theoretical short circuit current densities, but it is rather good evidence that the fabricator at present cannot anticipate or control the type of junction obtained and thus the resultant short circuit current characteristics are not optimized.

While the values of J_{sc} obtained depend very sensitively on the ability to accurately control the material, as pointed out by personnel of the Lewis Research Center, the feasibility of utilizing gallium phosphide solar cells at high temperatures can be determined from measurements of open circuit voltage at high temperatures using cells exhibiting the fundamental spectral response of 0.45 μ*.

---

* See Section VII on optimization of material for the 0.45 μ response.

From solar cell theory and for an ideal junction the open circuit voltage V_{oc}, is given by the following expressions:

$$V_{oc} = \frac{kT}{q} \ln \frac{J_L n_n}{2.23 \times 10^{31} qT^3 \left(\frac{D_p}{\tau}\right)^{\frac{1}{2}} e^{\frac{-Eg-\left(\frac{dEg}{dT}\right)\Delta T}{kT}}} \quad (7)$$

where T is the absolute temperature, n_n is the carrier concentration of the base material, D_p is the hole diffusion constant, $\tau = \tau_p = \tau_n$ is the minority carrier lifetime, Eg is the energy gap, $\frac{dEg}{dT}$ is the temperature coefficient of the energy gap and J_L is the short circuit current density.

Equation 7 has been calculated for gallium phosphide assuming an energy gap of 2.25 eV at 300° K, a temperature coefficient of energy gap of -5.4×10^{-4} eV/deg[20] and with τ_p taken as 10^{-10} sec. The results of the calculation are given on the linear plot of Figure 37. At 300° K an open circuit voltage of 1.68 volts would be expected for gallium phosphide.

It should be mentioned that in spite of the fact the major absorption occurs at the higher energies ($\lambda \approx 0.45\ \mu$) and more nearly corresponds to the "direct transition" band gap (contrary to some of the other semiconductors), the lower band energy of 2.25 eV was used in the calculation since it is assumed that electrons with higher energies will lose the energy difference between 2.75 and 2.25 eV through some energy consuming phonon interaction process in changing from upper to lower conduction band.

One can express the voltage-temperature plot of Figure 37 in terms of the simple linear relation:

$$V_{oc} = V_{oc(23)} - \beta (t-23) \quad (8)$$

where V_{oc} is the open circuit voltage at any temperature t, $V_{oc(23)}$

is the open circuit voltage at 23° C., t is the temperature in degrees centigrade and β is the temperature coefficient of the voltage.

On the basis of Equations 7 and 8 and Figure 37 we would expect for a gallium phosphide solar cell a β of about 3.0 mv/deg. In the succeeding paragraphs we shall discuss our experimental results obtained with cells having the 0.45 μ response.

One notes from Table XIII that β appears to vary from around 2.5 mv/deg to a maximum of 4.4 mv/deg. The majority of the cells appear to be close to the value of 3 mv/deg. In fact taking into account the uncertainty in the slopes, aside from sample NA30 SC31-3, most samples fall well within the calculated value of β.

It is of interest to examine the V_{oc}-temperature results obtained experimentally with that expected from theory as denoted in Eq. (7). This comparison is shown in Figure 37. The experimental and theoretical curves give about the same slope (β = 3 mv/deg) as already noted and this would tend to imply that the largest effect on temperature is the change in energy gap - this being the only factor in the expression in Eq. (7) permitted to vary with temperature (in first approximation). A second factor needs to be examined in Figure 37 and that is the absolute difference in magnitude existing (at any temperature) between that expected theoretically and that obtained experimentally. There is, for example, a difference of about .3 volts between the best experimental observation and theory. The difference cannot be simply accounted for in terms of lifetime or diffusion length as permitted in Eq. (7). While it is possible to account for the difference in terms of another phenomena such as recombination currents as has been pointed out by Wysocki and Rappaport[14] it is also of advantage to examine the spread in voltage of GaP solar cells shown on the figure. One may generally note from the

semiconductor of energy gap E_G and $N_{ph} E_{av}$ is the input power where N_{pn} is the number of incident photons and E_{av} is their average energy in electron volts.

For the ideal case where every photon generates an electron-hole pair in the semiconductor of energy $\geq$ 2.2 eV, and neglecting losses of any kind one calculates from expression (9) an efficiency of about 17%. If, however, we use the results obtained earlier in the discussion for a collection efficiency of 50%, then the conversion efficiency to be expected approaches 8% at room temperature.

To account for the difference between our experimentally obtained conversion efficiency of 1% and the calculated of 8% we note from Sections V D and E that large series junction resistances appear to dominate most of the cells. This statement draws additional direct and indirect support from a variety of measurements made in Section V such as the high values of n ($I = I_o e^{eV/nkT}$), $n \approx 6$, high values of apparent built in voltage ($\lessapprox 2$) which "require" the introduction of an "I" layer in the space charge region, evidence of negative resistance regions in the forward direction of I-V traces.

One explanation of the high series resistance is that it results from compensation or near compensation arising when an electrically active impurity (say zinc) is diffused into a region containing deep centers of the opposite type. Such an explanation has been proposed by Gershenzon and Mikulyak.[9] Other methods of obtaining this condition involving special combinations of donor, acceptor and trapping states are also possible.

The extrinsic cell, having its main spectral response at 0.7 μ, has given rise to a conversion efficiency of about 2% with a room temperature short circuit current density of about 5 ma/cm^2 and an open circuit voltage as high as 0.7 volts. Its high temperature char-

acteristics as already mentioned are inferior to the intrinsic cell.

It is,of course, surprising that one obtains such a large response at 0.7 μ with so little noted at the expected intrinsic response of 0.45 μ for GaP solar cells (Table XIV for cell NA21 SC21-3). In order to further verify that the results obtained were associated with GaP, a spectral response curve was taken of the starting material (SC21-3), using a gold dot on the surface and an alloyed Au-Sn-Kovar back contact. The curved showed definite spectral response features characteristic of GaP[16] i.e. a main response peak at ~ 0.46 μ and another peak at 0.56 μ. The shift in response (to 0.7 μ) on fabrication as deduced from these results appears to be related to the diffusion process and/or heat treatment.

While it is believed that the mechanism leading to current generation in the 0.7 μ cells must likely involve a two step excitation consisting either of two optical steps or one optical and one thermal step, the nature of the centers responsible for the 0.7 μ response in the epitaxial GaP is unknown. The 0.7 μ response has been found to occur as a major response at the fabrication, however, in epitaxial material grown initially with a low hydrogen flow rate (Table XXI).

Since the background level of ionized impurities in our material is 10^{18} cm^{-3} (see following paragraphs) with net carrier levels of 10^{16}, self compensation is suggested. To achieve the close compensation noted in many of the samples which still remain n-type, it is suggested that a deep donor which could correspond to the 0.7 μ level could be present. If this is so, it could be the same as the 0.4 eV donor postulated by Gershenzon and Mikulyak[1] and thought to be due to oxygen. This model remains to be verified.

From the point of view of examining the high series junction resistance found in the intrinsic 0.45 μ cells and the present limitations

on these solar cell characteristics, we have calculated the total number of ionized impurities, N_I, found in the starting n-type GaP. The data for the calculations were obtained from Table III. Only those samples were used which had the < 100 > orientation and from which GaP solar cells having the 0.45 μ response were fabricated. The calculation of N_I has been made for a 300° K temperature assuming the effective mass and free mass are the same, that the lattice mobility at 300° K is about 500 cm^2/volt sec and that the Brooks-Herring equation for ionized impurities holds. Typical data are shown in Table XXVI for N_I the total number of ionized impurities and the number of acceptors, N_A, and donors, N_D, leading to compensation and the measured carrier concentration as deduced from Hall measurements. These results indicate a large inherent background level of ionized impurities of the order of 10^{18} (since no impurities have been added) and a rather high degree of compensation.

To more clearly point up the direction for the material effort as well as show improvement in the solar cell characteristics with increased purity the open circuit voltage at 200° C of solar cells made from these samples was noted in column V of Table XXVI. The value at 200° C was chosen so that any surface (or extrinsic low temperature) effects would be minimized. It is noted that with decreasing impurity content, V_{oc} increases. A plot of Table XXVI is shown in Figure 39, where the value of V_{oc} at 200° C is plotted against N_I. The points shown have been plotted and it is noted that a straight line can be drawn through the points. If one extrapolates this line to the theoretical value of V_{oc} at 200° C as deduced from classical theory and Eq. (7) i.e. V_{oc} = 1.15 volts, one notes that the value of N_I must be reduced to $2 \times 10^{17}/cm^3$ or an improvement in the material of about an order of magnitude is required in order to approach the theoretical open circuit voltage at 200° C. This has also been noted in Table XXVI.

IX. CONCLUSIONS

A. Material Preparation

Thick, self supporting layers of GaP can be grown in an open tube system using hydrogen chloride transport. Rates in excess of 0.5 μ/min are feasible but structure and purity considerations appear to favor a lower rate of about 0.1 μ/min requiring long deposition times.

Smooth surfaced epitaxial layers free of major defects can be obtained by using slightly off (100) orientation substrate surfaces with present cleaning techniques (including a high temperature treatment of the substrate in hydrogen containing phosphorus vapor) and at moderate doping levels. It is probable that structure and/or growth rates can be improved under conditions of higher purity.

Contamination of the gallium phosphide originates in the hydrogen chloride transfer gas, in the phosphorus source and from reaction of the gases with the hot silica wall. Modest improvement in purity has been made using hydrogen reduction of $AsCl_3$ to generate HCl and tentatively by minimizing the vaporization temperature of phosphorus. The total electrically active impurity concentration of about 5×10^{18} atoms/cm^3 must be reduced by an order of magnitude or more in order to reach theoretical open circuit voltage in the gallium phosphide solar cells. The outlook for success is good.

A pronounced segregation of donor and/or acceptor impurities or difference in compensation mechanism exists among surfaces growing in different directions; order of magnitude differences in net carrier level being found for (111)B, (110), (100), and (111)A orientation in that order. The best direction is the < 100 > although with significant improvement in purity the (111)B might be preferred.

Doping with zinc, tellurium and tin has been demonstrated, but not fully developed. Low level tin doping apparently increases the Hall mobility but not the corresponding solar cell properties.

A significant improvement in structure and in economy of source material might be achieved by using an H_2O transport system rather than HCl transport but this is offset by the difficulty of working at the higher temperature required and the problem of maintaining purity at this high temperature.

Confirmation by XRD of successful deposition of single crystal GaP in early experiments using a close-space wet hydrogen technique make this method attractive for further exploration.

B. Solar Cell Fabrication

The ability to produce relatively large area epitaxial GaP has permitted p-n diffused junction GaP solar cells of 0.45 μ response to be fabricated having areas up to about 0.5 cm^2. From these cells we have been able to obtain at room temperature (in sunlight) a V_{oc} of 1.35 volts, a J_{sc} of 2 ma/cm^2 and a conversion efficiency of 1%. With increasing temperature the open circuit voltage decreases with temperature apparently following the variation of energy gap with temperature. However, at a temperature of 350° C., the open circuit voltage is still 0.4 volts which is lower than one expects on the basis of classical theory and an ideal junction.

Evidence accumulated on junction characteristics indicate that a limitation on the solar cell characteristics is imposed by the large series junction resistance which results from compensation effects probably arising during the diffusion of zinc to form the p-n junction.

The inability to control the junction characteristics closely enough which limits solar cell performance at present is partially a reflection however of the presence of large amounts of impurities of various types and forms present in the starting material. There are indications that even with measured net carrier concentrations of $10^{16}/cm^3$, the total number of ionized impurities may be in the $10^{18}/cm^3$ range with a high degree of compensation. Spectroscopic analysis has confirmed this.

That progress has been made in reducing the total impurity content in the starting material is reflected by the fact that the open circuit voltage has been raised at 350° C. from about 0.2 volts with an impurity content in the 10^{19} range to 0.4 volts with a total impurity content of about 10^{18}. Another order of magnitude decrease in total ionized impurity is indicated if the open circuit voltage is to be raised to the theoretical value of about 0.7 volts expected at 350° C. Further material purification may also lead to improved junction characteristics.

A second type of solar cell has been noted in the GaP which has a spectral response peak at 0.7 μ and has been labelled "extrinsic". The cell has a J_{sc} of about 5 ma/cm^2, a V_{oc} of about 0.7 volts and conversion efficiency of about 2% all at room temperature. This cell has inferior temperature properties to the intrinsic 0.45 μ cell and is believed to involve impurities although the generation mechanism leading to the current and voltage is not known.

X. RECOMMENDATIONS

A. Material Preparation

1. Epitaxial growth of gallium phosphide on gallium arsenide substrates by the open tube, HCl transport process should be continued. While there seem: to be definite limitations on the growth rates and yields that can be obtained in this system, it does have the advantage of permitting direct synthesis from the elements at relatively low temperatures and so may offer the best route to high purity gallium phosphide. Furthermore, controlled doping with either donors or acceptors is readily accomplished by injecting a volatile dopant source into the gas stream.

Specific recommendations to improve purity are as follows:

(a). High purity $AsCl_3$ is available which, with proper handling, on reduction in hydrogen, should provide an HCl source orders of magnitude purer than any yet employed and effectively eliminate the carrier gas as a source of contamination. Phosphorus trichloride, in equivalent purity would serve the same purpose and without reduction would also serve as a phosphorus source.

(b). To obtain a phosphorus source of higher purity than presently available, measures to purify phosphorus should be undertaken. Other sources such as PCl_3 or PH_3 should be investigated.

(c). Recently new high purity refractory materials including pyrolytic carbon and pyrolytic boron nitride have become available commercially. These should be tried as tube liners or substitutes for silica in the parts of the apparatus exposed to the reactive gases at high temperatures.

(c). Improvement in purity of polycrystalline GaP, either melt grown or solution grown, will make it more attractive as a source material for high purity epitaxial GaP. As such material becomes available, it should be tested.

Steps to improve the growth rates and yields as well as uniformity in electrical properties over large area epitaxial deposits should be taken. Redesign of the apparatus should make this possible.

2. The H_2O transport process in the open tube system should be investigated further. Although higher temperatures are required, higher growth rates and yields and improved structure have been indicated. Except for oxygen doping, toleration for which must be established, improved purity may also be possible through oxygen suppression of reaction with silica.

3. Investigation of close-space methods for growing epitaxial GaP should be continued. This method shows promise of producing the thick uniform layers required. The purity, however, will depend upon the availability of high purity polycrystalline GaP.

4. The investigations recommended above should continue studies of the effect of orientation on the growth and properties of epitaxial GaP.

5. Techniques to control doping should be refined and developed for both n- and p-type dopants, and the effect of doping on solar cell parameters investigated.

B. Material Evaluation

1. In addition to analytical investigations by emission spectroscopy and mass spectometry, and electrical characterization by Hall coefficient and resistivity measurements, structural studies should be made. These should include etch and decoration techniques to measure dislocation densities and strain birefringence measurements as well as the usual visual and microscopic examination for gross structural defects.

C. Solar Cell Fabrication

1. With evidence that the intrinsic GaP solar cells have potentially useful and interesting properties at temperatures in the range of 350° C. further attention must be paid to improving the junction characteristics and reducing the series junction resistance. The diffusion step leading to the p-n junction fabrication should be studied in greater detail with the initial objective of trying to obtain more abrupt junctions. A case in point is the zinc-phosphorus system in which the phosphorus may be influential in controlling the zinc surface concentration and junction depth. Other diffusants or diffusant systems providing both shallow and/or deeper levels may be studied.

2. A study of the optical and electrical properties such as Hall effect and resistivity with temperature would facilitate efforts to purify the material and provide knowledge of some of the levels present in the material.

3. A reanalysis of the theory of wide p-n junctions particularly as it pertains to the GaP solar cell would be useful.

4. Further work on improving contacts at temperatures above 300° C. both from an electrical and mechanical standpoint should be carried out.

XI. SAMPLES SENT TO NASA

Samples fabricated into solar cells and sent to Lewis Research Center NASA together with their characteristics are given in Table XXVII.

XII. REFERENCES

1. F. V. Williams and R. A. Ruehrwein, J. Electrochem. Soc., 108, 177C (1961).
2. R. R. Fergusson and T. Gabor, ibid 111, 585 (1964).
3. C. J. Frosch, ibid 111, 180 (1964).
4. M. Gershenzon and R. M. Mikulyak, J. Applied Phys., 35, 2132 (1964).
5. Second Quarterly Technical Report, "Gallium Phosphide Devices" July 14, 1963. Contract No. DA-36-039-AMC-00103. The Eagle-Picher Company.
6. F. V. Williams, J. Electrochem. Soc. 111, 886 (1964).
7. C. D. Thurmond and C. J. Frosch, ibid, 111, 184 (1964).
8. F. H. Nicoll, ibid, 110, 1165 (1963).
9. M. Gershenzon and R. M. Mikulyak, J. Appl. Phys. 32, 1338 (1961); Solid State Electronics 5, 313 (1962).
10. L. Chang and G. L. Pearson, Stanford Quarterly Research Review, No. 1, SE 1-62-109, p. 78-81 Stanford Electronics Laboratories; also J. Appl. Phys. 35, 1960 (1964).
11. H. Rupprecht and C. Z. LeMay, J. Appl. Phys. 35, 1970 (1964).
12. H. W. Allison, J. Appl. Phys. 34, 231 (1963).
13. R. A. Logan and A. G. Chynoweth, J. Appl. Phys. 33, 1649 (1962).
14. Final Report, Report No. 4, DA 36-039 SC-88889, Westinghouse Electric Corp., Central Research Laboratories
15. P. Lamond and B. Dale, Colloque International sur les dispostifs a' semiconducteurs, Paris, Vol. ,p635 (1961).
16. C. T. Sah, R. N. Noyce and W. Shockley, Proc. IRE, 45, 1228 (1958).
17. H. G. White and R. A. Logan, J. Appl. Phys. 34, 1990 (1963).
18. T. S. Moss, Solid State Electronics 2, 222 (1961).
19. H. C. Grimmeiss, A. Rabenau and H. Koelmans, J. Appl. Phys. 32, 2123 (1961).

20. T. S. Moss, "Optical Properties of Semiconductors" Butterworth's (1961) p. 224.

21. J. J. Wysocki and P. Rappaport, J. Appl. Phys. 31, 571 (1960).

22. A. R. Gobat, M. F. Lamorte, G. W. McIver, IRE Trans. Mil Electronics, p. 20, January, 1962.

23. H. C. Grimmeiss, A. Rabanau and H. Koelmans, J. Appl. Phys. 32, 2123 (1961)

24. J. J. Loferski, J. Appl. Phys. 27, 777 (1956).

25. W. Spitzer, M. Gershenzon, C. J. Frosch and D. F. Gibbs, J. Phys. and Chem. Solids 11, 339 (1950).

26. R. I. Stearns, Monsanto Company, Private Communication.

XIII. APPENDICES

Appendix A: Fabrication and Evaluation of Solar Cells formed using Cadmium as Diffusant

Use of cadmium as a diffusant to form p-n junctions in GaP has not been brought along as far as zinc and the preliminary results are recorded here. It will be noted from Tables XVIII (Fabrication) and XXIX (Evaluation) that the overall results are thus far inferior to those obtained using zinc. Cadmium, as expected, does not diffuse as rapidly as zinc.

Appendix B: Evaluation of Solar Cells made from GaP epitaxially prepared by other Methods.

In addition to GaP prepared epitaxially as described in the material preparation section, other methods of making GaP by epitaxial means have been tried. The evaluation of cells prepared from GaP prepared by the H_2O transport method and by another method at Monsanto are given in Table XXX. In these cases zinc was diffused in at 800° C. for 3 minutes to form a p-n junction. The fabrication procedure was similar to that described earlier in Section IV.

From Table XXX we note that the H_2O transport method appears to give values of V_{oc} and J_{sc} which compare with values obtained by the open tube method.

The values of V_{oc}, J_{sc} obtained with material made by the Monsanto method are lower than those obtained with GaP prepared by the H_2O transport method.

Further evaluations are required to make better judgments.

Appendix C: Thickness of Absorbed GaP Layer

Estimates have been made of the amount of solar energy

greater than 2.2 eV which is absorbed in GaP as a function of the thickness of GaP. In these calculations the absorption coefficient was approximated from the measurements of Spitzer, et al[25] and assumed to vary as the square of the photon energy, i.e., $\alpha(E) = A(E-E_o)^2$. Here $\alpha(E)$ is the absorption coefficient at a particular photon energy, A is a constant to be fitted ($A = 6.25 \times 10^3$ cm^{-1}/eV), $E_o = 2.2$ eV. The number of photons available as a function of energy (> 2.2 eV) was approximated from the available data on the solar spectrum in the energy range of interest for GaP (> 2.2 eV) by a parabola having the following form:

$$n(E) = n_o - \gamma (E-E_1)^2$$

where n(E) are the number of available photons as a function of energy, n_o, γ, E, are constants. The equation with the appropriate constants was found to be

$$n(E) = 3.5 \times 10^{17} - 2.43 \times 10^{16} (E-1)^2$$

The results of the calculations are plotted in Figure 40.

These approximate calculations indicate that for a GaP thickness of 15 microns about 80% of the energy > 2.2 should be absorbed.

LIST OF TABLES

LIST OF TABLES

TABLE I

Epitaxial Deposition of GaP on GaAs Substrate[1]

Run and Sample No.	Source Temp (°C)	Substrate[2] Temp (°C)	Substrate[2] Grad (°C/cm)	Flow Rates[3] (cc/min) HCl	Flow Rates[3] (cc/min) H_2	[4] P/Ga Mole Ratio	Time (Min)	[5] Thickness μ	[6] Growth Rates (μ/min)	[6] Growth Rates (μ/ccHCl)	Orient.
AP89D-4[7]	890	797	3.2	0.85	150	(6.6-4.5, $\overline{5.8}$)	60	5	.08	.10	<100>
SC4-2	875	808	2.6	0.92	150	(6.5-3.8, $\overline{5.3}$)	75	8[8]	.11	.12	<100>
SC5-3	895	810	3.5	0.95	150	(9.3-5.4, $\overline{7.3}$)	60	13[8]	.22	.23	<100>
SC6-3	888	805	4.2	(0.95)	150	(7.1-6.5, $\overline{6.8}$)	15				
				1.90	150	(3.2-1.3, $\overline{2.2}$)	157	10	.06	.032	<100>
SC7-3	886	814	6.2	(0.92)	150	(8.6-7.9, $\overline{8.3}$)	15				
				1.85	150	(3.9-1.6, $\overline{2.5}$)	239	19	.08	.042	<100>
SC8-3	888	823	10.3	(0.87)	150	(7.9-7.2, $\overline{7.5}$)	15				
				1.73	300	(3.6-2.1, $\overline{2.7}$)	118.5	40	.32	.18	<100>
SC9-3	889	825	10.3	0.66	150	(16.2-11.2, $\overline{13.6}$)	60	14	.23	.35	<100>
SC10-3	889	825	10.3	(0.86)	150	(11.5-7.9, $\overline{9.46}$)	60				
				1.72	300	(3.9-2.5, $\overline{3.1}$)	101	49	.37	.22	<100>
SC11-3	886	818	9.5	0.86	150	(10.3-4.5, $\overline{6.7}$)	240	43	.18	.21	<100>
SC12-4	936[9]	868	6.3	1.09	150	1.0[10]	720	24	.033	.031	<100>
-6		855	4.0					24	.033	.031	<100>
SC13-4	934[9]	827	6.6	1.04	150	1.0[10]	258	40	.16	.15	<100>
-6		809	5.4					40	.16	.15	<100>
SC14-2	886[9]	820	9.7	0.85	150	(16.9-7.3, $\overline{11.1}$)	240	30	.12	.15	<100>
SC15-3	887[9]	813	7.6	0.88	150	(8.9-4.6, $\overline{6.1}$)	240	40	.17	.19	<100>
SC16-3	887[9]	811	5.3	1.08	150	(5.1-2.6, $\overline{3.5}$)	240	50	.21	.19	<100>
SC17-3	887	808	5.7	1.18	150	(3.5-1.5, $\overline{2.2}$)	240	25	.10	.09	<100>
SC18-3	886	814	7.6	1.04	150	(5.1-1.9-$\overline{3.0}$)	240	26	.11	.10	<100>
-5		804	4.7					20	.08	.08	<100>
SC19-3	886	809	6.8	0.88	150	(9.9-3.7, $\overline{5.8}$)	243	34	.14	.16	<100>
-5		800	4.3					25	.10	.12	<100>

TABLE I (Continued)

Run and Sample No.	Source Temp (°C)	Substrate[2] Temp (°C)	Grad (°C/cm)	Flow Rates[3] (cc/min) HCl	H_2	P/Ga Mole Ratio[4]	Time (Min)	Thickness[5] μ	Growth Rates[6] (μ/min)	(μ/ccHCl)	Orient
SC20-3	886	818	9.7	1.07	300	(9.5-2.8, $\overline{5.0}$)	281	43	.15	.14	<100>
SC21-3	887	816	9.6	0.92	15	(12.7-4.9, $\overline{7.5}$)	243	10[8]	.04	.04	<100>
SC22-3	891	822	9.7	1.53	500	(6.5-4.7, $\overline{5.5}$)	50	15	.30	.20	<100>
SC23-3	887	817	8.9	1.39	500	(4.2-2.2, $\overline{3.0}$)	133	21	.16	.11	<100>
SC24-3	885	816	9.5	2.43	500	(1.4-0.66, $\overline{0.9}$)	245	70	.29	.12	<100>
-5		804	4.6					57	.23	.10	<100>
SC25-3	887	812	9.0	1.14(1.47)	150	(0.9-0.48, $\overline{0.66}$)	720	40	.06	.05	<100>
SC26-3	975	827	9.9	1.48(1.46)	150	(0.49-0.32, $\overline{0.40}$)	661	45	.07	.05	<100>
SC27-3	886	815[11]	11.2	0.85(1.14)	170	(5.1-2.1, $\overline{3.5}$)	240	25	.10	.12	<100>
SC28-3	886	811[11]	9.8	0.93(1.16)	170	(4.7-3.2, $\overline{3.7}$)	280	35	.12	.13	<100>
SC29-3	975	791	9.3	0.94(1.14)	150	(5.6-1.8, $\overline{3.4}$)	270	55	.20	.22	<100>
SC30-3	973	819	10.0	0.9	170	$\overline{3.9}$	10				
				2.1(2.35)	800	(1.9-0.79, $\overline{1.2}$	248	95	.38	.18	<100>
SC31-3	891	818	9.9	0.80(1.1)	95	(5.4-1.9, $\overline{3.1}$)	300	30	.10	.13	<100>
-5		806	5.0					12	.04	.05	<100>
SC32-3	976	874	22.7	3.32(3.2)	475	(1.5-0.44, $\overline{0.76}$)	332	130	.39	.12	<100>
-5		816	12.8					200	.60	.18	<100>
SC33-3	976	838	17.8	1.84(2.21)	300	(3.0-1.1, $\overline{1.7}$)	240	105	.44	.24	<100>
-5		791	11.6					97	.40	.22	<100>
SC34-3	896	826[12]	8.7	1.87(2.3)	310	(2.3-0.83, $\overline{1.3}$)	303	35	.12	.062	<100>
-5		817[12]	3.8					30	.10	.053	<100>
SC35-3	887	813	9.9	1.86(2.3)	310	(2.9-1.4, $\overline{2.0}$)	242	45	.19	.10	<100>
-5		800	5.0					30	.12	.067	<100>
SC36-3	906	830	7.0	1.64(2.15)	300	3.12	282	55	.20	.12	<100>
-5		820	2.8					45	.16	.10	<100>

TABLE I (Continued)

Run and Sample No.	Source Temp (°C)	Substrate[2] Temp (°C)	Substrate[2] Grad (°C/cm)	Flow Rates[3] (cc/min) HCl	Flow Rates[3] (cc/min) H_2	P/Ga Mole Ratio[4]	Time (Min)	Thickness[5] μ	Growth Rates[6] (μ/min)	Growth Rates[6] (μ/ccHCl)	Orient.
SC37-3	902	822	7.0	1.80(2.15)	300	0.79	1229	250	.20	.11	<100>
-6		812	2.3					95	.077	.043	<111>B
-10		803	4.0					290	.24	.13	<111>A
SC38-4	898	812	3.4	1.85(2.15)	300	0.49	1749	~170[13]	.10	.05	<111>A
-7		808	3.3					~12[13]	.007	.004	<100>
-10		787	5.6					~100[13]	.06	.03	<111>A
SC39-3	908	830	8.6	1.82(2.15)	300	1.43	697	135	.19	.11	<100>
-6		816	3.3					180	.26	.14	<111>A
SC40-3	898	827	7.0	1.94(2.2)	300	0.62	1616	115	.071	.037	<100>
-6		815	3.3					180	.11	.058	<111>A
SC41-3	901	831	7.3	1.88(2.1)	300	0.52	1655	100	.060	.03	<100>
-6		819[14]	3.4					25	.015	.008	<111>B
-8		812[14]	4.6					150	.090	.05	<111>A
-10		805[14]	5.3					140	.085	.045	<100>
SC42-3	904	817	3.4	1.88(2.1)	300	0.98	1070	165	.15	.08	<100>
-6		808	4.9					200	.19	.10	<111>A
-10		793	5.9					160	.15	.08	<111>B
SC45-3	908	826	7.6	1.86(2.15)	300	1.56	1074	160	.15	.08	<100>
-6		809	3.8					70	.065	.035	<111>B
SC46-3	926	837	8.3	2.00(2.15)	300	1.35	1316	325	.25	.12	<100>
-5		820	4.4					240	.18	.09	<110>
-7		809	5.9					105	.08	.04	<111>B
SC47-3	922	833	7.5	1.00(1.05)	150	0.48	1954	150	.07	.07	<100>
-5		819	4.2					100	.05	.05	<110>
-7		809	5.5					140	.07	.07	<111>B
SC48-2[15]	918	831	8.0	0.80(1.05)	150	0.89	3531	425	.12	.15	<100>
-4		819	4.0					500	.14	.18	<110>
-6		808	5.4					poly	-	-	<111>B

TABLE I (Continued)

Run and Sample No.	Source Temp (°C)	Substrate[2] Temp (°C)	Substrate[2] Grad (°C/cm)	Flow Rates[3] (cc/min) HCl	Flow Rates[3] (cc/min) H_2	P/Ga Mole Ratio[4]	Time (Min)	Thickness[5] μ	Growth Rates[6] (μ/min)	Growth Rates[6] (μ/ccHCl)	Orient
SC49-3[15]	915	833	8.4	- (1.05)	150	(0.89)	4301	460	.11	(.13)	<100>
-6		814	4.3					poly	-	-	<111>B
SC50-3	913	834	7.8	0.99(1.0)[16]	150	0.51	360	40	.11	.11	<100>
-5		822	3.9					-	-		<110>
-7		811	5.4					30	.08	.08	<111>B
SC51-3	920	831	7.9	0.97(1.0)[16]	150	0.62	373	45	.12	.12	<100>
-5		820	3.8					22	.06	.06	<110>
-7		809	5.5					40	.11	.11	<111>B
SC52-3[15]	920	835	8.9	0.52(1.0?)[16]	150	1.7	366	60	.16	.32	<100>
-5		823	3.6					27	.07	.14	<110>
-7		814	5.2					50	.14	.26	<111>B
SC53-3	916	832	7.8	0.91(1.05)	150	1.12	3237	150	.05	.05	<100>
-5		819	3.8					100	.03	.03	<110>
-7		809	5.3					125	.04	.04	<111>B
SC54-3[18]	917	825	3.6	1.00(1.05)	150	0.26	5471	0 - 48[17]	0-.01	0-.01	<100>
-5		817	4.7					21[17]	.004	.004	<110>
-7		808	5.8					57[17]	.010	.010	<111>B
SC55-3[18]	904	817	3.2	0.89(1.05)	150	0.88	2620	210	.08	.09	<100>
-5		810	4.3					160	.06	.07	<110>
-7		803	5.4					190	.07	.08	<111>B

TABLE I (Continued)

(1) Ga + P source used in all runs except SC-12 through SC-16.

(2) Substrate temperature and gradient based on thermocouples outside the tube in the deposition zone and a previous furnace calibration using a thermocouple inside the tube. Two different furnace systems were used; the first for runs through SC-35, the second for SC-36 through SC-55.

(3) HCl flow rates are based on Ga use rate assuming complete reaction of $HCl + Ga \rightleftharpoons GaCl + 1/2\ H_2$. For runs through SC-24 HCl was supplied directly from a cylinder of anhydrous HCl. For runs SC-25 on (except as noted) a cleaner, calibrated metering system was used with a 5% mixture of HCl in H_2. Flow rates based on the flowmeter calibration are given in parenthesis. H_2 rates (STP) are based on flowmeter readings.

(4) P./Ga mole ratios are based on weight loss of phosphorus and Ga sources. Because of a temperature gradient along the phosphorus evaporation zone in the first system, runs AP89-D through SC-35, the rate of phosphorus loss was not constant. A rough calculation based on the measured gradient and previous determination of phosphorus loss vs. temp. has been used to derive a maximum and minimum ratio as well as the average ratio during deposition. For runs SC-36 through SC-55 using the second system, having a uniform phosphorus evaporation zone, a single value is given.

(5) Layer thickness in most cases is an estimation based on cleaved sections of adjacent Hall bars and weight gain.

(6) For runs SC6, SC7, SC8, SC10 and SC30, in which HCl flow rate was doubled during course of the run, growth rates refer to the higher flow rate. For calculation, growth rate during initial low flow rate period assumed to be one half of that during the remaining time.

(7) Hall bar.

(8) Very ragged interfaces.

(9) GaP source.

(10) Phosphorus from source, no excess used during deposition.

(11) Substrates supported vertically parallel to flow.

(12) Substrates supported on long massive graphite bar.

(13) Substrates extensively etched, extremely ragged interfaces and poor adhesion.

(14) Wafer supported vertically, perpendicular to flow.

(15) 15 mm I. D. alumina tube liner, alumina boats and support plates.

(16) HCl generated by reduction of $AsCl_3$ in hot tube. As_4 product removed from stream by condensation.

(17) Substrates extensively etched and alloyed. extremely ragged interfaces.

TABLE I (Continued)

(18) Pretreatment in phosphorus/H_2 at 950°, phosphorus source at 400°.

TABLE II

Relative Growth Rates of GaP on Adjacent Substrates of Different Orientations

Hall Bar No.			Thickness (μ)			Ratio	
<100 >	<111 > B	<111 > A	<100 >	<111 > B	<111 > A	<111 > B/<100 >	<111 > A/<100 >
SC37-4	-5		181	105		0.58	
-8	-7	-9	106	90	358	0.85	3.38
SC39-4		-5	136		259		1.90
SC40-4		-5	73		184		2.52
SC41-4	-5		78.5	33.0		0.42	
SC42-4		-5	218		349		1.60
-8	-9	-7	156	128	349	0.82	2.24
-12	-11		215	194		0.90	
SC45-4	-5		147	37.5		0.26	

TABLE III

Properties of Undoped GaP Epitaxial Layers (n-type)

Sample No.	Source	Notes	Thickness μ	ρ	μ	n	Orient.
SC4-3	Ga + P (L)	1st HCl supply used for runs thru SC24	9	.14	75	6.8×10^{17}	<100>
SC5-3	Ga + P (F)		13	1.0	81	1.4×10^{17}	<100>
SC6-3	Ga + P (L)	Deposition repeated on same wafer. Evaluation made on fresh Hall bars each run.	10	2.65	68	3.5×10^{16}	<100>
SC7-3	"		19	1.37	53	1.7×10^{17}	<100>
SC8-3	"		40	.299	81	2.9×10^{17}	<100>
SC9-3	"		14	.386	72	2.8×10^{17}	<100>
SC10-3	"		49	.110	82	7.2×10^{17}	<100>
SC11-3	"		43	.651	93	1.3×10^{17}	<100>
SC6/11			175 Total	.250 Av	80 Av	3.4×10^{17} Av	
SC12-4	GaP(Merck #162)	$HgCl_2$ + $Mg(ClO_4)_2$ trap	27	1.13	53	2.0×10^{17}	<100>
-6			30	7.2	48	4.2×10^{16}	<100>
SC13-4	"	"	40	non-ohmic contacts			<100>
-6			40	"			<100>
SC14-2	Ga + P (L)	"	30	110	63	9.7×10^{14}	<100>
SC15-3	GaP + P(L) + Te (290°)	"	40	non-ohmic contacts			<100>
SC17-3	Ga + P (AA# 145)	"	25	1.2	68	1.4×10^{17}	<100>
SC24-3	"	$HgCl_2$ + $Mg(ClO_4)_2$ trap in dry ice	70	.10	88	7.3×10^{17}	<100>
-5	"		57	.14	89	5.1×10^{17}	<100>

TABLE III (Continued)

Sample No.	Source	Notes	Thickness μ	ρ	μ	n	Orient
SC25-3	Ga + P(AA # 145)	2nd HCl supply used for SC25 thru SC55 except as otherwise noted	40	13.4	68	2.5×10^{16}	<100>
SC26-3	" "		45	2.4	74	3.6×10^{16}	<100>
SC27-3	" "		25	2.7	74	4.8×10^{16}	<100>
SC28-3	" "		35	3.2	88	2.7×10^{16}	<100>
SC31-3	" "		30	Unreliable due to extreme insensitivity			<100>
-5	" "		12	"			<100>
SC32-3	Ga + P(AA#146)		130	0.54	94	1.9×10^{17}	<100>
-5			200	1.04	97	6.4×10^{16}	<100>
SC34-3	" "	Substrate supported on graphite bar	35	5.9	76	1.4×10^{16}	<100>
-5			30	8.8	79	1.0×10^{16}	<100>
SC35-3	" "		45	2.3	97	5.8×10^{16}	<100>
-5			30	13.0	69	1.9×10^{16}	<100>
SC36-3	" "		55	2.3	97	2.8×10^{16}	<100>
-5	"		45	3.1	81	2.6×10^{16}	<100>
SC37-3	" "		250	4.7	100	1.4×10^{16}	<100>
-6	"		95	0.055	120	1.1×10^{18}	<111> B
-10	"		290	hi	-	-	<111> A
SC38-4	" "		~170	102	53	1.2×10^{15}	<111> A
-7	"		~ 12	substrates extensively etched			<100>
-10	"		~100	114	29	1.9×10^{15}	<111> A
SC39-3	" "		135	3.9	96	2.1×10^{16}	<100>
-6	"		180	2.8×10^{3}	10	2.5×10^{14}	<111> A
SC40-3	" "		115	10.2	98	1.5×10^{16}	<100>
-6	"		180	hi	-	-	<111> A
SC41-3	" "		100	7.3	105	2.2×10^{16}	<100>
-6	" "		25	0.056	64	2.1×10^{18}	<111> B
-8	" "		150	Not evaluated			<111> A
-10	" "		140	>811	< 46	$< 1.68 \times 10^{14}$	<100>

TABLE III (Continued)

Sample No.	Source	Notes	Thickness μ	ρ	μ	n	Orient
SC42-3	Ga + P (AA # 146)		165	8.6	100	8.3×10^{15}	<100>
-6			200	6×10^{3}	< 10	$< 5 \times 10^{14}$	<111> A
-10			160	0.12	94	6.9×10^{17}	<111> B
SC45-3	Ga + P(M#105)		160	4.9	78	2.6×10^{16}	<100>
-6			70	0.075	59	1.9×10^{18}	<111> B
SC47-3	Ga + P(AA#222)		150	1.1	110	5.6×10^{16}	<100>
-5			100	0.358	66	2.7×10^{17}	<110>
-7			140	0.062	81	1.4×10^{18}	<111> B
SC48-2	" "	Alumina tube liner, boats	425	0.54	180	6.4×10^{16}	<100>
-4		and plates	500	0.39	46	3.5×10^{17}	<110>
-6			poly	-	-	-	<111> B
SC49-3	" "		460	0.33	180	1.1×10^{17}	<100>
-6			poly	-	-	-	<111> B
SC50-3	" "	HCl from $AsCl_3$	40	0.47	80	1.8×10^{17}	<100>
-5			-	-	-	-	<110>
-7			30	0.078	80	1.0×10^{18}	<111> B
SC51-3	" "	HCl from $AsCl_3$	45	9.3	62	2.7×10^{16}	<100>
-5		$HgCl_2$ and $Mg(ClO_4)$	22	-	-	-	<110>
-7		trap in dry ice	40	0.22	125	2.5×10^{17}	<111> B
SC52-3	" "	Same as above and alumina	60	0.54	84	1.4×10^{17}	<100>
-5		tube liner, boats and plates	27	-	-	-	<110>
-7			50	0.08	40	3×10^{18}	<111> B
SC53-3	Ga + P (K#996)		150	2.4	110	3.8×10^{16}	<100>
-5			100	0.55	81	1.4×10^{17}	<110>
-7			125	0.055	80	1.6×10^{18}	<111> B
SC54-3	" "	Minimum P evaporation	0-48	(1.0)	(86)	(7.6×10^{16})	<100>
-5		temp.	21	-	-	-	<110>
-7			57	(0.08)	(78)	(9.4×10^{17})	<111> B
SC55-3	" "	"	210	12.3	96	6.0×10^{15}	<100>
-5			160	-	-	-	<110>
-7			190	0.080	190	7.6×10^{17}	<111> B

TABLE IV

Semiquantitative Emission Analysis of Phosphorus, Source and Epitaxial GaP

Sample	Impurity Concentration (ppm)									
	Si	Fe	Mg	Ni	Al	Cu	Sn	Cr	V	Pb
P(AA-222)	50	10	1	5	5	5	N. D.	N. D.	5	10
P(AA-221)	50	10	1	5	5	5	N. D.	N. D.	1	10
P(M-105)	100	10	1	5	5	5	N. D.	N. D.	5	10
P(K-996) residue from SC55	50-100	10-50	10	10	5	5-10	N. D.	N. D.	10	10
P(AA-222) residue	50-100	10-50	10	10	5	10	10	10	10	10
SC47-3 <100>	50	10	1	-	10	5	-	-	10	-
-7 <111> B	50	10-50	1	-	10	5-10	-	-	50	-
-Source GaP	100	10	1	-	10	5-10	-	-	10	-
-Source Ga	N. D.		N. D.			.07-.10	N. D.			N. D.
SC48-2 <100>	50	10	1	-	10	5-10	-	-	10	-
-4 <110>	100	10	-	-	10	5	-	-	50	-
-6 <111> B	50	10	1	-	10	5	-	-	10	-
-Source GaP	50	10	5	-	10	10	-	-	10	-
-Source Ga	N. D.	N. D.	N. D.	-	-	1-5	N. D.	-	-	N. D.
SC49-2, 4 <100>	10	5	1	-	5	50	-	-	10	-
-6 <111> B	50	10	10	-	10	10	-	-	10-50	-
-Source GaP	50	50	1	-	10	5	-	-	50	-
-Source Ga	N. D.	N. D.	N. D.	-	-	.02	-	-	-	N. D.
SC50-Source GaP	50	10	5	-	10	50	-	-	50	-
-Source Ga	N. D.	N. D.	N. D.	-	-	.01	-	-	-	N. D.

Notes:
1. Phosphorus AA-222 used in all runs.
2. SC48 and SC49 run using alumina tube liner, boats and support plates; others in silica.
3. HCl from $AsCl_3$ used in SC50.
4. Ge (?) detected in source Ga samples SC47, SC48 and SC49; Ca <.03 ppm, and Cd 0.1-1.0 ppm detected in all four source Ga samples.

TABLE V

Segregation of Impurities with Substrate Position
< 100 > Hall Bars

No.	Run No.	Carrier Density (x 10^{-16}) 1st	2nd	3rd	4th	Mobility 1st	2nd	3rd	4th
1.	SC14 (GaP)	0.11	0.086			89	47		
2.	SC55	0.64	0.46			103	89		
3.	SC42	1.06	0.60	0.28	0.21	115	87	60	33
4.	SC34	1.4	1.4	0.69		67	85	73	
5.	SC37	1.7	1.14			105	94		
6.	SC40	2.6	0.48			126	70		
7.	SC36	2.8	2.8	2.4		105	89	73	
8.	SC39	3.1	1.2			99	94		
9.	SC28	3.7	1.6			95	82		
10.	SC45	3.7	1.04			83	77		
11.	SC41	4.0	0.47	0.17	(hi ρ)	111	100	46	(hi ρ)
12.	SC25	4.2	0.77			103	32		
13.	SC30 (Zn?)	4.3	2.1			103	90		
14.	SC51	4.7	0.75			73	50		
15.	SC53	6.0	1.7			122	101		
16.	SC27	6.4	3.2			105	44		
17.	SC48(Al_2O_3)	6.4*	9.2			181*	126		
18.	SC47	7.3	3.95			108	112		
19.	SC35	8.3	3.3	0.43		123	71	67	
20.	SC49(Al_2O_3)	8.4	14.1			242	124		
21.	SC33 (Sn)	8.7	3.3	6.1		235	133	75	
22.	SC52(Al_2O_3)	16.5	11.7			87	82		
23.	SC5	17.	10.			49	113		
24.	SC11	19.	7.0			92	95		
25.	SC50	23.	13.			81	79		
26.	SC17	15.	4.7			72	63		
27.	SC7	28.	5.8			55	51		
28.	SC32	31.	7.6	5.2		92	95	99	
29.	SC12(GaP)	32.	7.5	1.0		61	45	51	

TABLE V (Continued)

Segregation of Impurities with Substrate Position
<100 > Hall Bars

No.	Run No.	Carrier Density (x 10^{-16}) 1st	2nd	3rd	4th	Mobility 1st	2nd	3rd	4th
30.	SC8	36.	22.			92	71		
31.	SC9	38.	17.			79	65		
32.	SC46 (Sn)	60.	42.			82	98		
33.	SC19 (Te)	70.	54.	21		52	40	35	
34.	SC4	70.	67.			72	78		
35.	SC10	86.	57.			80	85		
36.	SC24	91.	56.	46		93	83	94	
37.	SC20 (Te)	170.	140.			78	80		
38.	SC23 (Te)	330.	300.			46	49		
39.	SC22 (Te)	390.	250.			44	46		
40.	SC16 (Te)	2900.	900.			29	36		

* Evaluation on Hall bar cut from wafer, substrate removed.

TABLE VI

Segregation of Impurities with Substrate Position
<111> B Hall Bars

Run No.	Carrier Density(10^{-18}) 1st	2nd	Mobility 1st	2nd
SC37	1.7	.59	84	160
SC41	1.3	2.8	61	67
SC42	1.5	.28	66	120
SC45	2.9	.83	44	74
SC46 (Sn)	2.0	.93	22	76
SC47	2.0	.84	71	91
SC50	.98	1.1	93	66
SC51	.32	.17	127	124
SC52 (Al_2O_3)	2.7	3.1	58	17
SC53	2.2	1.0	68	93
SC55	1.3	.20	102	277

TABLE VII

Electrical Properties of GaP Grown on Adjacent Substrates of Different Orientations

Hall Bar No.				Carrier Density (x 10^{-16})				Mobility				Carrier Ratio	
(100)	(111)B	(111)A	(110)	(100)	(111)B	(111)A	(110)	(100)	(111)B	(111)A	(110)	(111)B/(100)	(110)/(100)
SC37-4	-5			1.14	170			94	84			150	
-8	-7	-9		(+)	59	(hi ρ)		(+)	160	(hi ρ)		-	
SC39-4		-5		1.16		.01		99		13			
SC40-4		-5		.4		(hi ρ)		70		(hi ρ)			
SC41-4	-5			.4	130			100	61			280	
SC42-4		-5		.60		(hi ρ)		87		(hi ρ)			
-8	-9	-7		.28	150	.05		60	66	10		540	
-12	-11			.208	28			33	120			134	
SC45-4	-5			1.04	290			77	44			280	
SC46-4			-5	.42			55	98			84		1.3*
SC47-4			-5	4.0			27	112			66		6.8
SC48-3			-4	9.2			35	126			46		3.9**
SC53-4			-5	1.7			14	101			81		8.2

* Sn doped

** Al_2O_3 Tube

TABLE VIII

Properties of Doped GaP Epitaxial Layers

Sample No.	Source	Thickness μ (Approx)	ρ	μ	n	Orient.
SC16-3	GaP + P(L) + 3.0×10^{19} Te	50	.017	32	1.9×10^{19}	< 100 >
SC18-3	Ga + P(AA145)	26	.29	55	5.3×10^{17}	"
-5	+ 1×10^{18} Te	20	.66	53	2.0×10^{17}	"
SC19-3	Ga + P(AA145)	34	.23	46	6.2×10^{17}	"
-5	+ 1.3×10^{19} Te	25	.59	38	3.8×10^{17}	"
SC20-3	Ga, Te reused + P (AA145)	43	.052	79	1.5×10^{18}	"
SC21-3	"	10*	non ohmic contacts			"
SC22-3	"	15	.046	45	3.2×10^{18}	"
SC23-3	"	21	.043	47	3.1×10^{18}	"
SC29-3	Ga + P(AA145) + Zn (350°)	55	.037	(25)	(6×10^{18}) (p)	"
SC30-3	Ga, Zn reused + P (AA145)	95	2.4	96	3.2×10^{16}(n)	"
SC33-3	Ga, 1.65×10^{19} Sn	105	.86	180	6.0×10^{16}	"
-5	+ P(AA146)	97	1.40	100	4.6×10^{16}	"
SC46-3	Ga, 1.11×10^{20} Sn	325	.14	90	5.1×10^{17}	"
-5	+ P(M105)	240	.15	79	5.5×10^{17}	<110 >
-7		105	.115	49	1.45×10^{18}	< 111 > B

* Very ragged interface, non-standard growth conditions.

TABLE IX

Epitaxial Growth of GaP by Close-Space H_2O Transport

Physical Structure of GaP Source	Mils Spacing Between Source and Substrate Surfaces at Beginning	H_2 Flow Rate cc/min	Mils Thickness of Deposit	Notebook Page and Remarks on Visual and XRD Examination of Deposit
Finely powdered	30	4	3.0	545801 - Uniform matte finish. XRD found deposit to be <100 > GaP, with no visible evidence of a ternary Ga-As-P.
Finely powdered	10	1	7.2	545804 - Similar to above but some mechanical adherence of source GaP (evidently due to the close spacing)which could not be removed.
Polycrystalline Ingot	10	1	7.3	545803 - "Photographic" image of the source crystal planes was found on the deposit, with some places smooth and others rough, depending upon orientation of the adjacent source crystal plane. Deposit primarily single crystal < 100 > oriented GaP with some evidence of ternary at interface.
Polycrystalline Ingot	20	1	5.9	545805 - Image phenomenon above substantially reduced. Most of deposit area shiny, though wavy. Deposit is an alloy of GaAs and GaP (~ 6.3 mol % GaAs) and is predominantly < 100 > oriented. No pure GaP visible.

TABLE X

Solar Cell Fabrication

Diff. Run No.	Slice No.	Diffusant Source and Amt.	Diff Temp. (°C)	Diff Time (min)	P Surface Conc/cm^3	μ Of P Layer cm^2/volt sec	Junction Depth μ
NA-1	AP62-2	3.8 mg Zn_3As_2	800	3	4.7×10^{18}	48	1
NA-2	AP62-4	2.2 mg Zn	800	10	4.5×10^{18}	31	5
NA-3	AP48-2	2.2 mg Zn	800	3	-	-	3
NA-4	AP87-2	2.2 mg Zn	800	3	7×10^{18}	27	2
NA-4	bulk, poly	2.2 mg Zn	800	3	-	-	
NA-5	AP88-5	5.8 mg Zn	800	3	1×10^{19}	28	2
NA-6	AP60-2	2.2 mg Zn	850	1.5	-	-	< 1 μ
NA-7	SC5-3	5.8 mg Zn	850	2.5	1.3×10^{19}	23	2
NA-7	bulk, poly	5.8 mg Zn	850	2.5	-	-	-
NA-8	bulk, poly	5.8 mg Zn	800	30	-	-	16 (est. from spectral resp.)
NA-10	bulk, poly	5.8 mg Zn, 1.8 mg P	800	3	-	-	-
NA-11	AP88-2	5.8 mg Zn, 1.8 mg P	800	3	1.6×10^{19}	-	0.6
NA-11	bulk, poly	5.8 mg Zn 1.8 mg P	800	3	-	-	-
NA-13	bulk, poly	5.8 mg Zn, 1.8 P	800	10	-	-	-

TABLE X (Continued)

Solar Cell Fabrication
Diffusion Data

Diff. Run No.	Slice No.	Diffusant Source and Amt.	Diff. Temp (°C.)	Diff. Time (Min)	P Surface Conc/cm^3	μ of P Layer cm^2/volt sec.	Junction Depth μ
NA-14	bulk, poly	5.8 mg Zn, 1.8 mg P	800	3	-	-	-
NA-15	bulk, poly (old)	1.1 mg Zn	800	3	-	-	-
	bulk, poly (Lot 170)	1.1 mg Zn	800	3	1.9×10^{19}	30	-
NA-16	SC 6/11-3	5.8 mg Zn, 1.8 mg P	800	3	1×10^{19}	-	0.5
	SC14-2	"	800	3	4.2×10^{18}	36	1.5
	SC13-6	"	800	3	1×10^{19}	-	$\leq$ 0.5
NA-17	SC6/11-3	5.8 mg Zn, 1.8 mg P	800	3	high ρ	-	< 0.5
NA-18a	SC6/11-3	1 mg Zn_3As_2 in .3 ml volume tube	900	4	high ρ	-	1.5
NA-18b	SC6/11-3	5.8 mg Zn	800	30	$1.4\text{-}3 \times 10^{19}$	-	7-15
NA-20	SC13-4	5.8 mg Zn, 1.8 mg P	800	3	1.5×10^{19}	58	0.5
NA-20	SC15-3	"	800	3	1.5×10^{19}	81	$\leq$ 0.5
NA-20	SC16-3	"	800	3	-	-	< 0.5
NA-20	SC17-3	"	800	3	9.9×10^{18}	37	< 0.5
NA-21	SC18-3	"	800	3	6.4×10^{18}	28	< 0.4
NA-21	SC18-5	"	800	3	4.9×10^{18}	63	< 0.4
NA-21	SC19-3	"	800	3	8.5×10^{18}	31	< 0.4
NA-21	SC19-5	"	800	3	7.5×10^{18}	37	< 0.4
NA-21	SC20-3	"	800	3	7×10^{18}	22	0.4
NA-21	SC21-3	"	800	3	1.3×10^{19}	66	< 0.4
NA-22	SC13-6	"	800	10	1.2×10^{19}	35	3
NA-22	SC13-4	"	800	10	1.2×10^{19}	30	3
NA-22	SC19-5	"	800	10	7×10^{18}	27	5
NA-22	SC17-3	"	800	10	8.8×10^{18}	24	5
NA-22	SC21-3	"	800	10	1.1×10^{19}	31	4
NA-23	SC13-6	.5 mg Zn, 1.8 mg P	800	3	5×10^{18}	78	< 1

TABLE X (Continued)

Solar Cell Fabrication Diffusion Data

Diff. Run No.	Slice No.	Diffusant Source and Amt.	Diff Temp (C°.)	Diff Time (Min)	P Surface Conc/cm^3	μ of P Layer cm^2/volt sec.	Junction Depth μ
NA26	SC27-3	5.8 mg Zn, 1.8 mg P	800	3	3.3×10^{18}	27	1.5
NA26	SC28-3	"	800	3	4.9×10^{18}	27	1.0
NA26	SC29-3	"	800	3	----------No jct. found ----------		
NA26	SC30-3	"	800	3	6.5×10^{18}	24	0.7
NA29	SC31-5	5.8 mg Zn, 1.8 mg P	800	3	1.2×10^{19}	24	0.5
NA30	SC31-3	"	800	3	7×10^{18}	18	0.5
NA30	SC32-3	"	800	3	7.8×10^{18}	13	0.5
NA30	SC32-5	"	800	3	7.5×10^{18}	17	0.5
NA31	SC33-3	"	800	3	4.2×10^{18}	22	1.0
NA31	SC33-5	"	800	3	5.6×10^{18}	22	0.8
NA31	SC34-3	"	800	3	2.5×10^{18}	23	1.5
NA32	SC34-5	"	800	3	7.2×10^{18}	15	2.0
NA32	SC35-3	"	800	3	2.3×10^{19}	18	0.5
NA32	SC35-5	"	800	3	8.4×10^{18}	12	1.0
NA33	SC36-3	5.8 mg Zn, 1.8 mg P	800	3	6.8×10^{18}	13	0.5
NA33	SC36-5	"	800	3	1.4×10^{18}	40	1.5
NA33	SC37-3	"	800	3	2.5×10^{18}	18	1.0
NA33	SC37-6	"	800	3	2.0×10^{19}	2 (?)	0.5
NA34	SC38-4	"	800	3	3.2×10^{18}	23	0.5
NA34	SC38-7	"	800	3	No measurable values obtained		
NA34	SC38-10	"	800	3	1.5×10^{18}	21	1.0
NA34	SC39-3	"	800	3	1.8×10^{18}	21	1.0
NA34	SC39-6	"	800	3	9.2×10^{17}	21	0.5
NA34	SC40-3	"	800	3	1.5×10^{18}	21	1.5
NA34	SC40-6	"	800	3	3.5×10^{18}	26	0.5

TABLE XI

Variation in Surface Concentration with Zinc Concentration

Run No.	Sample No.	Carrier Conc., N	Diffusant * Source and Amt.	P Surface Conc.	Mobility of P Layer	Junction Depth (μ)
NA-16	SC13-6	1×10^{17}	5.8 mg Zn 1.8 mg P	1×10^{19}	-	< 0.4
NA-23	SC13-6	1×10^{17}	.5 mg Zn 1.8 mg P	5×10^{18}	78	< 1
NA-24	SC13-6	1×10^{17}	.1 mg Zn 1.8 mg P	6×10^{18}	78	< 0.5
NA-28	SC13-6	1×10^{17}	5.mg(95% Ga, 5% Zn)	9.6×10^{17}	4	0.5
NA-21	SC19-3	6.2×10^{17}	5.8 mg Zn 1.8 mg P	8.5×10^{18}	31	< 0.4
NA-23	SC19-3	6.2×10^{17}	.5 mg Zn 1.8 mg P	2.3×10^{18}	21	2
NA-24	SC19-3	6.2×10^{17}	.1 mg Zn 1.8 mg P	3×10^{18}	-	0.7
NA-28	SC19-3	6.2×10^{17}	5 mg (95%Ga, 5% Zn)	8.6×10^{18}	.1 (?)	0.5

* All diffusions were carried out at 800° C for 3 minutes.

TABLE XII

Solar Cell Evaluation Data at Room Temperature

Diff Run No.	Slice No.	Spectral Response Peak Microns λ_1	λ_2	λ_3	J_{sc} (ma/cm²) Sun	J_{sc} (ma/cm²) Tungsten	V_{oc} (Volts) Sun	V_{oc} (Volts) Tungsten	Area of Samples Cm²	Conversion Efficiency ** (using sun)
NA26	SC27-3	0.45			.81	.14	1.10	1.04	.25	-
NA26	SC28-3	0.45			1.2	.13	1.30	1.10	.10	1.1%
NA26	SC29-3		0.53		.06	.02	.68	.64	.16	-
NA26	SC30-3	0.45	0.55*	0.7 (broad)	.67	.08	.62	.31	.20	-
NA27	SC19-3	0.45	0.53		.13	.03	.82	.74	.11	-
NA27	SC25-3		0.53	0.8	.30	.07	1.0	.92	.10	-
NA28	SC13-6	0.43	0.52	0.8	.28	.11	.92	.82	.19	-
NA28	SC17-3	0.43	0.50		.007	.007	.05	.04	.14	-
NA28	SC19-3	---------Sample Broke----------								
NA28	SC19-5	0.44	0.50		.14	.27	.91	.92	-	-
NA28	SC26-3		0.6	0.75 (broad)	.03	.04	.79	.78	.31	-
NA29	SC31-5		0.50	0.7 (broad)	.10	.03	.92	.91	.26	-
NA30	SC31-3	0.45			1.2	.17	1.29	1.15	.03	0.45%
NA30	SC32-3	0.44		0.7 (broad)	.66	.07	.90	.90	.09	-
NA30	SC32-5	0.45	0.55*	0.7	1.0	.14	.92	.54	.17	-
NA31	SC33-3	0.45			0.61	.11	1.10	.94	.39	-
NA31	SC33-5	0.45			0.92	.13	1.30	1.00	.54	0.75%
NA31	SC34-3	0.45			1.43	.23	1.35	1.10	.57	1.1%
NA32	SC34-5	0.45			1.30	.15	0.76	1.20	.27	0.7%
NA32	SC35-3	0.45	0.50	0.8	0.54	.08	1.24	1.00	.48	-
NA32	SC35-5	0.45	0.50		0.88	.13	1.26	1.20	.43	0.6%
NA33	SC36-3	0.45	0.60*	0.7	0.74	.15	.52	.38	.23	-
NA33	SC36-5	0.45		0.7*	.50	.14	.64	.58	.30	-
NA33	SC37-3	0.45			.78	.12	1.20	1.12	.10	-
NA33	SC37-6	0.45			.20	.03	.96	.94	.20	-
NA33	SC37-10	---------No Output----------								

TABLE XII (Continued)

Solar Cell Evaluation Data at Room Temperature

Diff Run No.	Slice No.	Spectral Response Peak Microns λ_1	λ_2	λ_3	J_{sc} (ma/cm²) Sun	J_{sc} (ma/cm²) Tungsten	V_{oc} (Volts) Sun	V_{oc} (Volts) Tungsten	Area of Samples Cm²	Conversion Efficiency ** (using sun)
NA34	SC38-4	0.53			.04	.01	.83	.83	.18	-
NA34	SC38-7	------ No Output ----------								
NA34	SC38-10	------ No output ----------								
NA34	SC39-3	0.45			1.13	.15	1.35	1.02	.22	-
NA34	SC39-6		0.53		.00	.00	1.10	.99	.26	-
NA34	SC40-3	0.45			1.05	.14	1.30	1.10	.20	-
NA34	SC40-6		0.53		.06	.00	1.20	1.12	.17	-
NA16	SC14-2	0.46	0.50		0.30	0.04	1.05	1.0	.22	-
NA21	SC18-5	0.45			.69	.08	1.1	1.08	.20	-
NA21	SC19-3	0.45	0.50		.89	.14	1.0	1.0	.25	0.75%
NA21	SC19-5	0.45			.73	.09	1.05	.96	.13	-
NA25	SC22-3	0.45			.25	.06	.83	.90	.36	-
NA21	SC21-3			0.77 (broad)	5.0	5.0	.70	.74	.09	2.5%
NA25	SC23-3	0.45			.21	.06	1.05	1.05	.20	-
NA25	SC25-3	0.46			1.2	.19	1.08	.92	.24	1.0%
NA21	SC20-3	0.45			.26	.06	1.0	.92	.25	-
NA25	SC26-3	0.46	0.53		.11	.13	.92	.90	.39	-
NA16	SC13-6	0.46	0.53	0.59 0.7 (broad)	.03	.01	.58	.58	.06	-
NA20	SC13-4	0.46	0.54	0.7 (broad)	.16	.12	.76	.73	.26	-
NA20	SC15-3		0.53		.01	.03	.80	.75	.27	-
NA35	SC41-3	0.45			.50	.07	1.30	1.20	.13	-
NA35	SC42-3	0.45			.89	.11	.72	.58	.15	-
NA35	SC41-6	0.44		0.7	-	.09	-	.14	.17	-
NA35	SC41-8		0.55		-	.00	-	1.00	.21	-
NA35	SC41-10		0.50	0.6*	-	.13	-	1.02	.10	-
NA35	SC42-10			0.9	---------Shorted ----------				.18	-

TABLE XII (Continued)

Solar Cell Evaluation Data at Room Temperature

Diff Run No.	Slice No.	Spectral Response Peak Microns λ_1	λ_2	λ_3	J_{sc} (ma/cm²) Sun	Tungsten	V_{oc} (Volts) Sun	Tungsten	Area of Samples Cm²	Conversion Efficiency ** (using sun)
NA36	SC27-3	0.45			-	.14	-	1.29	.50	-
NA36	SC28-3	0.45			-	.12	-	1.08	.49	-
NA36	SC44-2	0.44			.79	.14	1.26	1.23	.14	-
NA36	SC44-5	0.48			.61	.10	1.33	1.32	.09	-
NA37	SC45-3	0.45			.44	.09	.94	.61	.23	-
NA37	SC46-3	0.45			.39	.05	.35	.23	.25	-
NA37	SC46-5	0.45			.33	.07	.00	.04	.09	-
NA39	SC47-3	0.45			.63	.10	1.10	1.00	.04	-
NA39	SC47-5		0.56*	0.7	.26	.02	.18	.03	.36	-
NA39	SC47-7	0.45			.25	.03	.14	.00	.15	-
NA39	SC48-2	0.45	0.57		.35	.00	.48	.00	.21	-
NA40	SC49-3	0.45			2.0	.15	1.25	1.18	.34	> 1% (estimated)
NA40	SC50-3	0.45			1.25	.13	1.30	.94	.16	-
NA40	SC50-5	0.45			1.17	.11	1.07	.76	.18	-
NA40	SC50-7	---------No Junction----------								
NA41	SC49-3				0	.01	.74	.64	.21	-
NA41	SC50-3	0.45		0.8	.24	.04	1.18	1.14	.20	-
NA42	SC49-3	0.45			.80	.07	1.26	1.12	.03	-
NA42	SC50-3	0.45			1.0	.11	1.34	1.14	.13	-
NA42	SC50-5	0.45			.96	.11	.44	.18	.19	-
NA44	SC51-3	0.45			1.2	.11	1.35	1.15	.17	1% (estimated)
NA44	SC51-5	0.45	0.47	0.8	1.1	.15	1.24	1.21	.25	-
NA44	SC51-7	0.45			.95	.07	1.28	1.22	.04	-

TABLE XII (Continued)

Solar Cell Evaluation Data at Room Temperature

Diff Run No.	Slice No	Spectral Response Peak Microns λ_1	λ_2	λ_3	J_{sc} (ma/cm²) Sun	Tungsten	V_{oc} (Volts) Sun	Tungsten	Area of Samples Cm²	Conversion Efficiency** (using sun)
NA45	SC51-3		0.51	0.9	.77	.13	1.28	1.22	.15	-
NA45	SC51-5		0.49		.80	.16	1.14	1.13	.18	-
NA45	SC51-7		0.48		.70	.12	1.05	1.09	.13	-
NA22	SC21-3			0.75	4.0	4.0	0.58	0.58	.18	1.6%

* Negative response.

** Measurements made from open window between 11:00 a.m. and 3:00 p.m. with sample pointed toward sun. A 10% standard silicon solar cell was also measured at the same time to provide an idea of the solar intensity level - if the incident intensity was lower than 80 mw/cm² measurements were not taken.

TABLE XIII

Open Circuit Voltage and Short Circuit Current vs. Temperature

Sample	Spectral Response Peak, Microns	V_{oc} * (23°C.)	Temp, Coefficient (β), mv/°C	V_{oc} at 350° C.	Slope, Δ E (ev) J_{sc} vs. 1/T
NA31 SC34-3	0.45	1.15	3.5	0.06	.06
NA30 SC31-3	0.45	1.20	4.4	-	indeterminate
NA26 SC27-3	0.45	1.05	2.8	0.27	.05
NA26 SC28-3	0.45	1.15	3.0	0.29	.047
NA32 SC34-5	0.45	1.2	3.5	0.25	.06
NA33 SC37-6	0.45	0.96	2.75	0.20	.062
NA33 SC37-3	0.45	1.20	2.88	0.36	.0478
NA34 SC40-3	0.45	1.24	2.8	0.40	.0496
NA31 SC33-5	0.45	1.30	2.5	0.31	.06
NA44 SC51-3	0.45	1.35	2.9	0.43	.0407
NA44 SC51-7	0.45	1.28	3.2	0.35	.055
NA42 SC49-3	0.45	1.26	3.2	0.26	.104
NA42 SC50-3	0.45	1.35	2.8	0.40	.054
NA22 SC21-3	0.7	0.58	2.8	0	0 } to 200° C., then
NA21 SC21-3	0.7	0.7	2.8	0	0 } J_{sc} decreases with increasing temp.

* Measured with tungsten source or sunlight

TABLE XIV

Spectral Response of Solar Cells Normalized Relative to Thermocouple

Diff Run No.	Slice No	P-Surface Conc/cm^3	Initial Base Conc (N) No/cm^3	λ_3, (μ)	I_3 (μa/μv)	λ_4 (μ)	I_4 (μa/μv)
NA16	SC13-6	1×10^{19}	1×10^{17}	.46	.014	.53	.039
Mesa	SC13-6			-	-	-	-
NA16	SC14-2	4.2×10^{18}	1×10^{15}	.46	.072	.495	.5
NA20	SC13-4	1.5×10^{19}	3.7×10^{16} (P-type)	.46	.047	.54	.176
NA20	SC15-3	1.5×10^{19}	graded	-	-	.53	.154
NA20	SC17-3	9.9×10^{18}	1.5×10^{17}	-	-	.53	.31
NA21	SC18-5 (Lo bump)	4.9×10^{18}	2×10^{17}(Te)	.45	6.35	-	-
NA21	SC19-3 (Lo bump)	8.5×10^{18}	6.2×10^{17} (Te)	.45	6.35	.50	1.65
NA21	SC19-3 (Hi bump)	8.5×10^{18}	6.2×10^{17} (Te)	.45	9.5	.50	2.44
NA21	SC20-3 (Hi bump)	7.0×10^{18}	1.5×10^{18}	.45	5.8	-	-
NA21	SC20-3 (Hi bump)	7.0×10^{18}	1.5×10^{18}(Te)	.45	5.95	.50	.44
NA21	SC19-5 (Lo bump)	7.5×10^{18}	3.8×10^{17}(Te)	.45	6.50	.50	1.30
NA21	SC19-5 (Hi bump)	7.5×10^{18}	3.8×10^{17}(Te)	.45	4.66	-	-
NA21	SC21-3	1.3×10^{19}	P-type	-	-	-	-
NA16	SC13-6	1×10^{19}	1×10^{17}	.58	.014	.7 (broad)	.0075
Mesa	SC13-6			.58	.255	.7 (broad)	.262
NA16	SC14-2	4.2×10^{18}	1×10^{15}	-	-	.7	.000185
NA20	SC13-4	1.5×10^{19}	3.7×10^{16} (P-type)	-	-	.73 (broad)	.21
NA20	SC15-3	1.5×10^{19}	graded	-	-	-	-
NA20	SC17-3	9.9×10^{18}	1.5×10^{17}	-	-	.76 (broad)	1.94
NA21	SC18-5 (Lo bump)	4.9×10^{18}	2×10^{17}(Te)	-	-	-	-

TABLE XIV (Continued)

Spectral Response of Solar Cells Normalized Relative to Thermocouple

Diff Run No.	Slice No.	P-Surface Conc/cm^3	Initial Base Conc (N) No/cm^3	λ_3, (μ)	I_3 (μa/μv)	λ_4 (μ)	I_4 (μa/μv)
NA21	SC19-3 (Lo bump)	8.5×10^{18}	6.2×10^{17}(Te)	-	-	-	-
NA21	SC19-3 (Hi bump)	8.5×10^{18}	6.2×10^{17}(Te)	-	-	-	-
NA21	SC20-3 (Lo bump)	7.0×10^{18}	1.5×10^{18}(Te)	-	-	-	-
NA21	SC20-3 (Hi bump)	7.0×10^{18}	1.5×10^{18}(Te)	-	-	-	-
NA21	SC19-5 (Lo bump)	7.5×10^{18}	3.8×10^{17}(Te)	-	-	-	-
NA21	SC19-5 (Hi bump)	7.5×10^{18}	3.8×10^{17}(Te)	-	-	-	-
NA21	SC21-3	1.3×10^{19}	P-type	-	-	.78 (broad)	11.7

TABLE XV

Typical I-V Characteristic Parameters of Fabricated Solar Cells *

Sample	Area Cm^2	from $I = I_o e^{ev/nkT}$ n	Saturation Current Density, J_o * amp/cm	ΔE (ev) $I_o T^{-5/2}$ vs. 1/T	Series Resistance ohm-cm^2 (at 5 ma forward current)
NA25 SC25-3	.24	5	8×10^{-8}	.18	14.4
NA21 SC21-3	.09	2.5	2.2×10^{-8}	.46	9
NA31 SC34-3	.57	4	5×10^{-9}	-	-
NA31 SC33-5	.54	6	2×10^{-7}	-	-
NA32 SC34-5	.27	5	1.1×10^{-8}	-	5
NA29 SC31-5	.26	-	-	-	245
NA25 SC26-3	.07	5	9×10^{-8}	-	1000
NA27 SC25-3	.10	-	10^{-8}	-	350
NA26 SC27-3	.25	5	4×10^{-8}	-	86

* Measurements made at 300° K.

TABLE XVI

Capacity-Voltage, Diffusion Length Data

Diffusion Run	Slice * No.	J_{sc} ** ma/cm^2	Carrier Concentration after Diffusion	Diffusion Length, μ	C-V	I Layer (μ)	Gradient, a (No/cm^4)
NA-1	AP62-2	.23	1×10^{16}	.47	$1/c^2$	-	-
NA-20	SC17-3	.37	1×10^{15}	4.0(?)	$1/c^3$	4.0	4×10^{19}
NA-20	SC15-3	.05	5×10^{16}	.27	$1/c^3$	.27	2.4×10^{22}
NA-20	SC13-4	1	3×10^{17}	.18	$1/c^3$	.17	1.5×10^{23}
NA-16	SC13-6	2	5×10^{18}	.045	$1/c^3$	.015	1.9×10^{24}
NA-22	SC13-6	.056	5×10^{17}	.16	$1/c^3$	.27	1.25×10^{23}
NA-23	SC13-6	.08	3×10^{16}	.88	-	.94	-
NA-24	SC13-6	.05	5×10^{14}	< 7.4 (?)	$1/c^3$	7.4	-
NA-21	SC21-3	3.5	5×10^{16}	< .0078	$1/c^3$	-	-
NA-21	SC19-5	.1	5×10^{14}	1	$1/c^3$	-	6.7×10^{18}

* Mesas of the samples have been used

** Measured using tungsten source

TABLE XVII

Effect of Top Metal Contact to GaP Solar Cell on Open Circuit Voltage

GaP Solar Cell NA-16, SC14-2

Total Cell Area Uncovered cm^2	Open Circuit Voltage V_{oc} Volts
.22 (total cell area)	1.05
.16	1.03
.11	1.00
.077	.98
0	0

TABLE XVIII

Effect of Junction Depth on J_{sc}

Diff. Run No.	Slice No.	Junction Depth (μ)	V_{oc} (Volts)	J_{sc} (ma/cm^2)
NA16	SC13-6	< 0.5	0.58	0.01
NA20	SC13-4	0.5	0.73	0.12
NA21	SC19-5	< 0.4	0.96	0.12
NA20	SC17-3	< 0.5	0.60	0.20
NA21	SC21-3	< 0.4	0.74	5.0
NA22	SC13-6	3	0.65	0.005
NA22	SC13-4	3	0.74	0.006
NA22	SC19-5	5	0.92	0.06
NA22	SC17-3	5	0.96	0.04
NA22	SC21-3	4	0.62	1.14

TABLE XIX

Solar Cell Characteristics vs. Surface "bump" Density

Diff Run No.	Slice No.	V_{oc} * Volts	J_{sc} * ma/cm²	"Bump" Density bumps/cm²
NA 21	SC 18-3	1.18	.06	11
NA 21	SC 18-5	1.08	.08	25
NA 21	SC 19-3	1.00	.14	215
		.98	.16	139
NA 21	SC 19-5	.96	.09	372
		.96	.12	138
NA 21	SC 20-3	.92	.06	19
		.98	.06	7
NA 25	SC 22-3	.90	.06	42
		.56	.04	63
NA 25	SC 23-3	1.1	.06	109
NA 25	SC 24-3	1.1	.06	39
		1.0	.04	67
NA 25	SC 24-5	1.1	.07	75
		1.0	.06	69
NA 25	SC 25-3	.92	.19	121
		.80	.15	105
NA 25	SC 26-3	.90	.13	112
		.92	.07	157

* Measured with tungsten source

TABLE XX

Open Circuit Voltage (in sunlight) vs. Effect of Crystal Orientation

Sample	Orientation	V_{oc}* (Volts)	Temp. Coeff of V_{oc}, mV/deg
NA33 SC37-3	<100>	1.20	2.8
NA34 SC39-3	<100>	1.35	2.4
NA34 SC40-3	<100>	1.30	2.8
NA35 SC41-3	<100>	1.30	3
NA35 SC42-3	<100>	0.58	-
NA36 SC27-3	<100>	1.29	3
NA36 SC28-3	<100>	1.08	3.2
NA33 SC37-6	<111> B	0.96	2.6
NA33 SC44-2	<111> B	1.26	2.8
NA34 SC38-4	<111> A	0.83	-
NA34 SC39-6	<111> A	1.10	-
NA34 SC40-6	<111> A	1.20	-

* Measured in sunlight.

TABLE XXI

Relationship of Growing Conditions, Short Circuit Current, Spectral Response Peaks for GaP Solar Cells

Run No.	Slice No.	H_2 Flow Rate cc/min	Source Temp °C.	Spectral Response Peaks (Microns)				J_{sc} (ma/cm²) ± Sunlight
NA21	SC21-3	15	890				0.77	5.0
NA30	SC31-3	95	890	0.45				1.2
NA29	SC31-5	95	890		0.50		0.7	0.10
NA16	SC14-2	150	890	0.46	0.50			0.30
NA20	SC15-3	150	890		0.53			0.025
NA20	SC17-3	150	890		0.53		0.76	0.28
NA21	SC19-3	150	890	0.45	0.50			0.89
NA21	SC19-5	150	890	0.45				0.73
NA25	SC25-3	150	890	0.45				1.2
NA26	SC27-3	170	890	0.45				0.81
NA26	SC28-3	170	890	0.45				1.15
NA21	SC20-3	300	890	0.45				0.26
NA31	SC34-3	310	895	0.45				1.43
NA32	SC34-5	310	895	0.45				0.76
NA25	SC22-3	500	890	0.45				0.25
NA25	SC23-3	500	890	0.45				0.21
NA25	SC24-5	500	890	0.45				0.29
NA16	SC13-6	150	935	0.45	0.53	0.59	0.7	0.03
NA20	SC13-4	150	935	0.46	0.54		0.7	0.16
NA25	SC26-3	150	975	0.46	0.54			0.11
NA26	SC29-3	150	975		0.53			0.06
NA30	SC32-3	475	975	0.44			0.7	0.66
NA30	SC32-5	475	975	0.45	0.53	0.58*	0.8	1.0
NA26	SC30-3	800	975	0.45	0.55*		0.8	0.67

± Measurements made from open window vetween 11:00 a.m. and 3:00 p.m. with sample pointed toward sun. A 10% standard silicon solar cell was also measured at the same time to provide an idea of the solar intensity level - if the incident intensity was lower than 80 mx/cm² measurements were not taken.

* Negative response

TABLE XXII

Relationship between Epitaxial Growth Conditions and Temperature Dependence of Short Circuit Current for Cells having only 0.45 μ Response

Run No.	Slice No.	H_2 Flow Rate cc/min	Source Temp. °C	J_{sc} (ma/cm²) (Sunlight)	Slope, ΔE (ev) J_{sc} vs. 1/T	Conversion* Efficiency
NA30	SC31-3	95	890	1.2	Indeterminate	0.45%
NA21	SC19-5	150	890	0.73	.045	-
NA25	SC25-3	150	890	1.2	.044	1.0%
NA26	SC27-3	170	890	0.81	.05	-
NA26	SC28-3	170	890	1.15	.047	1.1%
NA21	SC20-3	300	890	0.26	.07	-
NA31	SC34-3	310	895	1.43	.06	1.1%
NA32	SC34-5	310	895	0.76	.06	0.7%
NA25	SC22-3	500	890	0.25	.04 .08	-
NA25	SC23-3	500	890	0.21	.08	-
NA25	SC24-5	500	890	0.29	.04 .08	-

* See footnote of Table XXI concerning solar measurement.

TABLE XXIII

Relationship between Phosphorus Flow Rate used in Epitaxial Growth and Solar Cell Properties

Run No.	Slice No.	Phosphorus ± Flow Rate (cc/min)	P/Ga Mole Ratio	V_{oc} ** (Volts)	J_{sc} ** ma/cm^2	Spectral Response Peaks Microns
NA33	SC36-3	1.28	3.12	0.52	0.74	0.45, 0.6*, 0.7
NA33	SC36-5	1.28	3.12	0.64	0.50	0.45 0.7*
NA33	SC37-3	0.36	0.79	1.20	0.78	0.45
NA34	SC39-3	0.647	1.43	1.35	1.13	0.45
NA34	SC40-3	0.30	0.62	1.30	1.05	0.45
NA35	SC41-3	0.24	0.52	1.30	-	0.45

± Source temp., H_2, HCl flow rates maintained constant, fixed orientation < 100 >.

* Negative Response.

** Measured in sunlight.

TABLE XXIV

Relationship between V_{knee}, Spectral Response and V_{oc}

Run No.	Slice No.	V_{knee} (Volts) (from $I_f - V_f$ Trace)	Spectral Response Peaks (Microns)				V_{oc} (Volts) (Sunlight)	J_{sc} (ma/cm²) (Sunlight)
NA26	SC27-3	1.1	0.45,				1.17	0.81
NA26	SC28-3	1.2	0.45,				1.27	1.15
NA25	SC25-3	1.1	0.46,				1.05	1.2
NA30	SC31-3	1.3	0.45,				1.30	1.2
NA16	SC13-6	0.9	0.46,	0.53,	0.59,	0.7	0.58	0.03
NA23	SC13-6	1.6		0.53,	0.6	0.7	0.50	0.03
NA20	SC13-4	1.1	0.46,	0.54		0.7	0.76	0.16
NA20	SC15-3	3		0.53,			0.80	0.03
NA27	SC25-3	1.6	0.45,	0.53,		0.75	1.0	0.30
NA26	SC30-3	6	0.45,	0.55*,		0.8	0.62	0.67
NA28	SC26-3	12			0.58,	0.75	0.79	0.05
NA25	SC26-3	5	0.46,	0.53			0.95	0.29
NA29	SC31-5	0.8		0.50		0.70	0.92	0.10
NA30	SC32-5	4.5	0.45,	0.53	0.58*	0.8	0.92	1.0
NA30	SC32-3	0.7	0.44			0.7	0.90	0.66

* Negative Response.

TABLE XXV

Open Circuit Voltage * vs. Temperature

Sample	V_{oc} (23°C)	Temp. Coefficient (β) mv/°C	t_m (°C) Max. Temp.	V_{oc} at t_m (°C)	$n_{Initial}$
NA31 SC34-3	1.15	3.5	225	0.5	1.4×10^{16}
NA32 SC34-5	1.2	2.78	225	0.63	1.05×10^{16}
NA31 SC33-5	1.0	2.5	225	0.6	4.6×10^{16}
NA26 SC28-3	1.15	3.0	350	0.28	2.7×10^{16}
NA26 SC27-3	1.05	2.83	350	0.26	4.8×10^{16}
NA30 SC31-3	1.20	4.4	325	0.07	2×10^{16}
NA21 SC20-3	.96	3.74	275	0.12	1.5×10^{18}
NA33 SC37-3	1.20	2.88	350	0.36	illegible
NA33 SC37-6	.96	2.75	350	0.20	1.1×10^{18}
NA34 SC40-3	1.24	2.8	350	0.40	1.5×10^{16}

* Measured with tungsten source or sunlight.

TABLE XXVI

V_{oc} vs. Total Ionized Impurity Concentration for Samples having 0.45 μ Response < 100 > Orientation

Sample	Carrier Conc (No/cm^3)	Mobility (cm^2/volt sec)	N_I (calc) (No/cm^3)	V_{oc} at 200° (volts)	N_A (calc) (No/cm^3)	N_D (calc) (No/cm^3)
NA34 SC40-3	1.5×10^{16}	98	1.08×10^{18}	0.84	5.3×10^{17}	5.5×10^{17}
NA35 SC41-3	2×10^{16}	100	1.1×10^{18}	0.82	5.4×10^{17}	5.6×10^{17}
NA26 SC28-3	2.7×10^{16}	88	1.38×10^{18}	0.74	6.8×10^{17}	7.1×10^{17}
NA26 SC27-3	4.8×10^{16}	74	1.9×10^{18}	0.70	9.4×10^{17}	9.8×10^{17}
NA25 SC24-5	5.1×10^{17}	89	2.28×10^{18}	0.69	8.9×10^{17}	1.4×10^{18}
NA21 SC19-3	6.2×10^{17}	46	4.6×10^{18}	0.54	2×10^{18}	2.6×10^{18}
From theory and extrapolation			2×10^{17}	1.15		

TABLE XXVII

Samples sent to Lewis Research Center

Sample:	NA-31 SC 34-3	NA-31 SC 33-5	NA-32 SC 34-5	NA-22 SC 21-3
Growth Conditions:				
Source Temp. (°C)	895	975	895	890
Substrate Temp. (°C)	825	790	815	815
H_2 Flow Rate (cc/min)	310	300	310	15
HCl Flow Rate (cc/min)	2.3	2.2	2.3	0.92
P_4 Flow Rate (cc/min)	.9	.78	.9	2.0
Layer Thickness (μ)	35	.78	.9	2.0
ηCarrier Conc. (No/cm^3)	1.4×10^{16}	4.6×10^{16}	1.1×10^{16}	P-type**
μ(cm^2/volt sec)	76	100	79	-
ρ (ohm-cm)	5.9	1.40	8.8	-
Diffusion:				
Dopant	zinc	zinc	zinc	zinc
Temp (°C)	800	800	800	800
Time (min)	3	3	3	10
Cell Evaluation:				
P-layer conc (no/cm^3)	2.5×10^{18}	5.6×10^{18}	7.2×10^{18}	1.1×10^{19}
μ(cm^2/volt sec)	23	22	15	31
Jct. Depth (μ)	1.5	~0.8	2.0	4
Forward I-V Trace, V_{knee}(volts)	1.1	1.2	1.2	.6
Max. power (in sum) (mw)	.608*	.38*	.182*	.224 ±
V_{oc} (volts)	1.35	1.30	1.30	0.58
J_{sc} (ma/cm^2)	1.43	0.92	0.76	4.0
Cell area (cm^2)	0.57	0.54	0.27	0.18
Efficiency (in sun) (relative to std. Si solar Cell), (%)	1.1*	0.75*	0.7*	1.68 ±
Spectral Response (μ)	0.45	0.45	0.45	0.75(broad)
Slope J_{sc} vs. 1/T (ev)	.06	.06	.06	-
D. C. I_f-V_f : $I_o \exp \frac{ev}{nkT}$; n	4	6	5	2

* Based on solar intensity, as measured with Si solar cell, of 94 mw/cm^2

** From C-V data

± Based on solar intensity, as measured with Si solar cell, of 74 mw/cm^2

TABLE XVIII (Continued)

Samples to Lewis Research Center

Sample:	NA34 SC39-3	NA34 SC40-3
Growth Conditions:		
Source Temp. (°C)	908	898
Substrate Temp. (°C)	830	827
H_2 Flow Rate (cc/min)	300	300
HCl Flow Rate (cc/min)	2.15	2.2
P_4 Flow Rate (cc/min)	0.65	0.3
Orientation	<100 >	< 100 >
Layer thickness (μ)	135	115
n Carrier Conc (no/cm^3)	2.1×10^{16}	1.5×10^{16}
μ (Cm^2/volt sec)	96	98
ρ (ohm-cm)	3.9	4.3
Diffusion:		
Dopant	Zinc	Zinc
Temp (°C)	800	800
Time (min)	3	3
Cell Evaluation:		
p-layer conc (No/cm^3)	1.8×10^{18}	1.5×10^{18}
μ (cm^2/volt sec)	21	21
jct. depth (μ)	1	1
Cell area (cm^2)	0.22	0.20
Spectral Response peak (μ)	0.45	0.45
J_{sc} (ma/cm^2) at 23°C in sunlight	1.13	1.05
V_{oc} (volts) at 23°C in sunlight	1.35	1.30
Temp. Coeff. V_{oc}, β, (mv/deg)	~2.5	~2.9
V_{oc} at 300° C	0.52	0.54

TABLE XVIII (Continued)

Samples to Lewis Research Center

Sample:	NA36 SC27-3	NA36 SC28-3
Growth Conditions:		
Source Temp. (°C)	890	890
Substrate Temp. (°C)	815	815
H_2 flow rate (cc/min)	170	170
HCl flow rate (cc/min)	1	1
P_4 flow rate (cc/min)	.75	.87
Orientation	< 100 >	< 100 >
Layer thickness (μ)	25	35
n Carrier Conc. (No/cm^3)	4.8×10^{16}	2.7×10^{16}
μ (cm^2/volt sec)	74	88
ρ (ohm cm)	2.7	3.2
Diffusion:		
Dopant	Zinc	Zinc
Temp. (°C)	800	800
Time (min)	2	2
Cell Evaluation:		
P-layer conc (No. /cm^3)	3.3×10^{18}	4.9×10^{18}
μ(cm^2/volt sec)	27	27
Jct. dpth (μ)	1.5	1.0
Cell area (cm^2)	.50	.49
Spectral Response Peak (μ)	0.45	0.45
V_{oc} (volts) st 23° C in tungsten	1.29	1.08
Temp. Coeff. V_{oc}, β, (mv/deg)	3	3.1
V_{oc} at 300 ° C	0.48	0.43

TABLE XXVIII

Solar Cell Fabrication, Cadmium Diffusion

Run No.	Slice No.	P Diffusant and Amount	Diffusion Temp (°C.)	Diffusion Time (Mins)	Ave. P-Surface Conc. No/cm^3	Ave. Surface Mobility Cm^2/volt sec.	Junction Depth (μ)
38	521046-3	30 mg Cd	850	10	Could not Measure		$\ll$ 0.5
38	SC34-5	"	850	10	"		$\ll$ 0.5
38	SC40-3	"	850	10	"		$\ll$ 0.5
43	521038-3	6 mg Cd 1.8 mg P	900	10	"		-
43	SC34-5	"	900	10	"		-
43	SC40-3	"	900	10	"		-

TABLE XXX

Evaluation of Solar Cells made from GaP epitaxially prepared by other methods

Run No.	Slice No.	GaP Prep. Method	V_{oc} (Volts)	J_{sc} * (ma/cm^2)	Temp. Coeff ± of V_{oc}, β (mv/deg)	Cell Area Cm^2	Spectral Response Peak (Microns)
NA36	SC44-2	H_2O Transport	1.26	0.79	2.8	.14	0.44
NA36	SC44-5	"	1.33	0.61	7	.09	0.48
NA35	521044-1	Monsanto	0.62	0.50	-	.06	0.45, 0.55
NA23	521038	"	0.65	-	-	-	0.46

* Measured in sunlight

± Measured using tungsten source (see third quarterly report)

LIST OF FIGURES

LIST OF FIGURES

LIST OF FIGURES

LIST OF FIGURES

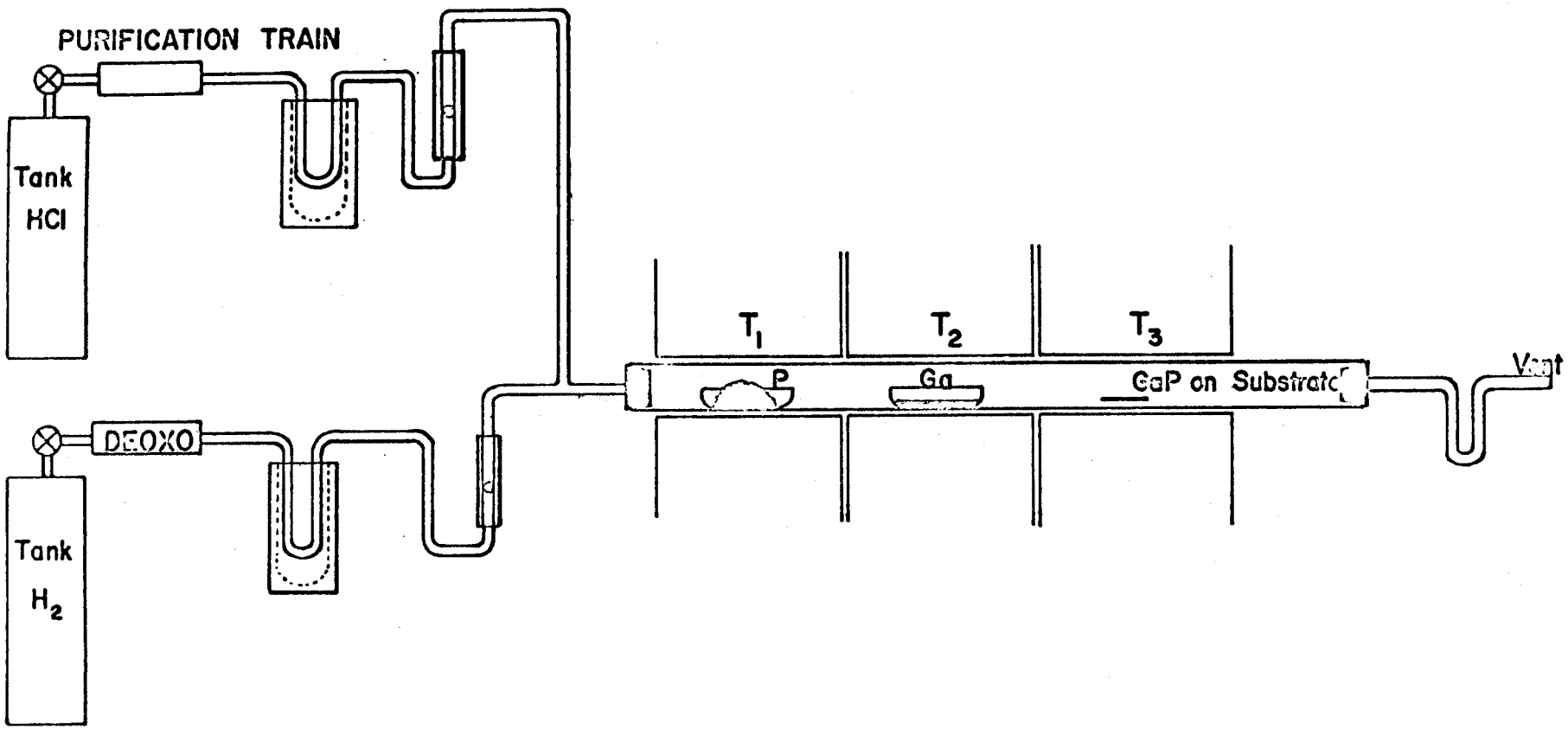

Figure 1 - Schematic of system for growth of single crystal GaP by vapor phase deposition.

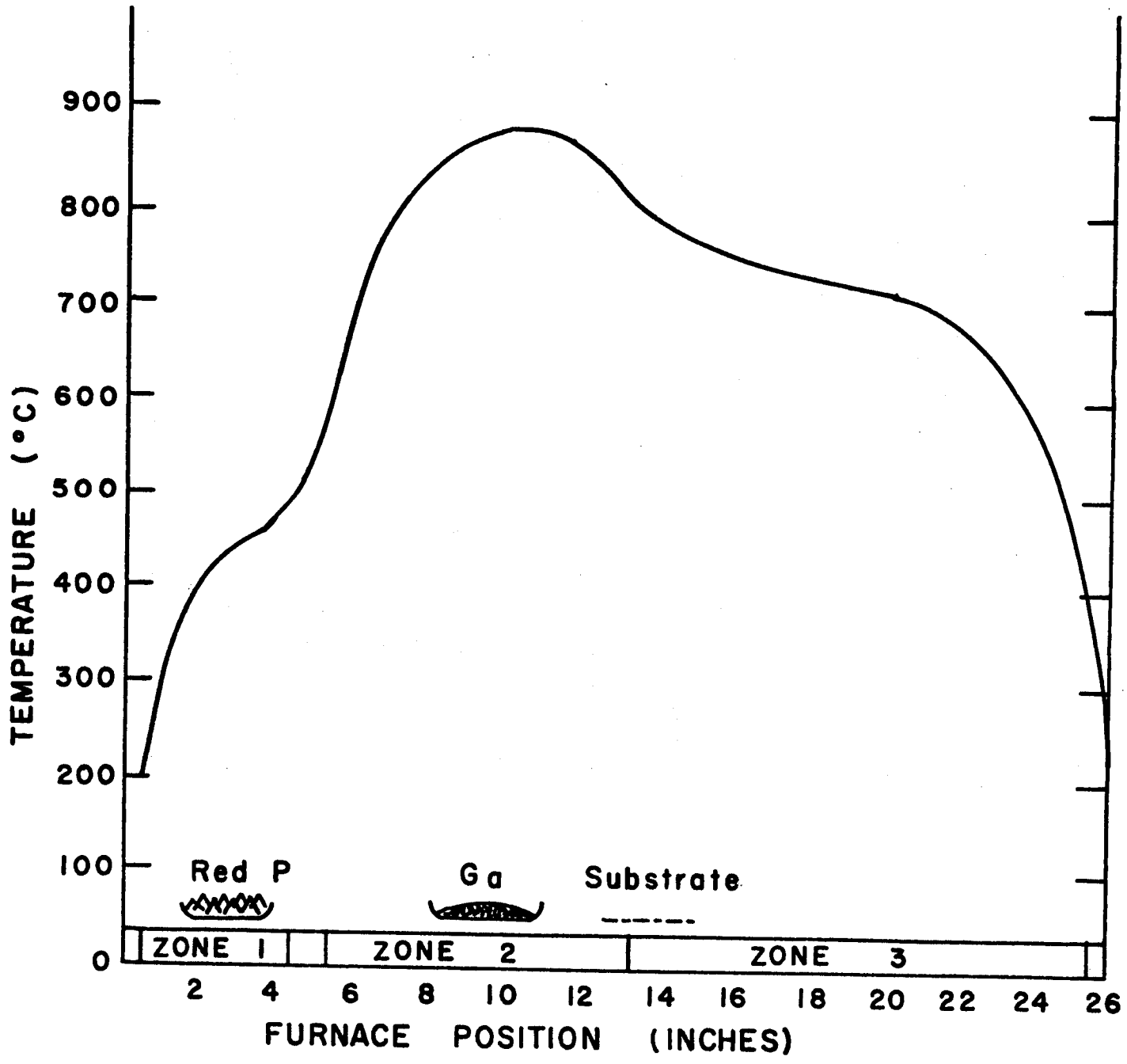

Figure 2 - Typical Temperature Profile and Sample Positions.

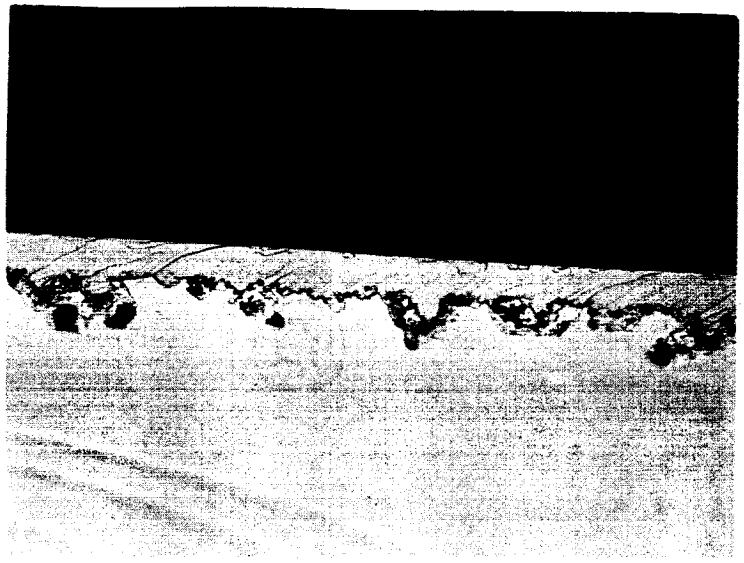

Figure 3

SC5-4 Extremely ragged interface
with large voids. 500X

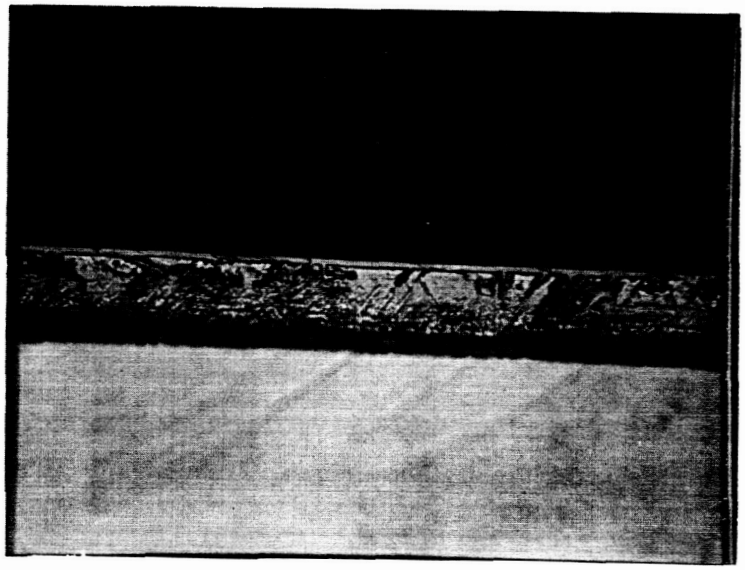

Figure 4

Sample NA-5, AP88-5 Sectioned to show P-N junction. Magnification - 500x; P layer depth - 2 μ, note ragged junction and relatively poor GaP-GaAs interface.

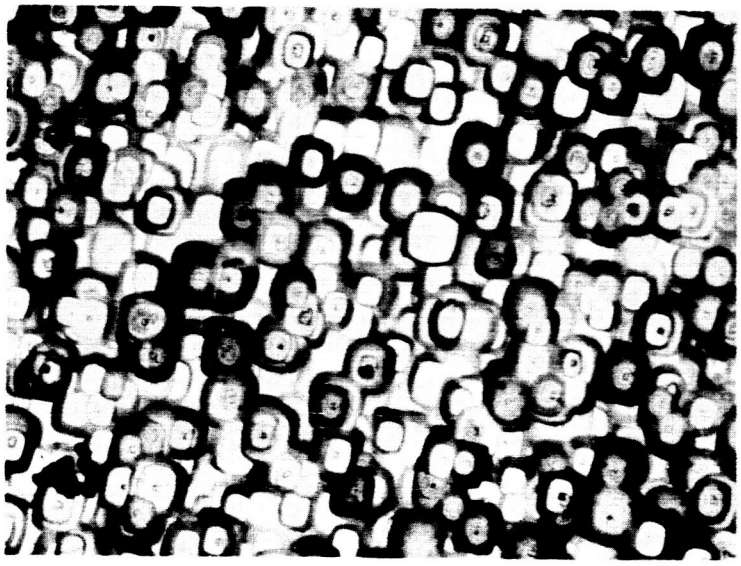

Figure 5

AP89-2 10 μ Typical bumps grown on < 100 > surface without high temperature pretreatment with phosphorus in hydrogen. 50X.

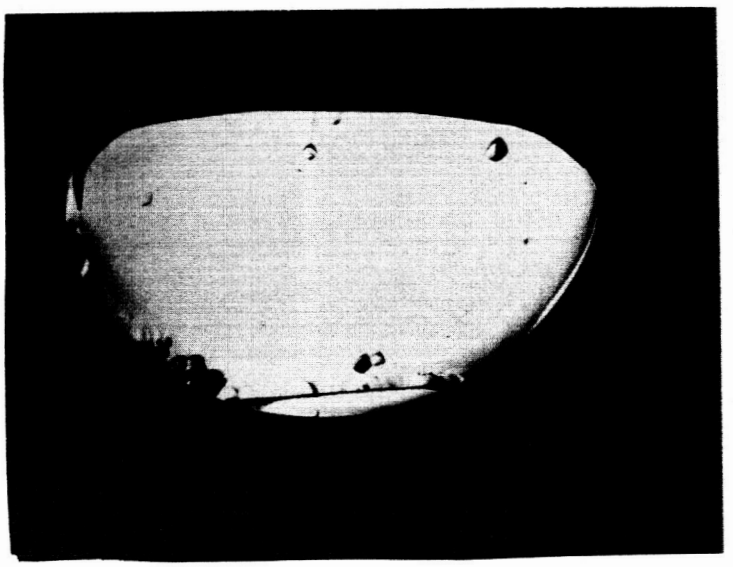

Fig. 6 - SC27-3, 25 μ. nearly bump free surface showing effect of orientation

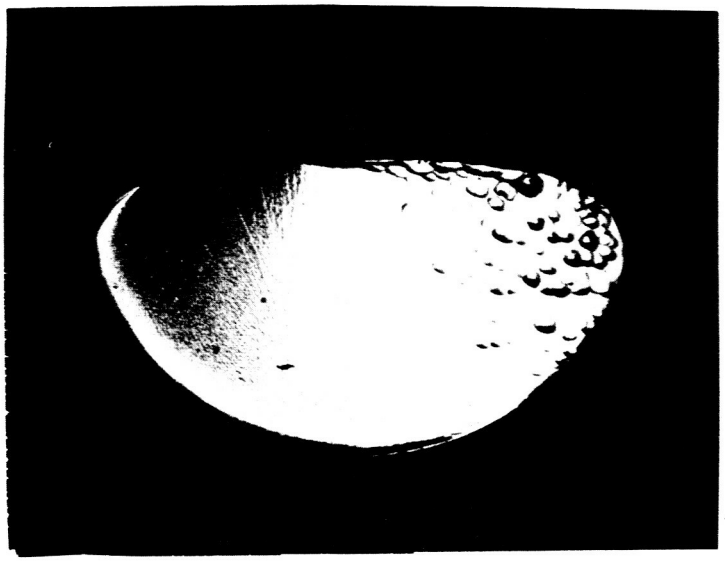

Figure 7 - SC32-3 130 μ Grown at 874° in steep temperature gradient.

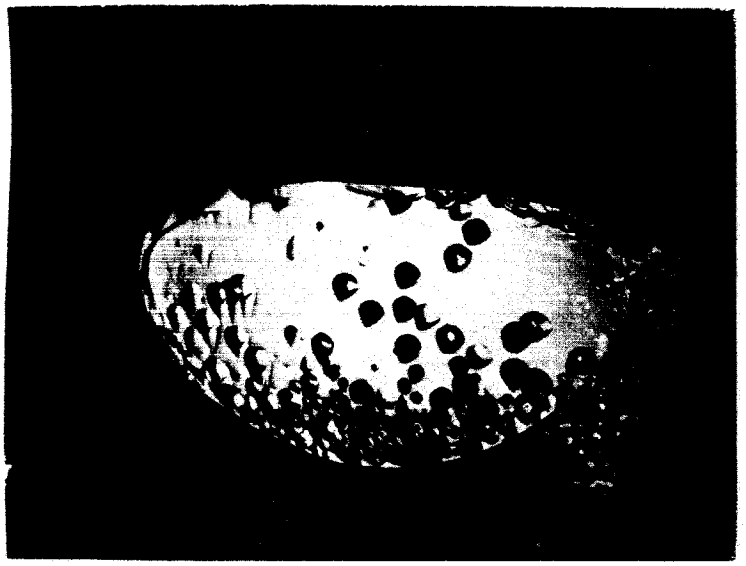

Figure 8 - SC30-3 95 μ showing relatively small bumps which may have nucleated after about half the thickness had been grown. Compare with SC27-3 25 μ in Figure (6).

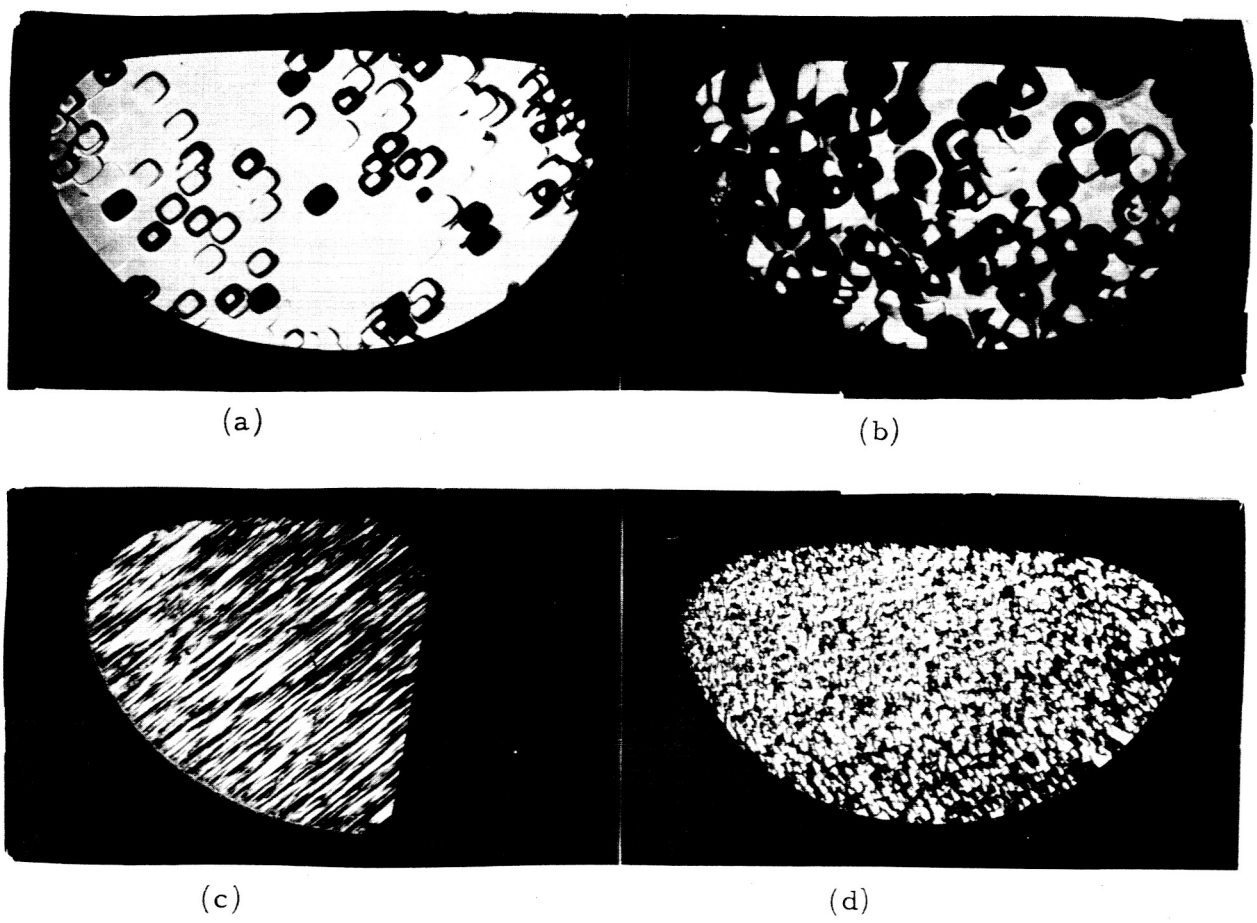

Fig. 9 - (a) SC18-5, 20 μ, 2.0×10^{17}, "rounded rectangular" bumps, many with flat tops. (b) SC24-5, 57 μ, 5.1×10^{17}, "square pyramidal" bumps. (c) SC16-3 50 μ, 1.9×10^{19}, parallel ridges caused by very heavy tellurium doping. (d) SC29-3, 55 μ, 6×10^{18} (p), high concentration of bumps elongated in "A" direction caused by zinc doping.

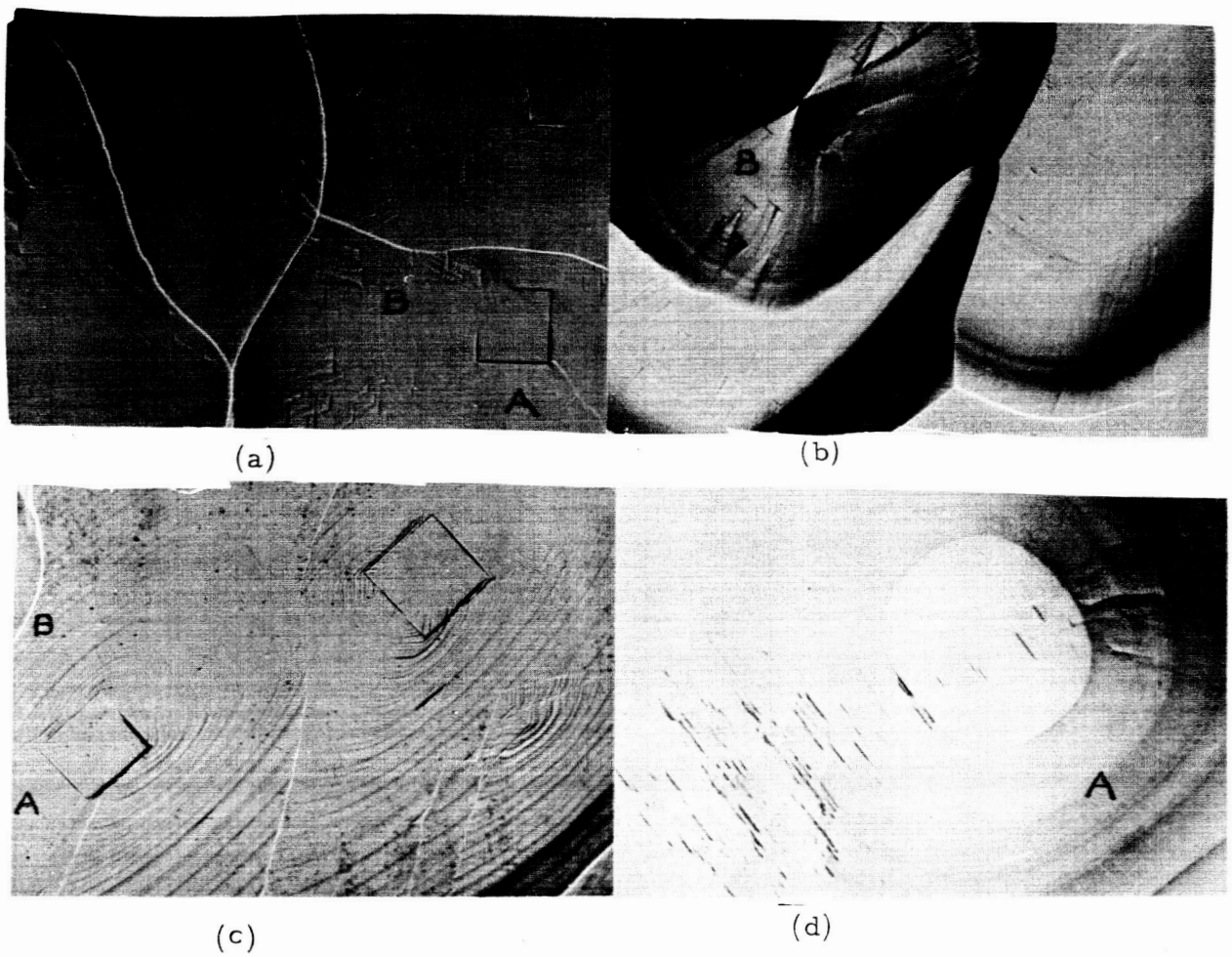

Fig. 10 - (a) SC26-3, 45 μ, < 3.6 x 10^{16}, overlapping "square pyramidal bumps, 100x. (b) SC19-3, 34 μ. 6.2 x 10^{17}, peaked rounded rectangular bumps. 100x. (c) SC29-3, 55 μ, 6 x 10^{18} (p). Zn doped. well developed "p-type" elongated oval bumps, 200x. (d) SC30-3, 95 μ. 3.2 x 10^{16} (n) Zn doped. small peaked "p-type" rounded rectangular bump, 100x.

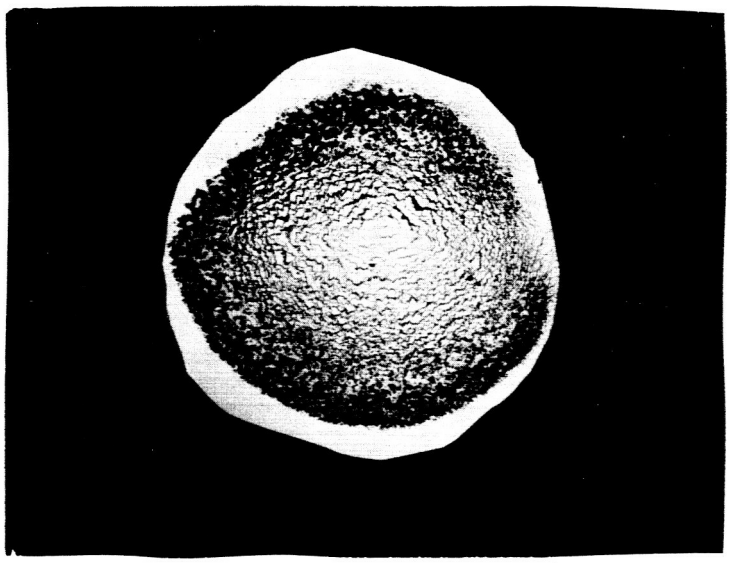

Figure 11 SC37-10 Typical Growth on < 111 > A Surface. Edge 370 μ, Center 215 μ

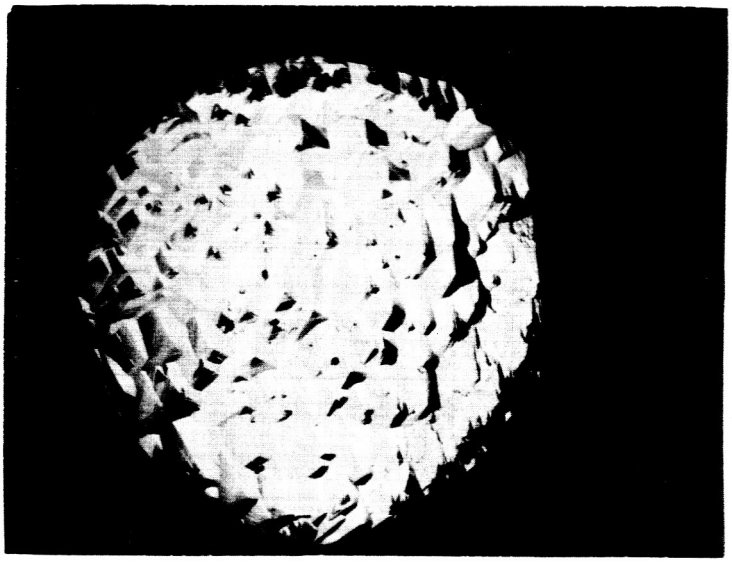

Figure 12 SC37-6 Typical Growth on < 111 > B Surface. ~ 95 μ

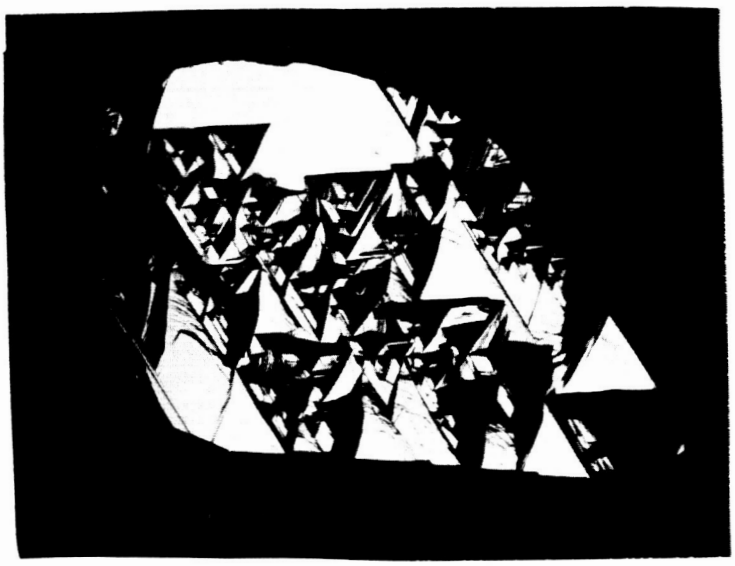

Figure 13 - SC53-5 Typical Growth on (110) surface. 100 μ

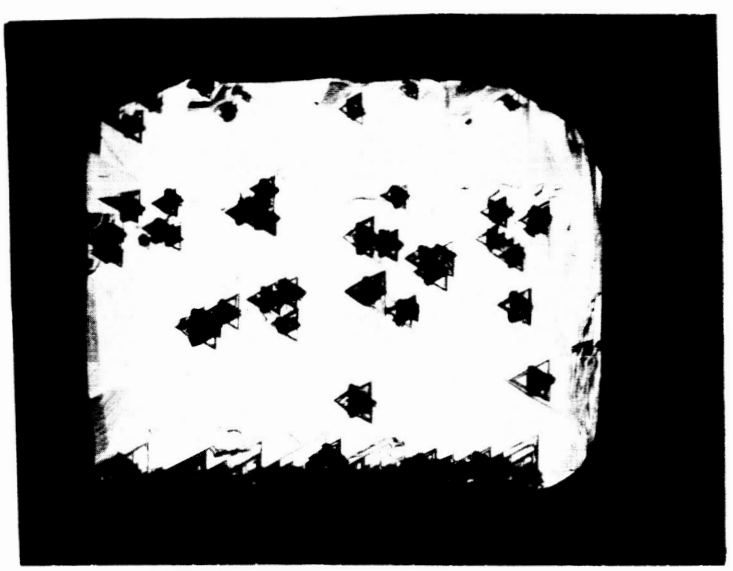

Figure 14 - SC53-7 Growth on (111)B surface. 125 μ

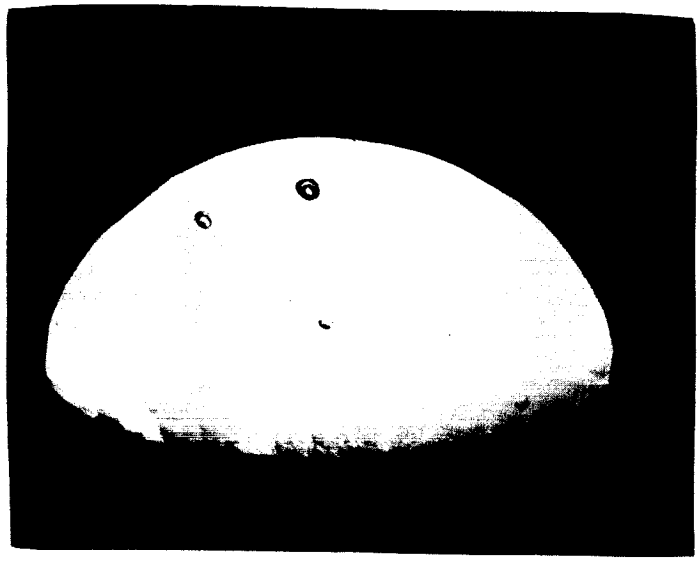

Figure 15 - SC51-3 Growth on (100) surface
45 μ

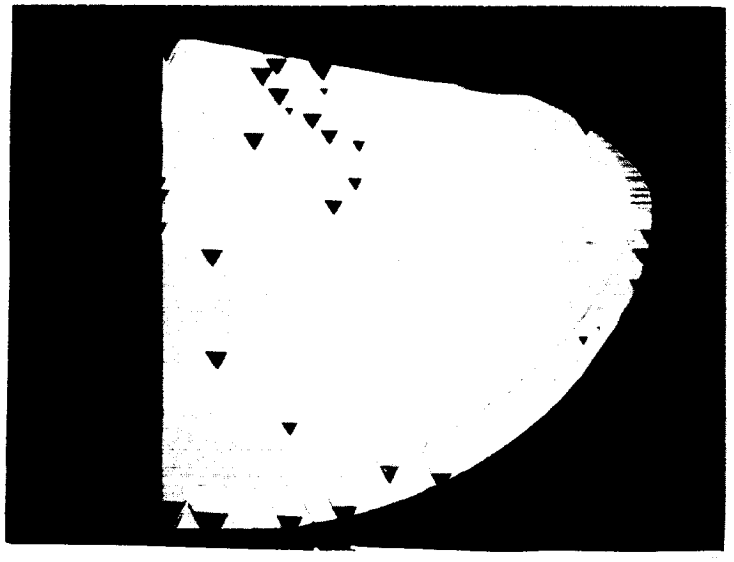

Figure 16 - SC51-5 Growth on (110) surface
22 μ

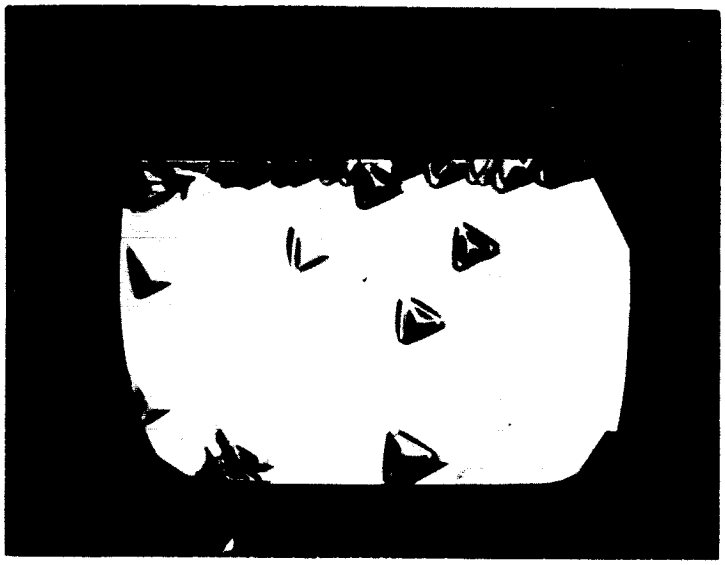

Figure 17 - SC51-7 Growth on (111)B. 40 μ

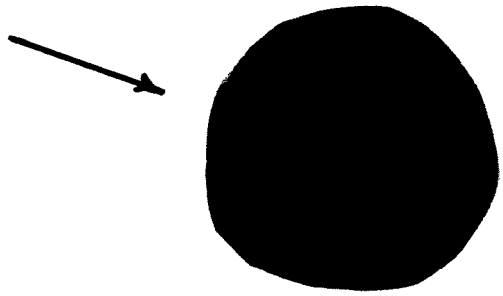

Figure 18 SC44-2 Growth on < 111 > B Surface by H_2O transport. Note < 110 > facets.

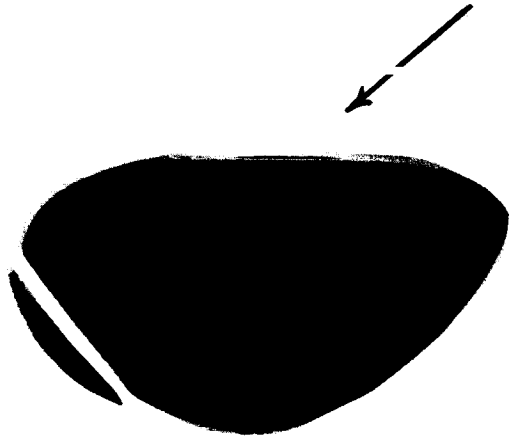

Figure 19 SC44-5 Growth on < 100 > Surface by H_2O transport. Sides heavily etched. Arrow shows direction of gas flow.

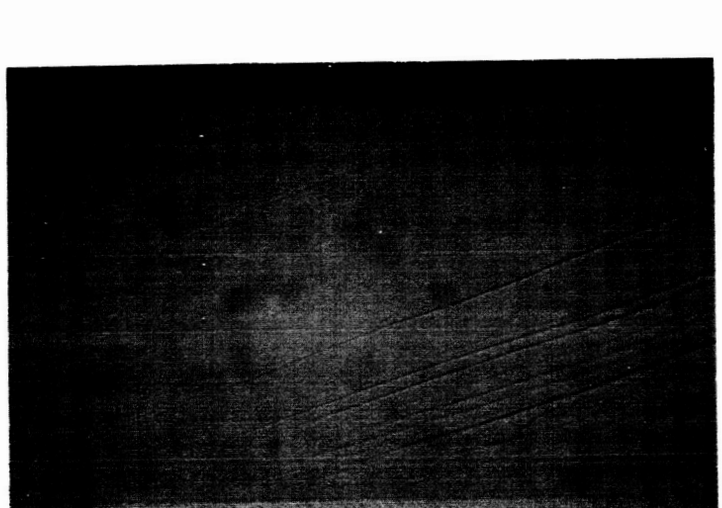

Figure 20 SC44-3 Spontaneously cleaved section of GaP layer grown by H_2O transport on GaAs. Not etched. 500X.

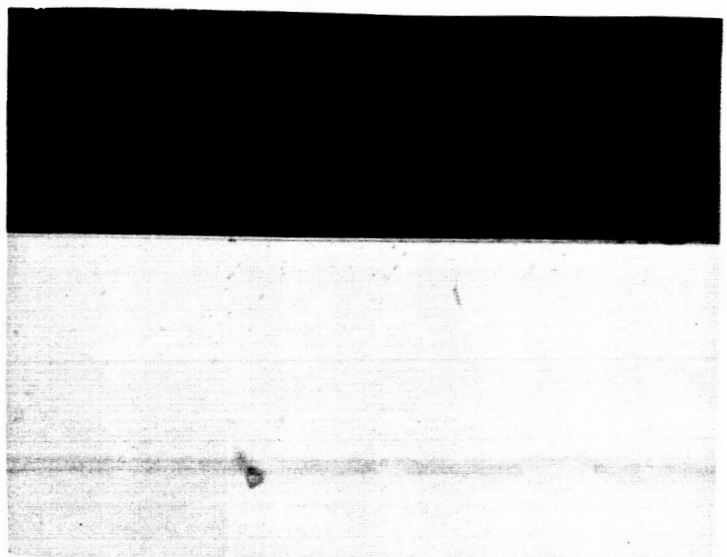

Figure 21: Delineated Junction of sample NA26 SC30-3, showing improved junction front; junction located .7 μ below surface; Magnification 500X.

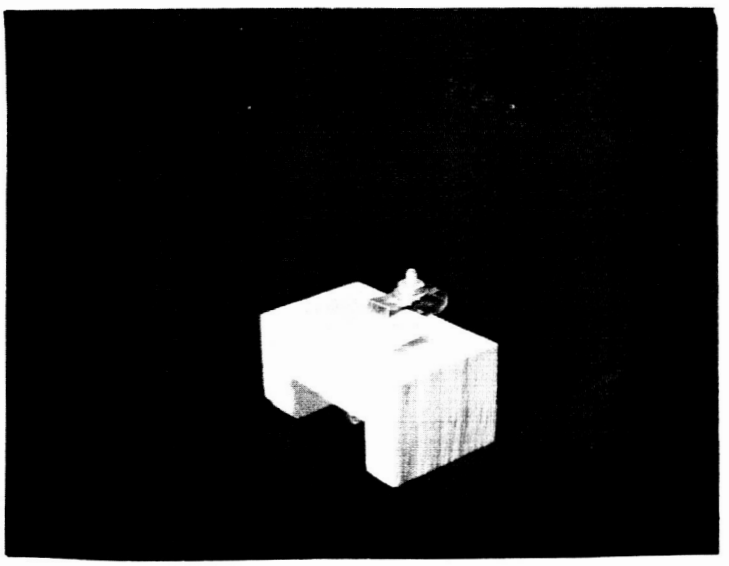

Figure 22: Lavite Holder for Measuring Temperature Characteristics of Solar Cell.

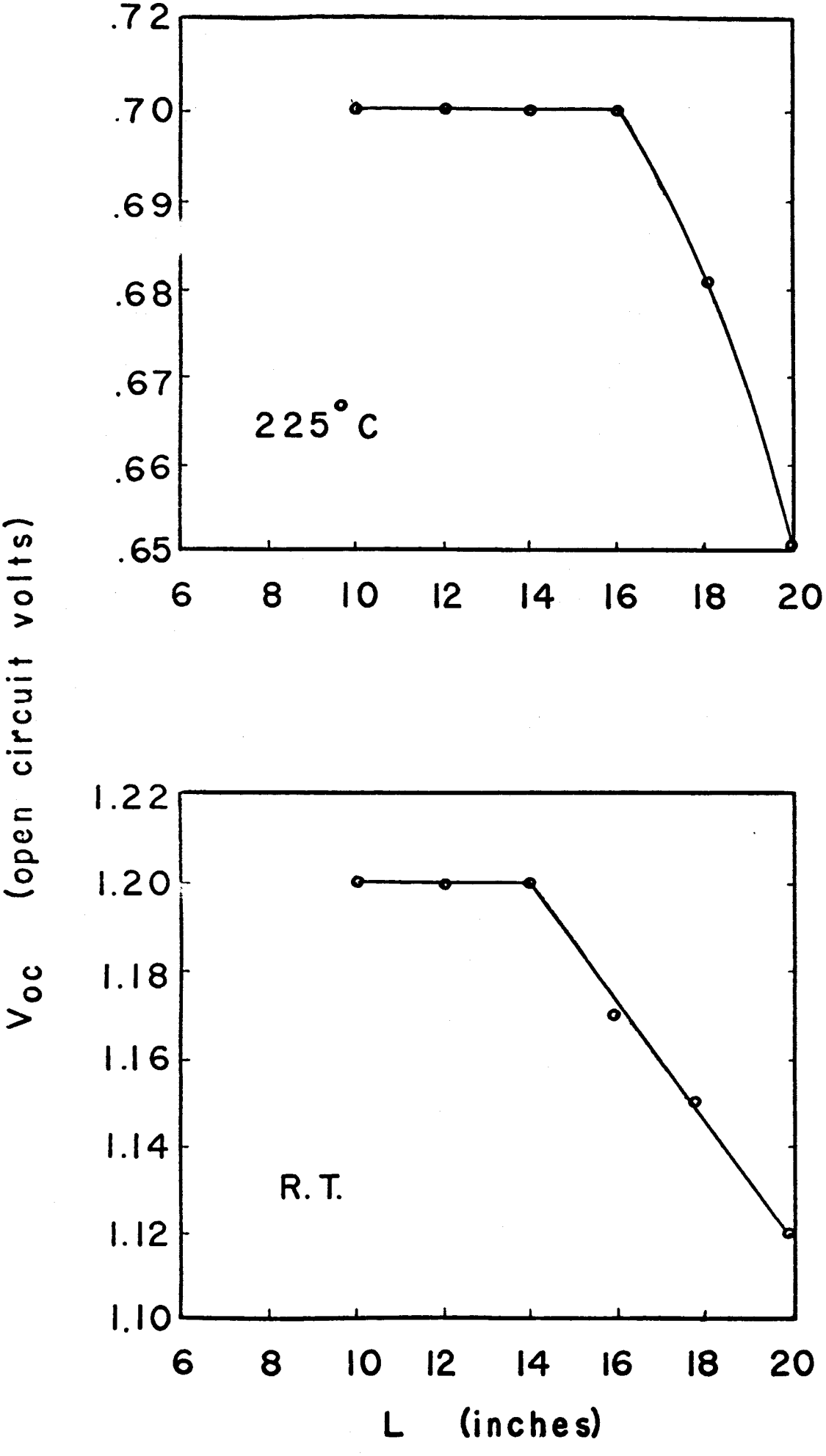

Figure 23: V_{oc} vs. Source-Sample Separation with Tungsten Source at room temperature and 225° C.

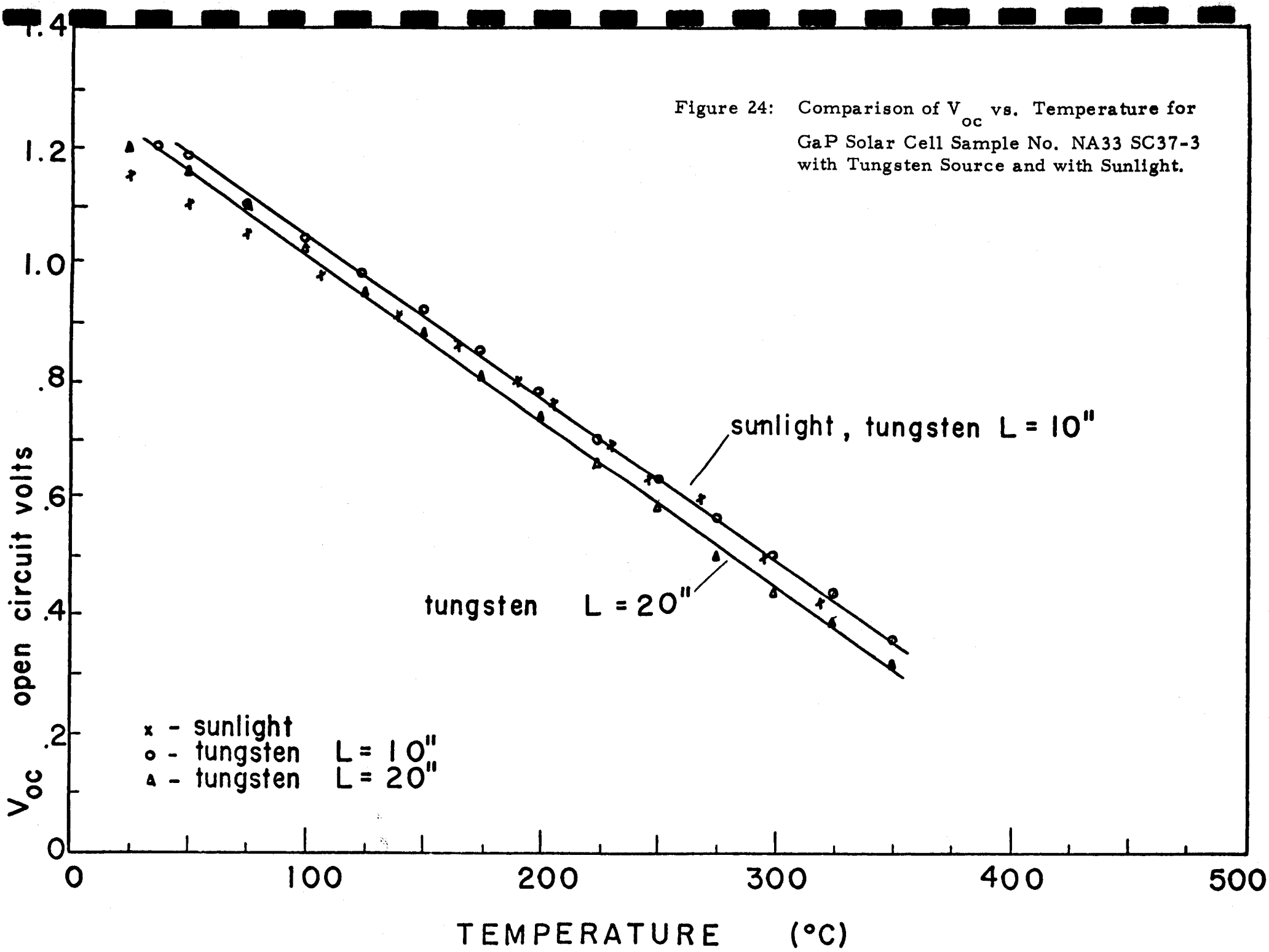

Figure 24: Comparison of V_{oc} vs. Temperature for GaP Solar Cell Sample No. NA33 SC37-3 with Tungsten Source and with Sunlight.

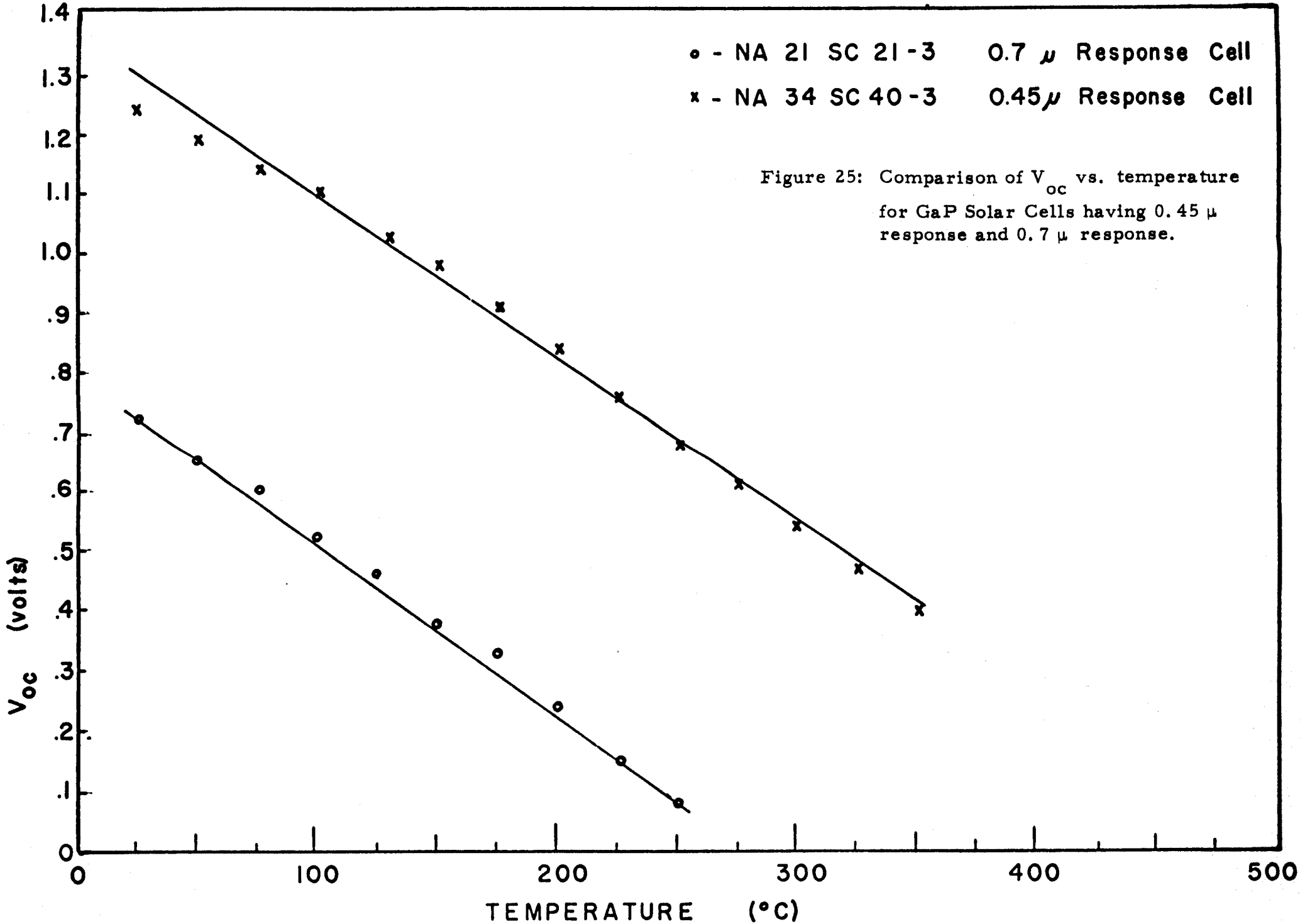

Figure 25: Comparison of V_{oc} vs. temperature for GaP Solar Cells having 0.45 μ response and 0.7 μ response.

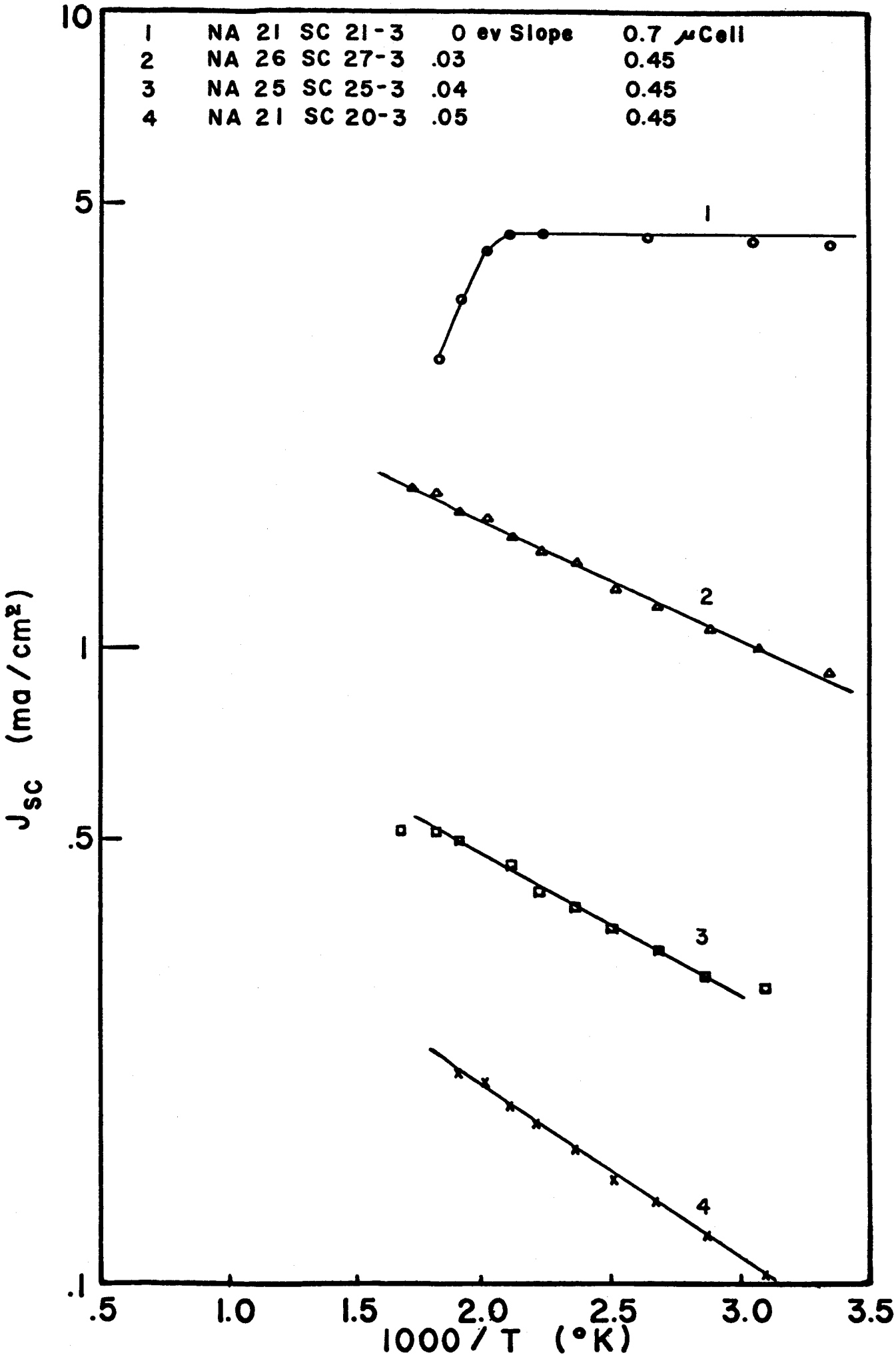

Figure 26: Curves of Short Circuit Current Density vs. Temperature for both 0.45 μ and 0.7 μ response cells.

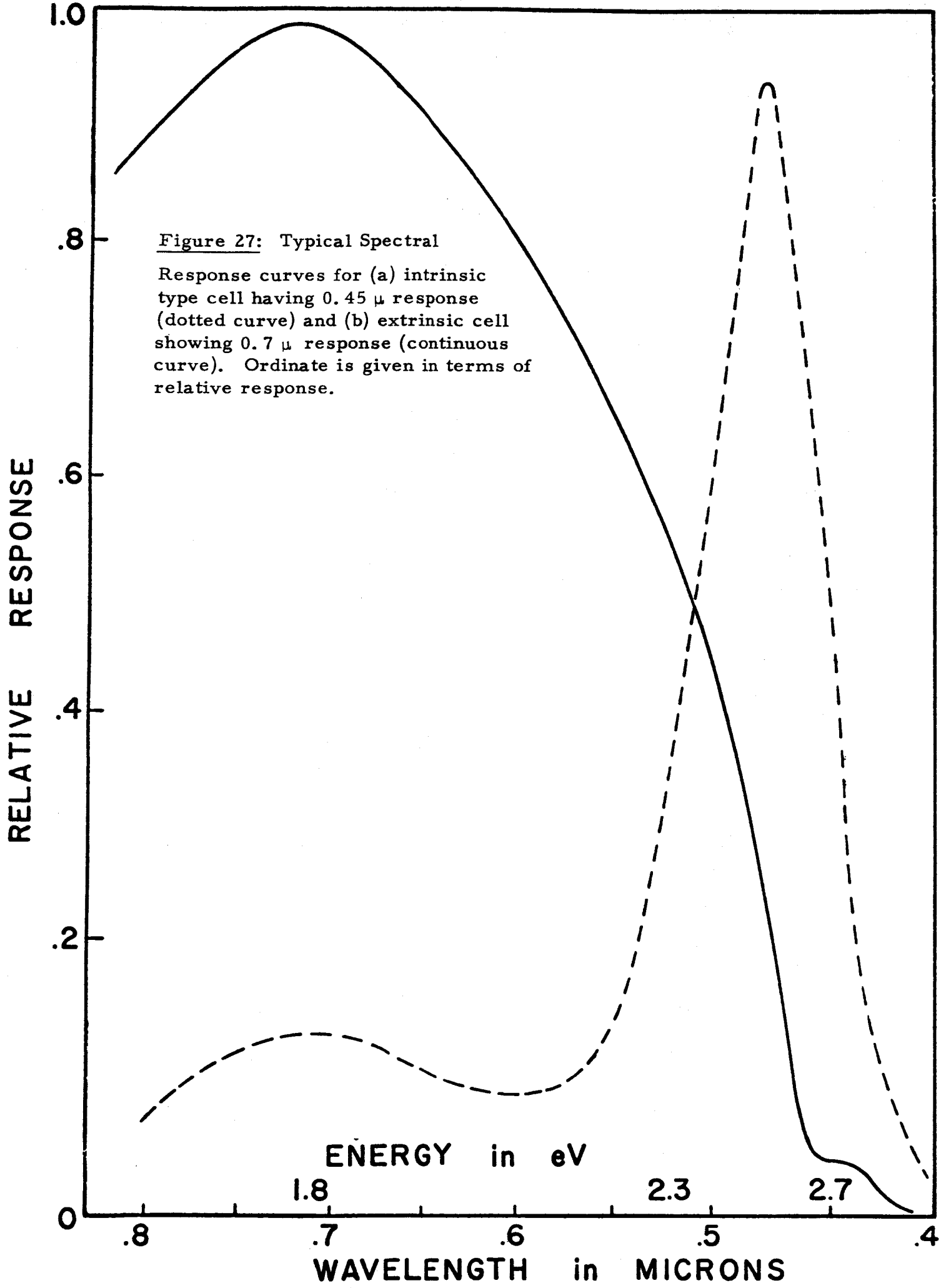

Figure 27: Typical Spectral

Response curves for (a) intrinsic type cell having 0.45 μ response (dotted curve) and (b) extrinsic cell showing 0.7 μ response (continuous curve). Ordinate is given in terms of relative response.

Figure 28: E-I curves taken in sunlight for sample NA31 SC34-3 with and without grid. Sample exhibits main spectral response at 0.45 μ. Conversion efficiency increases from 0.94% to 1.1% with use of grid.

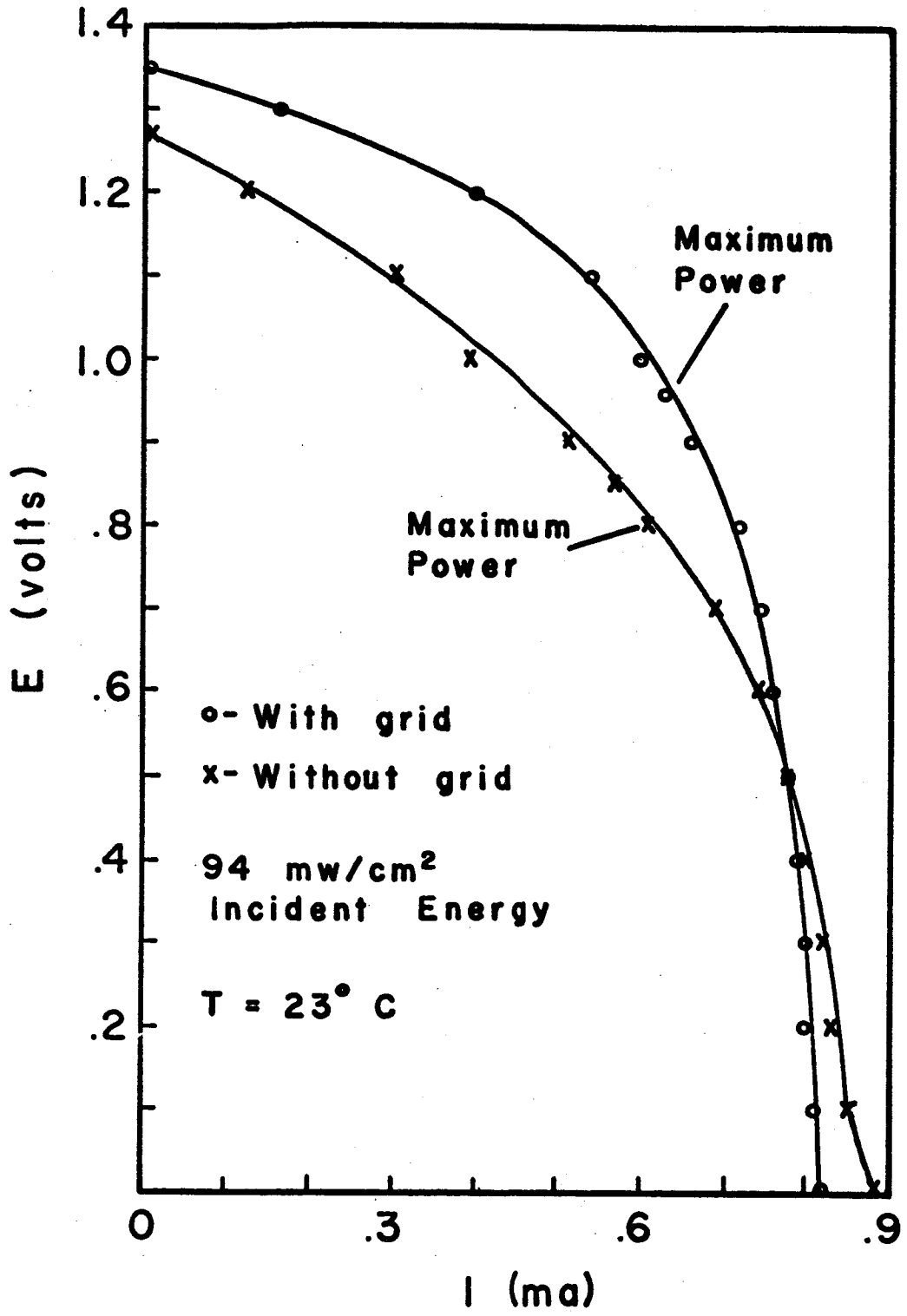

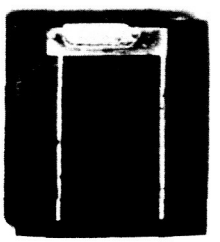

Figure 29: Solar Cell Sample NA31 SC34-3 with grid.

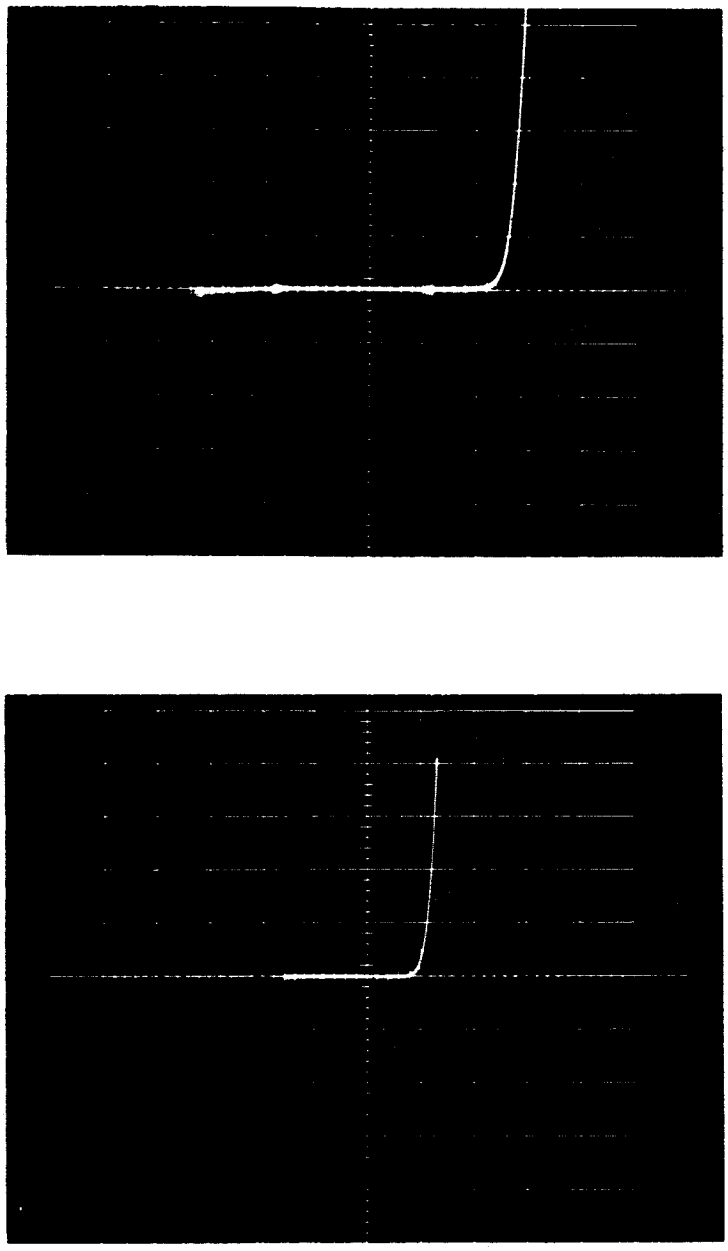

Figure 30: Best current-voltage traces obtained for a 0.45 μ cell and a 0.7 μ cell. Current, vertical axis, 0.2 ma/cm; voltage, horizontal axis, 0.5 volts/cm for both traces. Top trace, sample NA32 SC34-5, represents a 0.45 μ cell. Lower trace, sample NA22 SC21-3, represents a 0.7 μ cell.

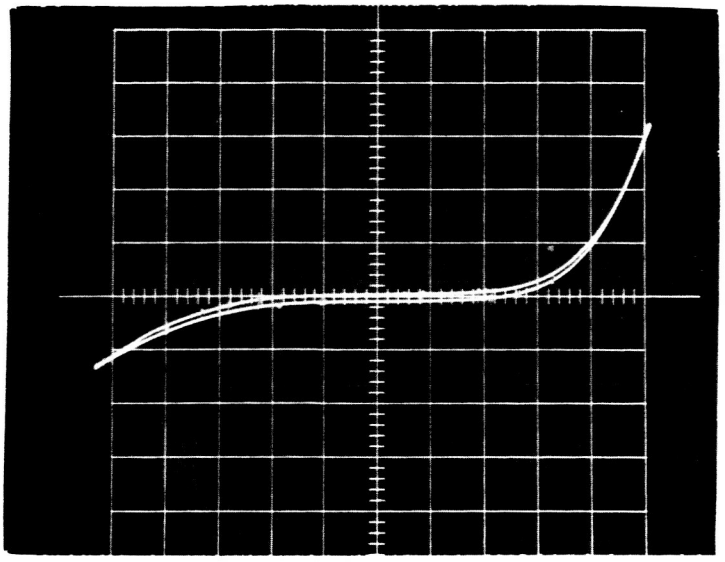

Figure 31: Typical I-V characteristic of fabricated GaP Solar Cell, for sample NA44 SC51-3, vertical:current, I, 0.2 ma/cm; horizontal, voltage, V, 0.5 volts/cm.

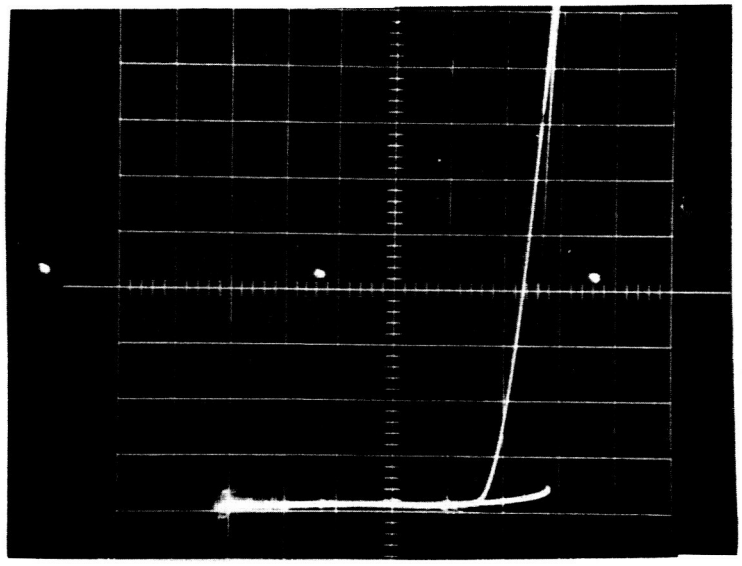

Figure 32: Negative resistance in forward direction for GaP (mesa) cell NA24 SC13-6. Vertical: Current, I, 0.2 ma/cm. Horizontal: Voltage, V, 1.25 volts/cm.

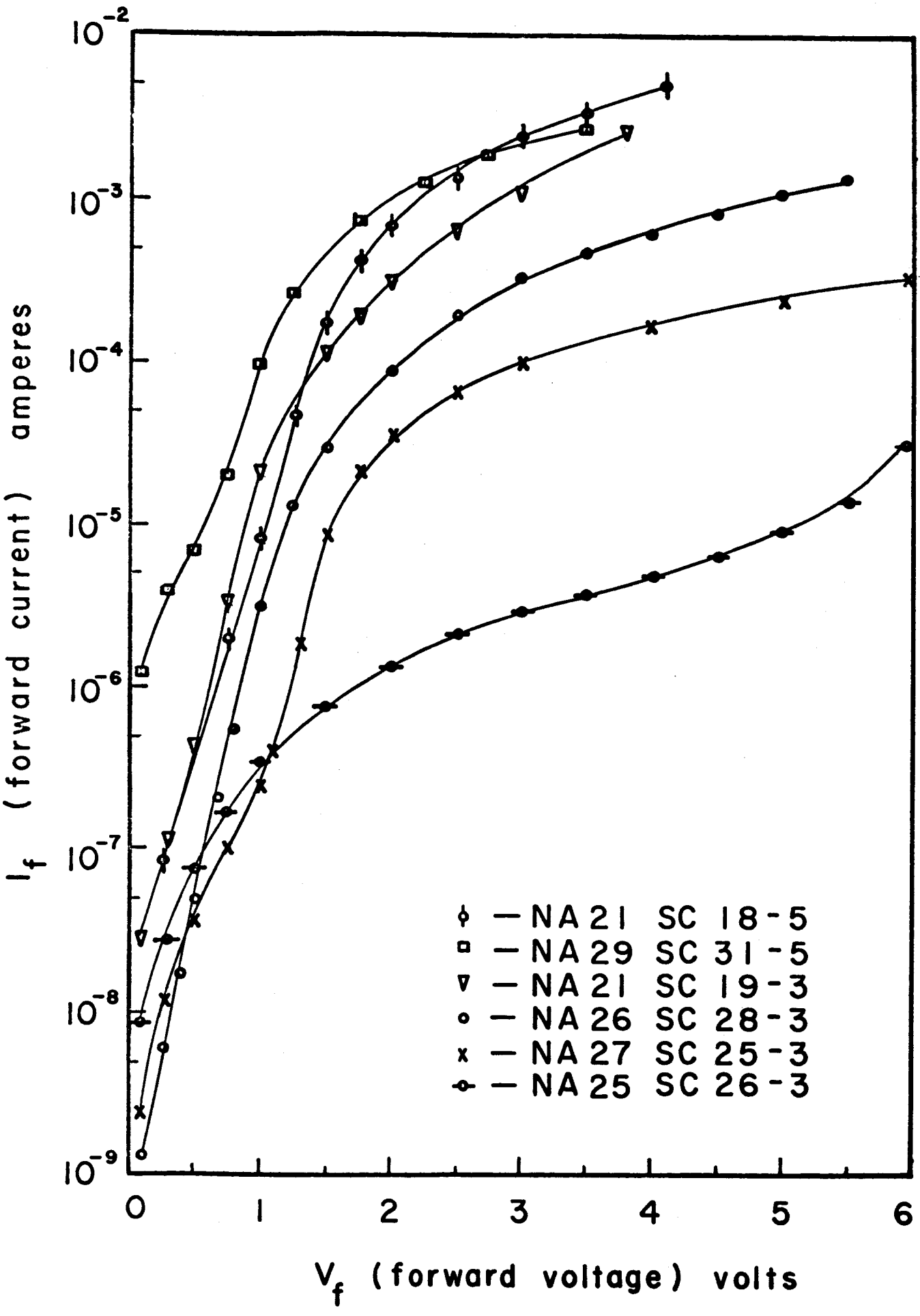

Figure 33: Representative forward I-V characteristics at 300° K of GaP Solar Cells.

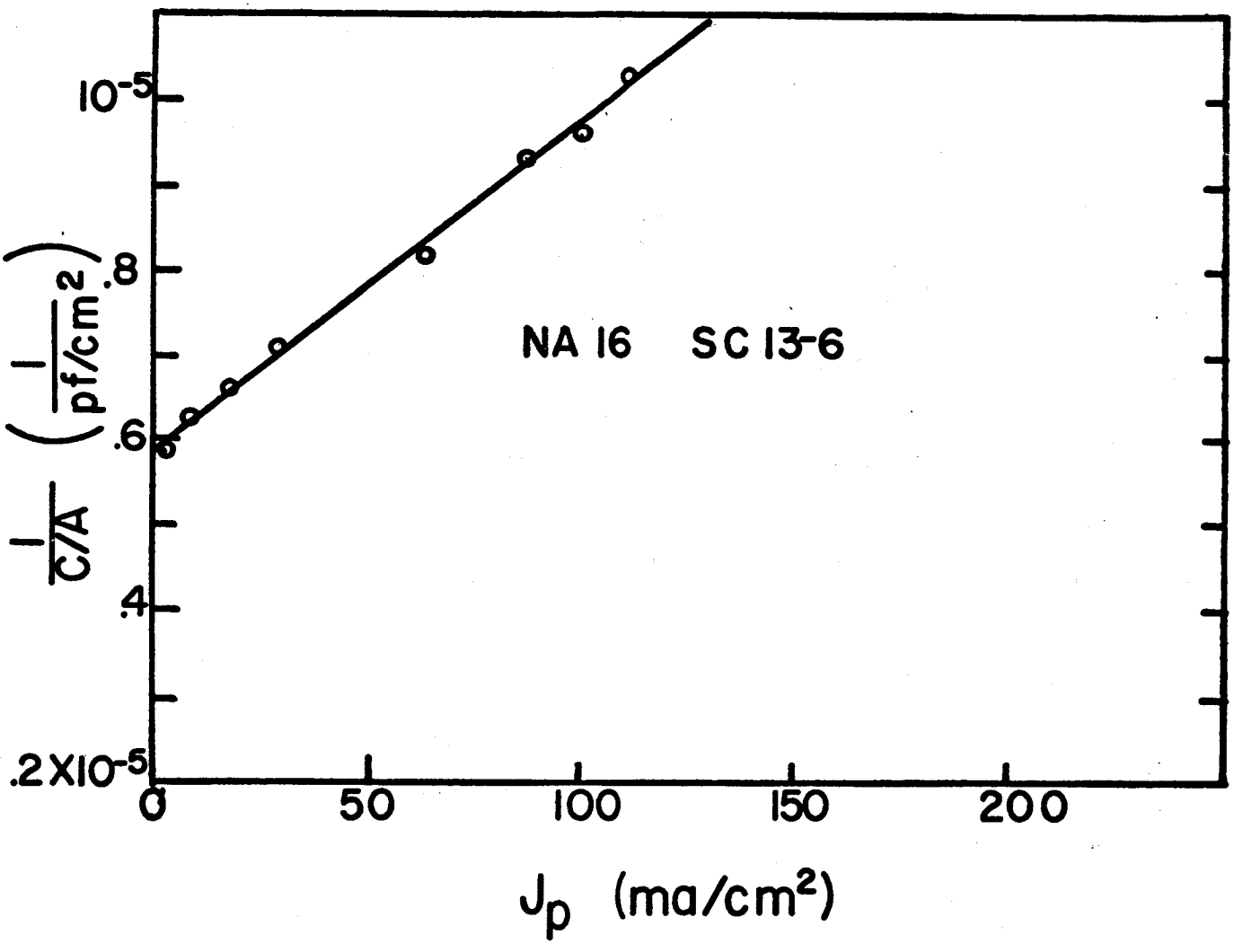

Figure 34: Sample of plot used for determining minority carrier diffusion length (from plot, L_D = 150 Å)

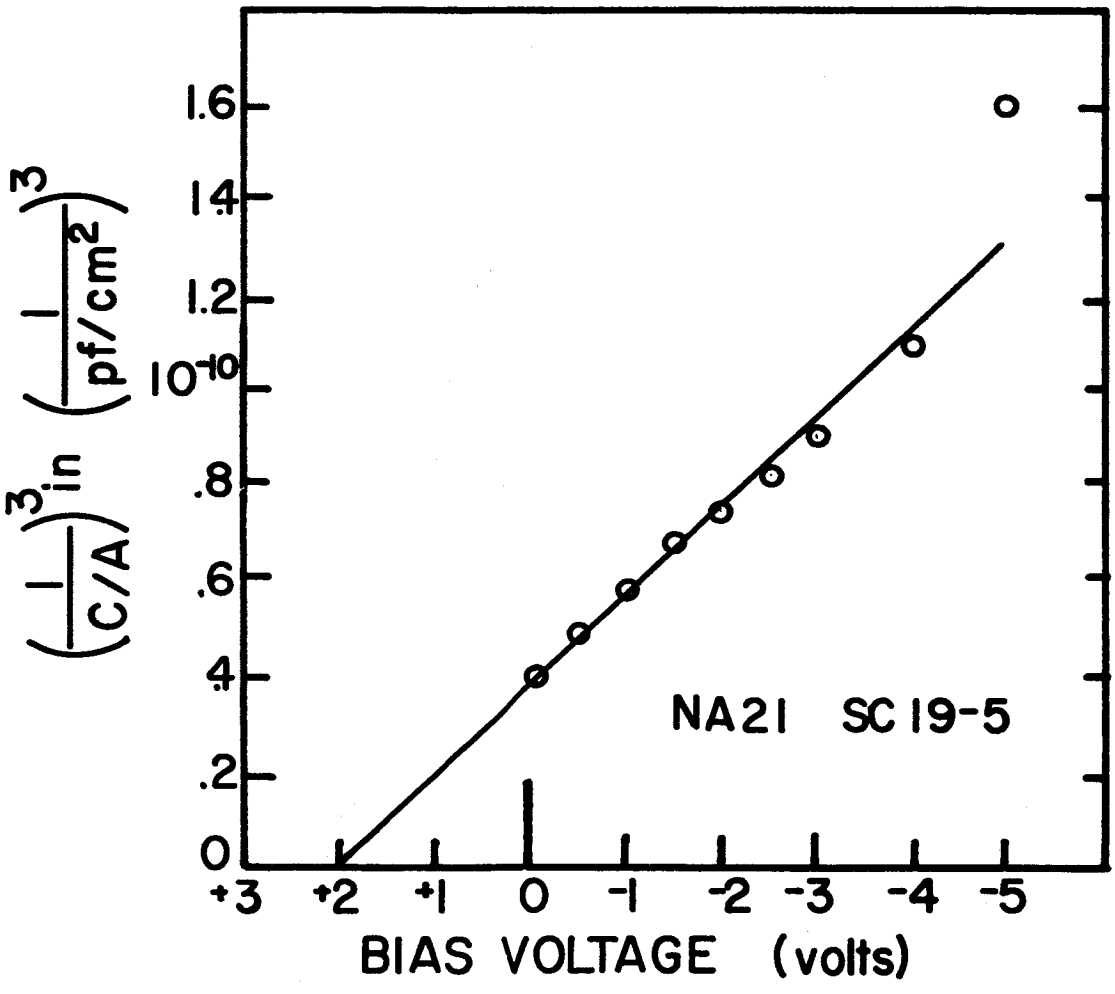

Fig. 35: - Plot of $1/c^3$ vs voltage for sample NA21 SC19-5

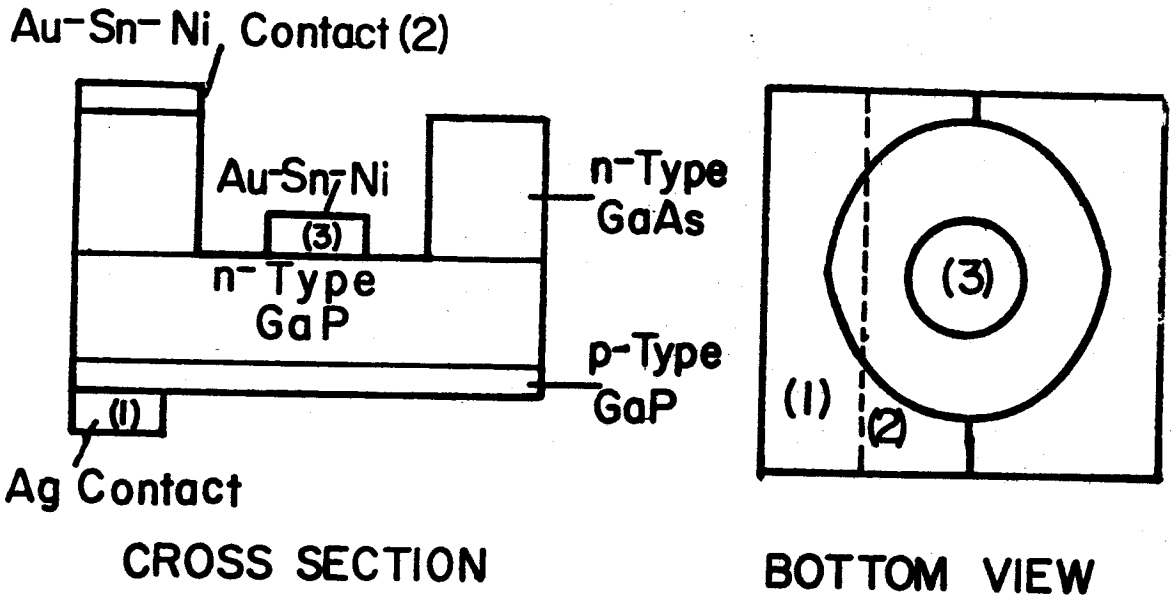

Figure 36: Experimental arrangement for checking effect of GaP-GaAs interface.

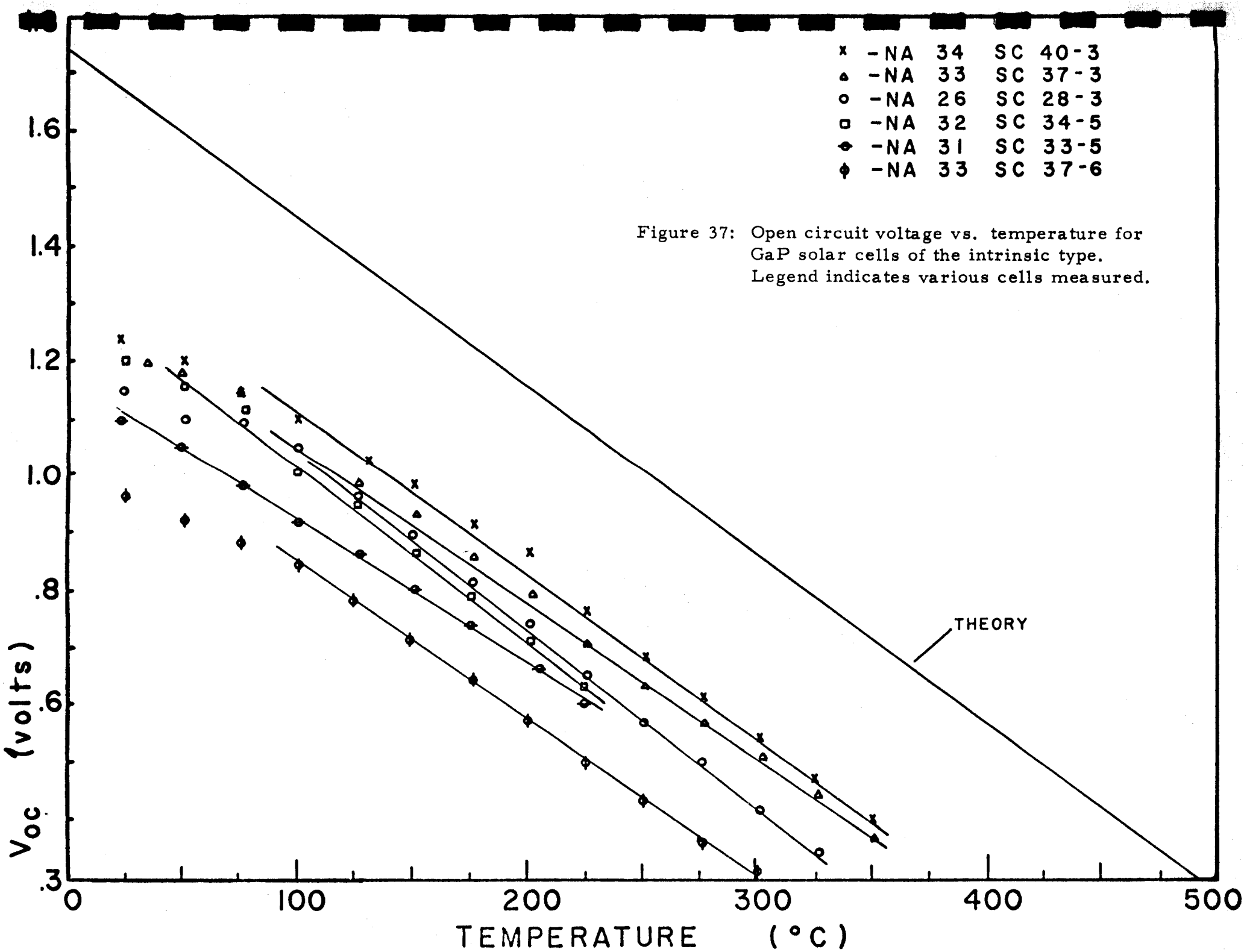

Figure 37: Open circuit voltage vs. temperature for GaP solar cells of the intrinsic type. Legend indicates various cells measured.

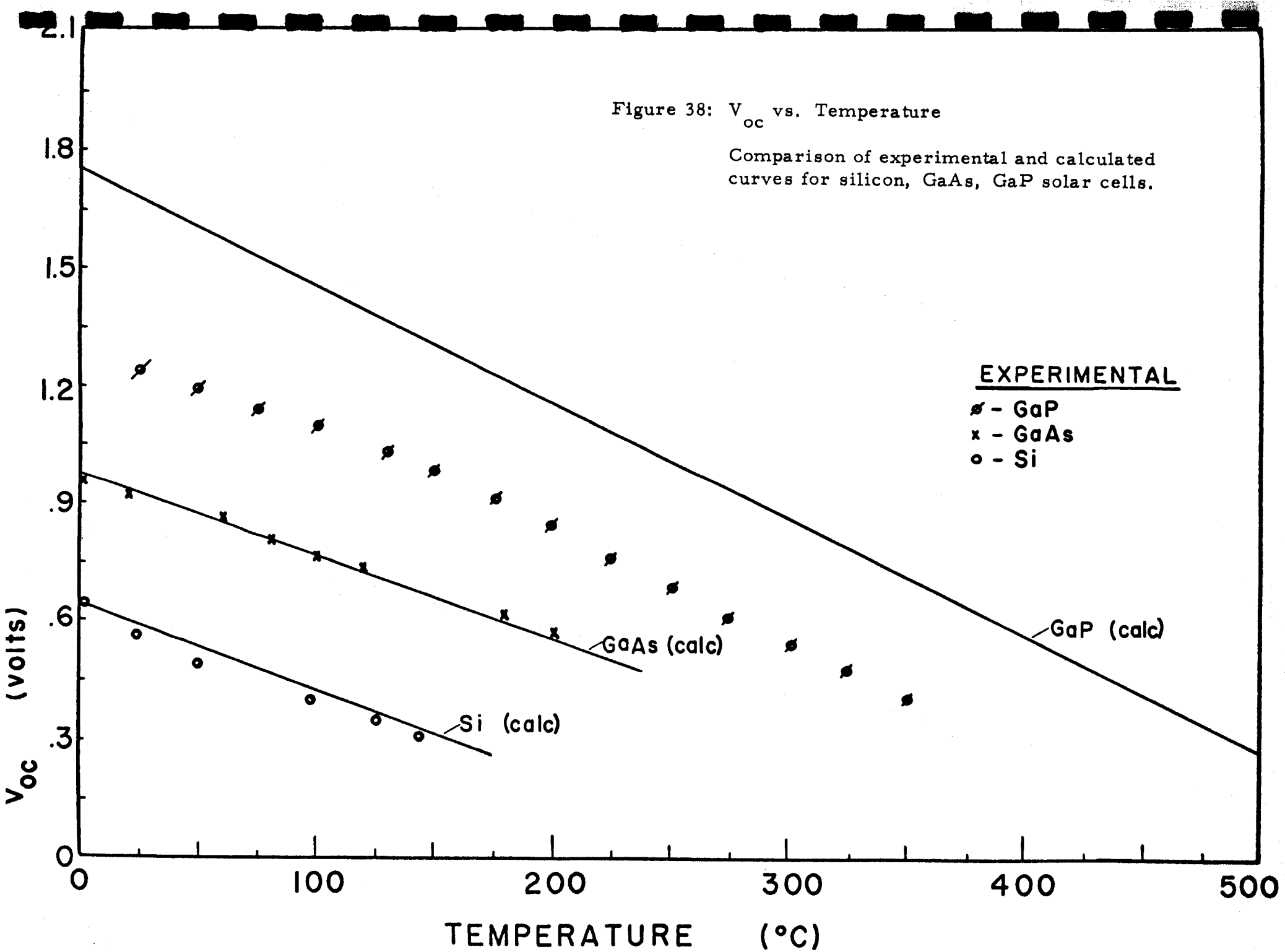

Figure 38: V_{oc} vs. Temperature

Comparison of experimental and calculated curves for silicon, GaAs, GaP solar cells.

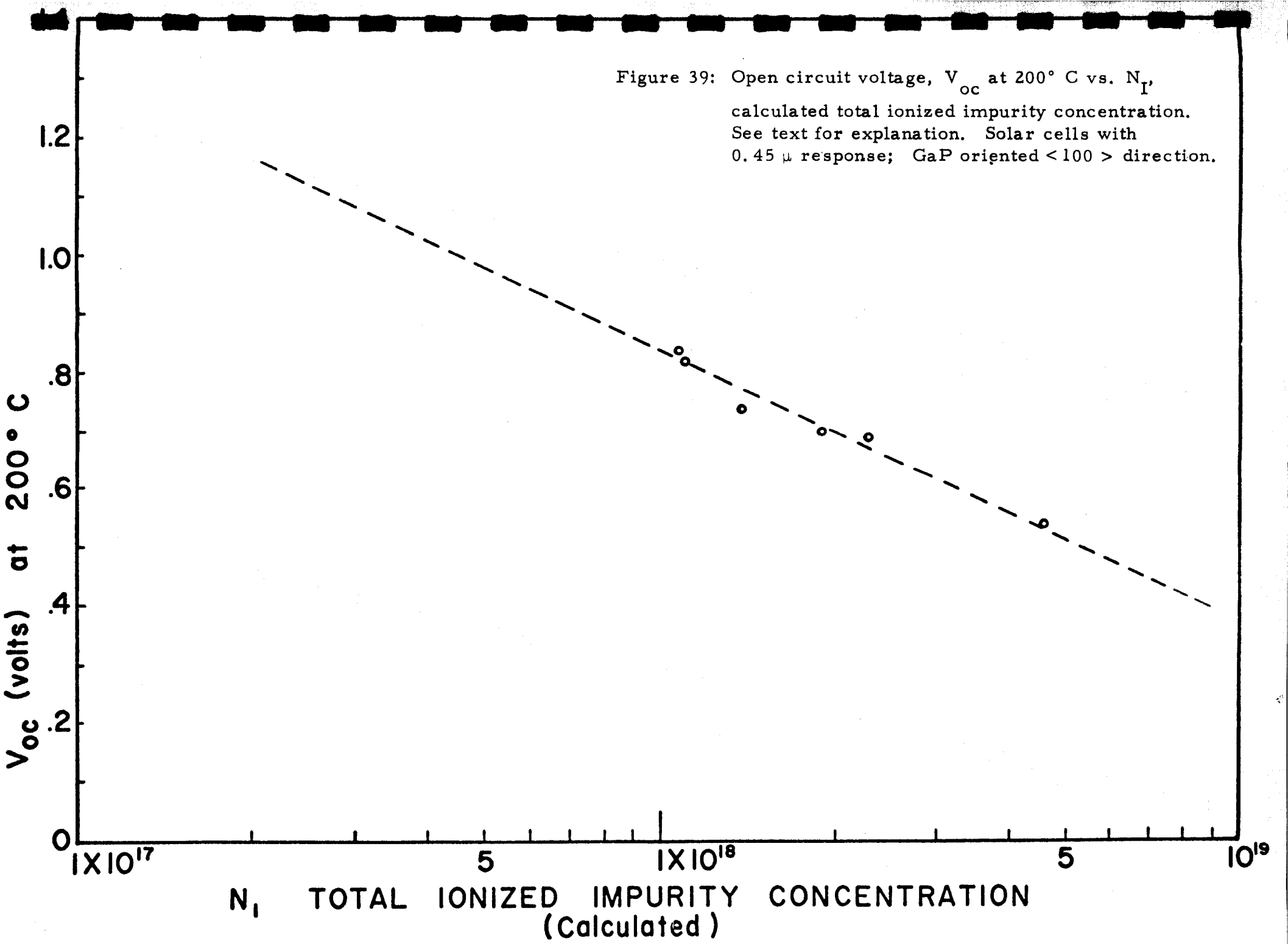

Figure 39: Open circuit voltage, V_{oc} at 200° C vs. N_I, calculated total ionized impurity concentration. See text for explanation. Solar cells with 0.45 μ response; GaP oriented < 100 > direction.

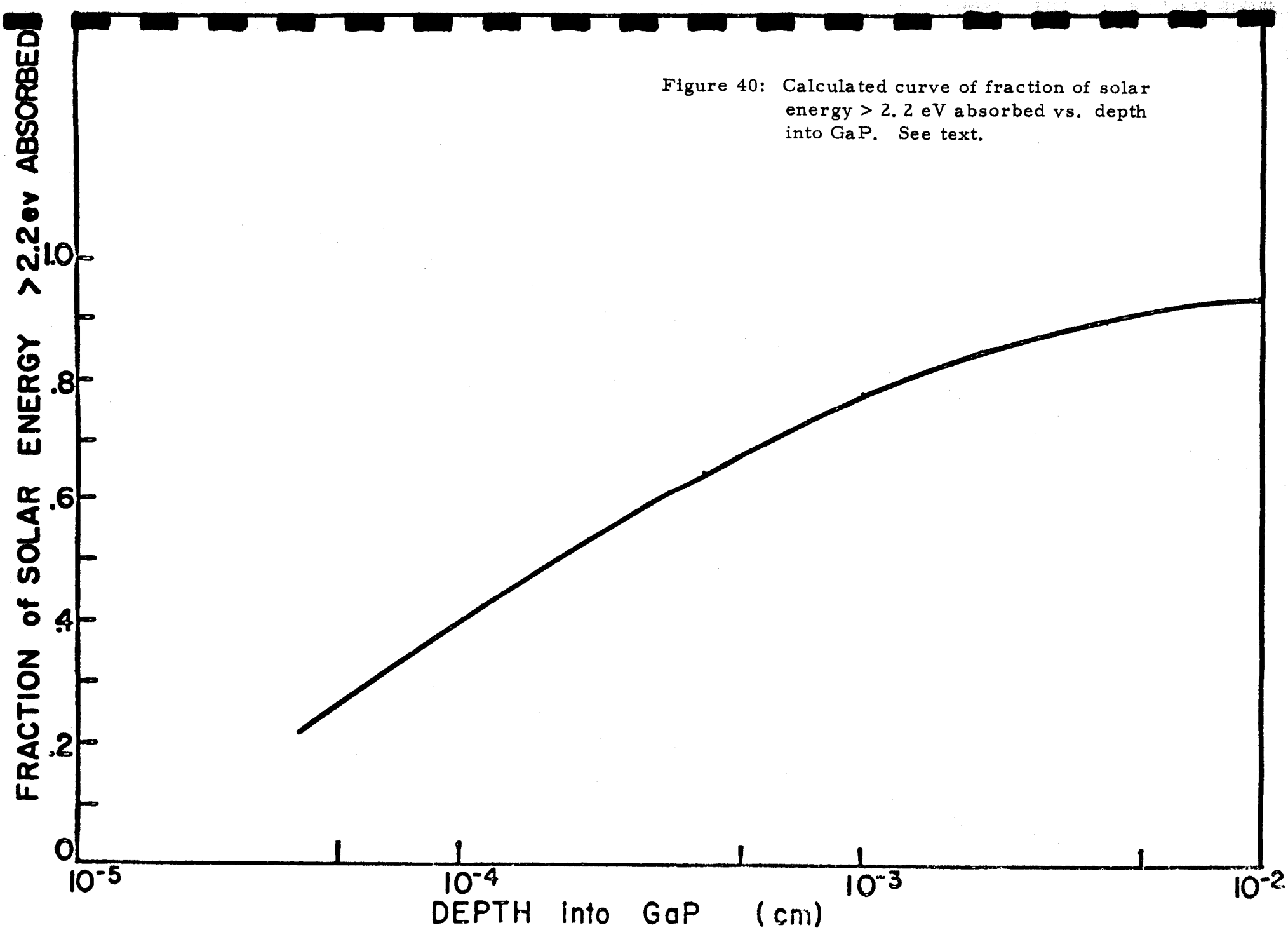

Figure 40: Calculated curve of fraction of solar energy > 2.2 eV absorbed vs. depth into GaP. See text.

Fig. 40

DISTRIBUTION LIST

National Aeronautics and
Space Administration
Washington, D. C. 20546
Attn: Arvin Smith/RP (1)
J. L. Sloop/RP (1)

NASA Goddard Space Flight Center
Greenbelt, Maryland 20771
Attn: W. R. Cherry (1)
M. Schach (1)
B. Mermelstein,
Code 672 (1)
J. W. Callaghan,
Code 621 (1)

NASA Lewis Research Center
21000 Brookpark Road
Cleveland, Ohio 44135
Attn: J. J. Fackler,
MS 86-1 (1)
B. Lubarsky,
MS 86-1 (1)
H. Schumaker,
MS 86-1 (1)
R. L. Cummings,
MS 86-1 (1)
C. K. Swartz,
MS 86-1 (1)
N. D. Sanders,
MS 302-1 (1)
J. Broder,
MS 302-1 (1)
J. Mandelkorn,
MS 302-1 (1)
A. E. Potter,
MS 302-1 (1)
C. S. Corcoran,
MS 100-1 (1)
N. T. Musial,
MS 77-1 (1)
L. R. Scudder,
MS 500-201 (3)
Library, MS 3-7 (2)
G. Mandel, MS 5-5 (1)

NASA Langley Research Center
Langley Station
Hampton, Virginia 23365
Attn: W. C. Hulton (1)
E. Rind (1)

NASA Scientific and Technical
Information Facility
Box 5700
Bethesda, Maryland
Attn: NASA Representative (50)

Philco Corporation
Blue Bell, Pennsylvania
Attn: Mr. A. E. Mace (1)

Radio Corporation of America
RCA Research Laboratories
Princeton, New Jersey
Attn: P. Rappaport (1)

Radio Corporation of America
Semiconductor and Materials
Division
Somerville, New Jersey
Attn: Dr. F. L. Vogel (1)

Sandia Corporation
Albuquerque, New Mexico
Attn: F. Smits (1)

Solid State Electronics Laboratory
Stanford Electronics Laboratory
Stanford University
Stanford, California
Attn: Prof. G. L. Pearson (1)

Westinghouse Electric Corporation
Research and Development
Laboratories
Churchill Borough, Pa.
Attn: H. C. Chang (1)

Westinghouse Electric Corporation
Semiconductor Division
Youngwood, Pennsylvania
Attn: Don Gunther (1)

Massachusetts Institute of Technology
Security Records Office (1)
Room 14-0641
Cambridge 39, Massachusetts

Clevite Research Center
540 East 105th Street
Cleveland, Ohio 44108
Attn: Dr. Hans Jaffe (1)

The Eagle-Picher Company
Chemical and Material Division
Miami Research Laboratories
200 Ninth Avenue, N. E.
Miami, Oklahoma
Attn: John R. Musgrave (1)

Harshaw Chemical Company
Solid-State Division
2240 Prospect Avenue
Cleveland, Ohio 44115
Attn: James C. Schaefer (1)

Heliotek Corporation
12500 Gladstone Avenue
Sylmar, California
Attn: Eugene Ralph (1)

Hughes Aircraft Company
Aerospace Group, R and D Division
Culver City, California
Attn: C. A. Escoffery (1)

Leesona Moos Laboratories
90-28 Van Wyck Expressway
Jamaica 18, New York
Attn: Stanley Wallack (1)

National Cash Register Company
Physical Research Department
Dayton 9, Ohio
Attn: R. R. Chamberlin (1)

North American Aviation, Inc.
Autonetics Division
Anaheim, California
Attn: R. R. August (1)

Jet Propulsion Laboratory
4800 Oak Grove Drive
Pasadena, California 91103
Attn: P. Goldsmith (1)
Don W. Ritchie (1)

Institute for Defense Analysis
Connecticut Avenue, N. W.
Washington, D. C. 20546
Attn: R. Hamilton (1)

Advanced Research Projects Agency
Department of Defense, Pentagon
Washington, D. C. 20546
Attn: Dr. C. Yost (1)

Naval Research Laboratory
Department of the Navy
Washington, D. C. 20546
Attn: E. Broncato,
Code 6464 (1)
M. Wotaw,
Code 5170 (1)
Dr. L. Linnenbom,
Code 7450 (1)
Dr. C. Klick,
Code 6440 (1)

U. S. Army Advent Management Agency
Mission Equipment Department
Ft. Monmouth, New Jersey
Attn: William Scherr,
SIGFM/PAM-5 (1)

U. S. Army Signal Research and Development Laboratory
Fort Monmouth, New Jersey
Attn: Power Sources Branch (1)

Air Force Cambridge Research Center
Air Research and Development Command
USAF, Hanscem Field
Bedford, Massachusetts
Attn: Col. G. de Giacomo (1)

Air Force Ballistic Missile Division
Air Force Unit Post Office
Lost Angeles 45, California
Attn: Col. L. Norman, SSEM (1)
Lt. Col. G. Austin, SSZAS (1)
Capt. A. Johnson, SSZDT (1)
Capt. W. Hoover, SSTRE (1)
Lt. Col. A. Bush, SSZME (1)

Wright Air Development Division
Wright-Patterson Air Force Base
Dayton, Ohio
Attn: P. R. Betheand (1)
Mrs. E. Tarrants/ WWRNEM-1 (1)

Flight Accesories Aeronautics Systems Division
Wright-Patterson AFB
Dayton, Ohio
Attn: Joe Wise/ASRMFP-2 (1)

Aerospace Corporation
P. O. Box 95085
Los Angeles 45, California
Attn: Dr. G. Hove (1)
Dr. F. Mozer (1)
V. J. Porfune (1)
Dr. I. Spiro (1)

Battelle Memorial Institute
505 King Avenue
Columbus, Ohio
Attn: L. W. Aukerman (1)
R. E. Bowman (1)
T. Shielladay (1)

Bell and Howell Research Center
360 Sierre Madre Villa
Pasadena, California
Attn: Alan G. Richards (1)

Bell Telephone Laboratories
Murray Hill, New Jersey
Attn: W. L. Brown (1)
U. B. Thomas (1)

Bendex Corporation
Research Laboratories Division
Southfield (Detroit), Michigan
Attn: Frank Adams (1)

Johns Hopkins University
Charles and 34th Street
Baltimore, Maryland
Attn: Walter Allen (1)

Solar Systems, Inc.
San Diego, California
Attn: R. L. Bachner (1)

Electro-Optical Systems, Inc.
125 North Vinedo Avenue
Pasadena, California
Attn: P. Bachwansky (1)

General Electric Company
1 River Road
Schenectady 5, New York
Attn: J. K. Baker (1)

Texas Instruments, Inc.
13500 North Central Expressway
Box 5474
Dallas 22, Texas
Attn: Kenneth E. Bean (1)

International Telephone and
Telegraph Corporation
320 Park Avenue
New York 22, New York
Attn: Robert B. Beltz (1)

Dow Corning Corporation
Box 592
500 South Saginaw Road
Midland, Michigan
Attn: A. H. Blake (1)

Libby Owens Ford Glass Company
811 Madison Avenue
Toledo 2, Ohio
Attn: J. W. Blumer (1)

General Instrument Corporation
65 Gouverneur Street
Newark, New Jersey 07104
Attn: Karl Boer (1)

General Motors Corporation
Allison Division
Speedway
Indianapolis 6, Indiana
Attn: R. C. Bourke (1)

United Aircraft Corporation
400 Main Street
East Hartford, Connecticut
Attn: L. Cavanaugh (1)

Lockheed Aircraft Corporation
Missiles and Space Division
3251 Hanover Street
Palo Alto, California
Attn: L. G. Chidester (1)

Martin Company
Baltimore, Maryland 21203
Attn: E. W. Colehower (1)

Thompson Ramo Woolridge, Inc.
Space Technology Laboratories
1 Space Park
Redondo Beach, California
Attn: Joseph Denney (1)

International Rectifier
233 Kansas Street
El Segundo, California
Attn: J. Gault (1)

Aero Geo Astro Corporation
Edsall and Lincolnia Roads
Alexandria, Virginia
Attn: R. F. Julius (1)

Ion Physics Corporation
P. O. Box 98
Burlington, Massachusetts
Attn: W. J. King (1)

Brown University
Providence, Rhode Island
Attn: J. Loferski (1)

Grumman Aircraft Engineering
Corporation
Bethpage, Long Island, New York
Attn: E. Miller (1)

Fairchild Stratos Corporation
Hagerstown 10, Maryland
Attn: Mir Vilayet Ali (1)

Boeing Company
P. O. Box 3707
Seattle 24, Washington
Attn: Henry Oman (1)

Hoffman Electronics Corporation
1009 Cafritz Building
1625 Eye Street, N. W.
Washington, 6, D. C.
Attn: Bernd Ross (1)

Tyco Laboratories, Inc.
Hickory Drive
Bear Hill
Waltham 54, Massachusetts
Attn: George Rupprecht (1)

Republic Aviation Corporation
Conklin Street
Farmingdale, Long Island, New York
Attn: M. Schwartzburg (1)

Aerospace Corporation
2400 East El Segundo Boulevard
East Segundo, California
Attn: W. T. Sheng (1)

Douglas Aircraft Company, Inc.
1100 17th Street, N. W.
Washington, 36, D. C.
Attn: R. D. Stevenson (1)

General Electric Company
General Atomic Division
P. O. Box 608
San Diego, 12, California
Attn: V. Van Lint (1)

General Motors Corporation
General Motors Building
Detroit, 2, Michigan
Attn: J. J. Werth (1)

U. S. Army Electronics Command
Research and Development Laboratory
Fort Monmouth, New Jersey
Attn: James Kespeies (1)